Expression and characterization of cytochrome b_5 from *Giardia lamblia*

A thesis submitted to the Committee of Graduate Studies in partial fulfillment of the requirements for the degree of Master of Science in the Faculty of Arts and Science

Trent University
Peterborough, Ontario, Canada

Environmental and Life Sciences M.Sc. Graduate Program
July 15

ABSTRACT

Expression and characterization of cytochrome *b*5 from *Giardia lamblia*

Samiah Alam

Giardia lamblia is an intestinal parasite found globally in freshwater systems that is responsible for endemic outbreaks of infectious diarrhea. As a unicellular parasite that lacks mitochondria, a respiratory chain and lives in the anaerobic environment of its host's intestine, Giardia was assumed for decades to lack heme proteins. However, its genome encodes several putative heme proteins, including three with sequence similarity to the cytochrome *b*5 family, referred to as Giardia cytochromes b_5 (gCYTb_5). Recombinant expression of one of these genes (gCYTb_5-I), results in a protein (17-kDa) that is isolated with noncovalently bound heme. Resonance Raman and UV-visible spectra of gCYTb_5-I in oxidized and reduced states resemble those of microsomal cytochrome b_5, while sequence alignment and homology modelling supports a structure in which a pair of invariant histidine residues act as axial ligands to the heme iron. The reduction potential of gCYT*b*5-I measured by cyclic voltammetry is -165 mV *vs* the standard hydrogen electrode and is relatively low compared to those of other family members. The amino- and carboxy-terminal sequences that flank the central heme-binding core of the gCYT*b*5 are highly charged and do not occur in other family members. An 11-kDa core gCYT*b*5-I variant lacking these flanking sequences was also able to bind heme; however, we observe very poor expression of this truncated protein as compared to the full-length protein.

Keywords: Giardia intestinalis, cytochrome *b*5, *b*-type cytochrome, heme/heam protein, electron transfer protein, protozoan protein, recombinant protein, molecular cloning, sequence homology, cyclic voltammetry, spectroelectrochemistry, Ultraviolet spectrophotometry, Resonance Raman, Mass Spectrometry

ACKNOWLEDGEMENTS

I would like to express sincere gratitude to my advisors Dr. Janet Yee and Dr. Steven Rafferty for allowing me to conduct research in the supportive and caring environment of their lab. Thank you for always being there to share your expertise and guide me with all aspects of graduate school. You challenged me when I needed to work hard, inspired me when I needed motivation and were patient with me when I struggled. This thesis would be impossible without your considerate and compassionate attitude.

I would like to thank Dr. Ray March for teaching me mass spectrometry and sharing your knowledge and experiences. I am indebted to Dr. Shin-ichi Joseph Takayama of Dr. Grant Mauk's lab in UBC for performing the cyclic voltammetry experiments and Dr. Logan Donaldson in York University for his assistance with NMR experiments. Special thanks to Linda Cardwell, Jane Rennie, Dr. Huda Al-Haddad, and all the graduate staff for their words of encouragement and support throughout my Trent career.

Next to all members of the Yee and Rafferty lab both past and present, I thank you for creating a pleasant and friendly working environment. To Joella, Colin, Chase, Amber, Aaliya and Gail, thank you for teaching and advising. To Katie, Mirfath, Wendy, Megan, Jen, Daniel, and Elizabeth thank you for your help and enthusiasm that always created a cheerful atmosphere in the lab, it was much appreciated. To my friends Eva, Rolinda and Simanga for your friendship, emotional support, for helping me get through difficult times, and for all the happy moments we spent together. I will always treasure those times.

Finally, to my husband Faraz, my siblings, and extended family thank you for your love and moral support. Most importantly, to my parents; I am truly grateful for everything you have done to raise me, support me, teach me, and give me the best life possible.

TABLE OF CONTENTS

LIST OF FIGURES

LIST OF TABLES

LIST OF ABBREVIATIONS AND SYMBOLS

α	alpha (protein), absorption coefficient
A	Absorbance
ALA	δ-Aminolevulinic acid
BLASTp	Basic local alignment search tool (protein)
bp	Base pair
CV	Cyclic voltammetry
Da	Dalton
DNA	Deoxyribonucleic acid
dNTP	deoxynucleotide triphosphates
ε	Extinction coefficient, molar absorptivity ($M^{-1}cm^{-1}$)
E	Potential of an electrode versus a reference
E°	Standard potential of an electrode or a couple
E°'	Formal potential of an electrode
E_{eq}	Equilibrium potential of an electrode
$E_{1/2}$	Measured half wave potential in voltammetry
F	Faraday constant (charge on one mole of electrons)
gCYT*b*5	Giardia cytochrome *b*5
ΔG	Free energy
gFLHb	Giardia flavohemoglobin
GiardiaDB	Giardia database
HPLC	High performance liquid chromatography
HSQC	Heteronuclear single quantum coherence
$\mathbf{i_{pa}}$	Peak anodic current
$\mathbf{i_{pc}}$	Peak cathodic current
IMAC	Immobilized metal-affinity chromatography
IPTG	Isopropyl-β-D-thiogalactoside
l	Path length of cuvette in spectrometry
MS	Mass spectrometry
$\mathbf{M_r}$ **MW**	Molecular weight
n	Number of electrons transferred
NHE	Normal hydrogen electrode = SHE
NMR	Nuclear magnetic resonance
O	Oxidized species in **O** + *ne* ↔ R
OD	Optical density
OM	Outer mitochondrial
OTTLE	Optically transparent thin-layer electrode
ppm	Parts per million
PCR	Polymerase chain reaction
R	Reduced species in O + *ne* ↔ **R**
RR	Resonance Raman
rpm	Revolutions per minute
SDS-PAGE	Sodium dodecyl sulfate polyacrylamide gel electrophoresis
SHE	Standard hydrogen electrode = NHE
TCEP	Tris(2-carboxyethyl)phosphine
UV-Vis	Ultraviolet-visible
λ	Wavelength of light, switching time in CV
1D, 2D, 3D	One-, two-, three-dimensional

INTRODUCTION

1: *Giardia lamblia*

The protozoan parasite *Giardia lamblia* is one of the most common causes of waterborne diarrheal disease, known as giardiasis or 'Beaver fever' that infects humans, domestic animals and wildlife (Adam 2001). Giardiasis occurs worldwide, but has a higher prevalence in developing countries due to poor sanitation and limited access to clean water (Younas *et al.* 2008). Giardiasis has been included in the Neglected Diseases Initiative by World Health Organization due to its significant role in morbidity and association with poverty (Savioli 2006).

1.1: *Giardia lamblia* life cycle

Giardia enters its host as an infectious and inert cyst ingested through contaminated water, food, or direct fecal-oral contact (Figure 1). Exposure of these cysts to the acidic environment of the stomach triggers their excystation into flagellated trophozoites that adhere to the epithelial cells of the upper small intestine, where they reproduce by asexual binary fusion. Attachment of trophozoites to the intestinal lumen causes malabsorption, chronic diarrhea, dehydration, weight loss, cognitive impairment in children, and chronic fatigue in adults (Dunn *et al.* 2010). During infection, the trophozoites that are swept downstream to the lower intestine must encyst before they are excreted in feces, so they can survive outside the host and can start another infectious cycle.

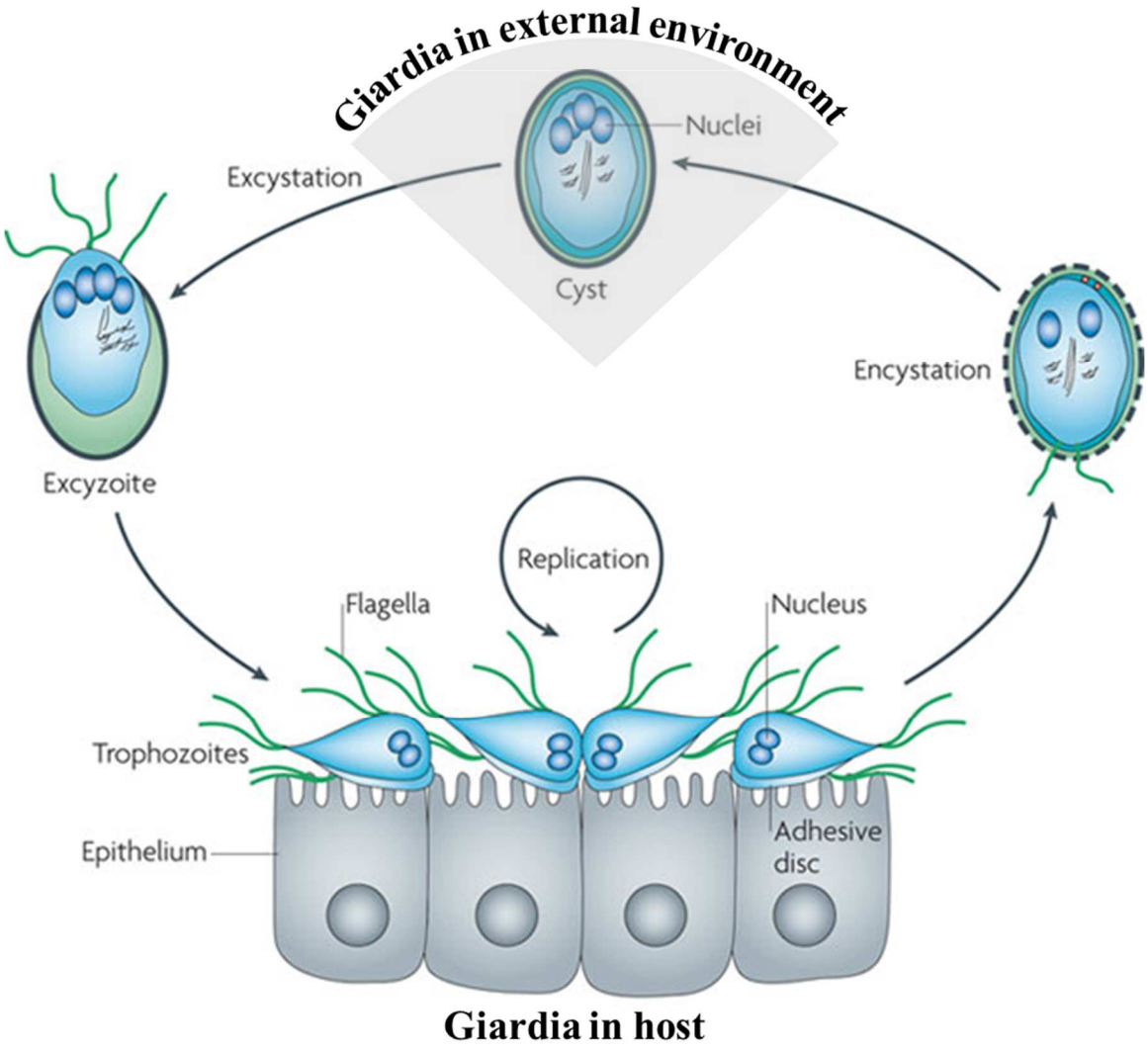

Figure 1: Life cycle of *Giardia lamblia*. Infectious cysts are ingested from environment into the gastrointestinal tract of the host. Excystation into the trophozoite form in the small intestine leads to replication by binary fission. The pathogen is excreted in the cyst form to complete the infectious cycle (Ankarklev *et al.* 2010).

Besides its impact on human and animal health, Giardia is a peculiar organism. Although it is classified as a eukaryote, it has many unusual features that set it apart from other eukaryotes. These differences in cell structure, metabolism, and genome arise not only due to Giardia's parasitic mode of existence but also from its evolutionary divergence. Giardia is classi fied as an early diverging eukaryote in a number of gene phylogenies because it lacks typical eukaryotic organelles, such as peroxisomes, and only has rudimentary versions of others, such as a Golgi apparatus (Adam 2001; Svärd 2003). This classification has been challenged by the discovery of vestigial mitochondria in Giardia, called mitosomes that have retained the ability to form iron-sulfur clusters but lack the capacity for oxidative phosphorylation (Tovar *et al.* 2007). Hence, there are suggestions that Giardia is a highly derived eukaryote that has recently evolved as a parasite from a typical aerobic free-living flagellate (Lloyd and Harris 2002; Philippe 2006; Embley and Martin 2006).

1.2: *Giardia lamblia* metabolism

Giardia obtains its nutrients, such as glucose, amino acids, and complex lipids, from the small intestine of its host. Giardia uses substrate-level phosphorylation for energy production; being an anaerobe it does not have a citric acid cycle or an electron transport chain for oxidative phosphorylation (Embley and Martin 2006; Han and Colin 2012). Glucose is metabolized into pyruvate through glycolysis followed by reduction of the pyruvate to regenerate NAD^+. Since Giardia is a microaerotolerant facultative anaerobe, the pyruvate can be reduced to either ethanol under aerobic conditions or alanine and acetate under anaerobic conditions.

As heme proteins that are involved in oxidative metabolism, such as cytochromes, are not required under anaerobic conditions, it was thought that Giardia did not require heme as a cofactor. Furthermore, Giardia lacks any known pathway for either heme uptake or heme biosynthesis, and it does not have fully functional mitochondria where heme is synthesized in other eukaryotes.

1.3: *Giardia lamblia* genome analysis

The sequencing of the Giardia genome revealed that it has a compact genome size of 11.7 Mb with 6470 genes distributed over five chromosomes (Morrison 2007). This genome size is much smaller than most eukaryotic genomes and is of similar size to that of yeast (Morrison 2007). Upon *in silico* sequence analysis of this genome, genes encoding for seven putative heme-containing proteins were identified, which was surprising, given the presumptions that Giardia did not make heme or have a need for it. One of these is a flavohemoglobin, while three are members of the cytochrome *b5* family.

2: *Heme binding proteins*

Heme, which is an iron-containing porphyrin cofactor of proteins, functions as a prosthetic group in many critical cellular processes (Figure 2). Heme is a versatile molecule that can perform diverse functions depending upon its surrounding protein environment. For example, in hemoglobin of red blood cells the heme transports oxygen; in cytochromes the heme transports electrons; in monooxygenases and peroxidases it catalyses the reaction of oxygen with biomolecules; and in nitric oxide synthase the heme catalyzes production of the signaling molecule, nitric oxide.

As heme is redox-active and hydrophobic, free heme is toxic to cells and thus heme synthesis, acquisition, and transport are highly regulated (Hamza 2006). In eukaryotes heme is synthesized in part in the mitochondrial matrix through a specific pathway and is exported only as required to heme-binding proteins found in the cytoplasm and membrane-bound organelles (Severance & Hamza 2009). It has also been speculated that heme synthesis and transport is different in bacteria and yeast as compared to eukaryotic animals (Weissman & Kornitzer 2004).

2.1: Flavohemoglobin

Flavohemoglobin (gFLHb) was one of giardia's heme-binding proteins that was successfully expressed from the pathogen's genome and characterized as a functional recombinant protein by Rafferty *et al.* and Mastronicola *et al.* (2010). The protein was highly expressed with heme and FAD cofactors bound to it. The NAD(P)H oxidase and nitric oxide dioxygenase enzymatic activities and UV-visible spectroscopy of gFlHb were similar to other flavohemoglobins. Due to its sequence similarity to flavohemoglobins of Gram negative bacteria, it is thought that Giardia acquired the protein through lateral gene transfer with bacteria found in intestinal flora.

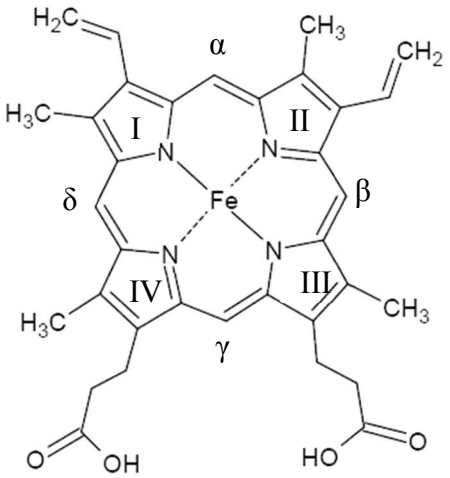

Figure 2: Molecular structure of heme b: protoporphyrin IX coordinated to an iron ion that cycles between the Fe (II) and Fe (III) oxidation states. The porphyrin donates four nitrogen ligands to the iron ion's coordination sphere in a planer arrangement. In cytochrome b_5, the ε-nitrogen atom of histidines in the protein's side-chain provide the fifth and the sixth axial ligands to complete iron's octahedral ligand coordination sphere and make the iron low spin. Pyrrole rings are denoted by Roman numerals and *meso*-positions by Greek letters.

3: *Cytochrome b_5*

In addition to the gFLHb gene, the Giardia genome also encodes several proteins similar in sequence to cytochrome b_5. Cytochrome b_5 is a hemoprotein that has been identified in variety of organisms, including aerobic, anaerobic, and photosynthetic bacteria, fungi, plants, and eukaryotes (Jagow 1980). These *b*-type cytochromes have diverse properties and function at various locations within cells depending on the redox or electron transfer reaction they are involved in (Schenkman and Jansson 2003; Vergéres and Waskell 1995). They are membrane-bound when found in the endoplasmic reticulum or mitochondria, and water-soluble when found in erythrocytes, bacteria, viruses or some animal tissues (Aono *et al.* 2010; Reid *et al.* 2013).

Membrane-bound mammalian cytochrome b_5 are found in the membranes of the endoplasmic reticulum (type A microsomal cytochrome b_5, CYB5A or Mcb_5) and the outer mitochondrial membrane (type B mitochondrial cytochrome b_5, CYB5B or OMb_5). The different subcellular localization of the two isoforms of the proteins is a result of gene duplication as the mammalian cytochromes b_5 are more similar to each other than to those of insects, plants or fungi (Guzov *et al.* 1996). The microsomal cytochrome b_5 has been identified in many organisms, but the mitochondrial cytochrome b_5 has only been isolated from rat liver, and human testis (Sergeev *et al.* 2006).

3.1: Structural features of cytochrome b_5

Membrane-bound cytochrome b_5 such as the microsomal and mitochondrial isotypes, are small (MW 15.2 kDa - 16.7 kDa) monomeric proteins made up of a single polypeptide chain of 131 to 146 amino acid residues (Sergeev *et al.* 2006). These cytochromes are composed of two functional domains: a hydrophilic amino-terminus

globular domain that contains the heme-binding catalytic site (~90 residues) and a hydrophobic carboxy-terminus domain that serves as a membrane anchor (~28 or 40 residues). The N-terminal domain extends out of the membrane to participate in electron transfer reactions and is more soluble than full-length protein. The carboxy-terminus domain contains a hydrophobic segment (~14-18 residues) that inserts into the membrane and is connected to the globular domain *via* a proline containing hinge/linker region (~7-15 residues) (Schenkman and Jansson 2003). The final portion of this domain is a C-terminal hydrophilic segment (~7 residues) that is exposed on the surface of membranes and encodes the posttranslational membrane-targeting region (Silvestris *et al.* 1995). The protein is targeted to outer mitochondrial membrane if this region contains positively charged amino acids, and to endoplasmic reticulum membrane if these positively charged amino acids are absent (Mitoma and Ito 1992). The targeting region of mitochondrial cytochrome b_5 tends to be longer than the microsomal protein (Kuroda 1998).

The soluble mammalian cytochrome b_5 contains around 98 amino acids with sequence and structure similar to the hydrophilic heme-binding amino domain of the microsomal membrane-bound protein (Guzov *et al.* 1996). The soluble and membrane-bound cytochrome b_5 are coded by the same gene and the two forms arose at the level of mRNA splicing (Chudaev *et al.* 2001).

The hydrophobic nature of the transmembrane domain causes the full length protein to aggregate in aqueous solution and thus structural studies of the protein have focused on the heme binding functional segment without the transmembrane domain, which can be cleaved enzymatically from the native protein or expressed recombinantly from a DNA sequence that does not encode the anchor.

3.1.1: Heme binding domain of cytochrome b_5

Cytochromes b_5 are made up of five β-strands consisting of one central β sheet and various β-turns, five α-helices and a short C-terminal α helix (α6) (Figure 3). The order of the secondary structure strands of heme domain from N-terminal to C-terminal is as follows, β1-α1-β4-β3-α2-α3-β5-α4-α5-β2-α6 (Mathews *et al.* 1979). The curved beta sheet divides the protein into two hydrophobic cores on both sides of beta sheets; core 1 is larger and holds the heme (α2 to α5), while the smaller core 2 (β1- β4, α1 and α6) stabilizes core 1. The heme-binding core forms a cleft, on each side of which are a pair of short alpha helices connected by a turn. In core 2, the bottom side of the beta sheet forms one side of a barrel, with N-terminal helix α1 on the other side of the barrel and a turn of helix α6 at C-terminus closing off the bottom of barrel (Lederer 1994).

The amino-terminal domain of cytochrome b_5 has a non-covalently bound iron ion complexed by protoporphyrin IX, or heme *b*, as a prosthetic group. Cytochrome b_5 exhibits a six-coordinate geometry around the iron with an octahedral arrangement of ligands. The ε-nitrogen atoms of two conserved histidine residues (His 39 and 63) provide the fifth and sixth heme axial ligands (Figure 3). The His 39 residue resides in the HPGG loop motif between α2 and α3, while His 63 resides in the VGHS loop motif between α4 and α5 (Mathews *et al.* 1971). These strong field axial ligands do not permit spin state changes and the iron atom is low spin in both Fe(II) and Fe(III) oxidation states. This electron configuration effects the reactivity as low-spin iron tends to hold on to its ligands more strongly. The bis-histidine (bis-His) coordination means that there are no positions for further coordination thus small exogenous ligands such as O_2, CO or NO cannot directly bind to heme.

The heme is oriented within the crevice such that its two-propionate groups are situated at the opening of the heme-binding pocket with the heme edge and one propionate group extending out of the protein exposed to the environment (Figure 3). The heme-binding pocket is made up of highly conserved hydrophobic amino acid residues, which assist in stabilizing the oxidized and the reduced forms of heme. The aromatic-ring side chains of amino acids, such as phenylalanine, tyrosine and tryptophan interact with the heme through T and π stacking interactions (Lederer 1994; Smith *et al.* 2010). The placement and conformation of heme within the protein is determined by its hydrophobic interactions and hydrogen bonds with surrounding protein amino acid residues. Due to the non-covalent interaction between heme and protein in *b*-type cytochromes, there are two stereoisomers of the protein that differ by a 180° rotation of the heme about an axis defined by the α-γ meso carbons (Figure 4, Walker 1988).

The geometry around the heme is generated by the rigid protein fold, which does not relax readily. This protein fold leaves the coordination sphere of the iron complete, and it undergoes minimal structural rearrangement upon a change in iron oxidation state.

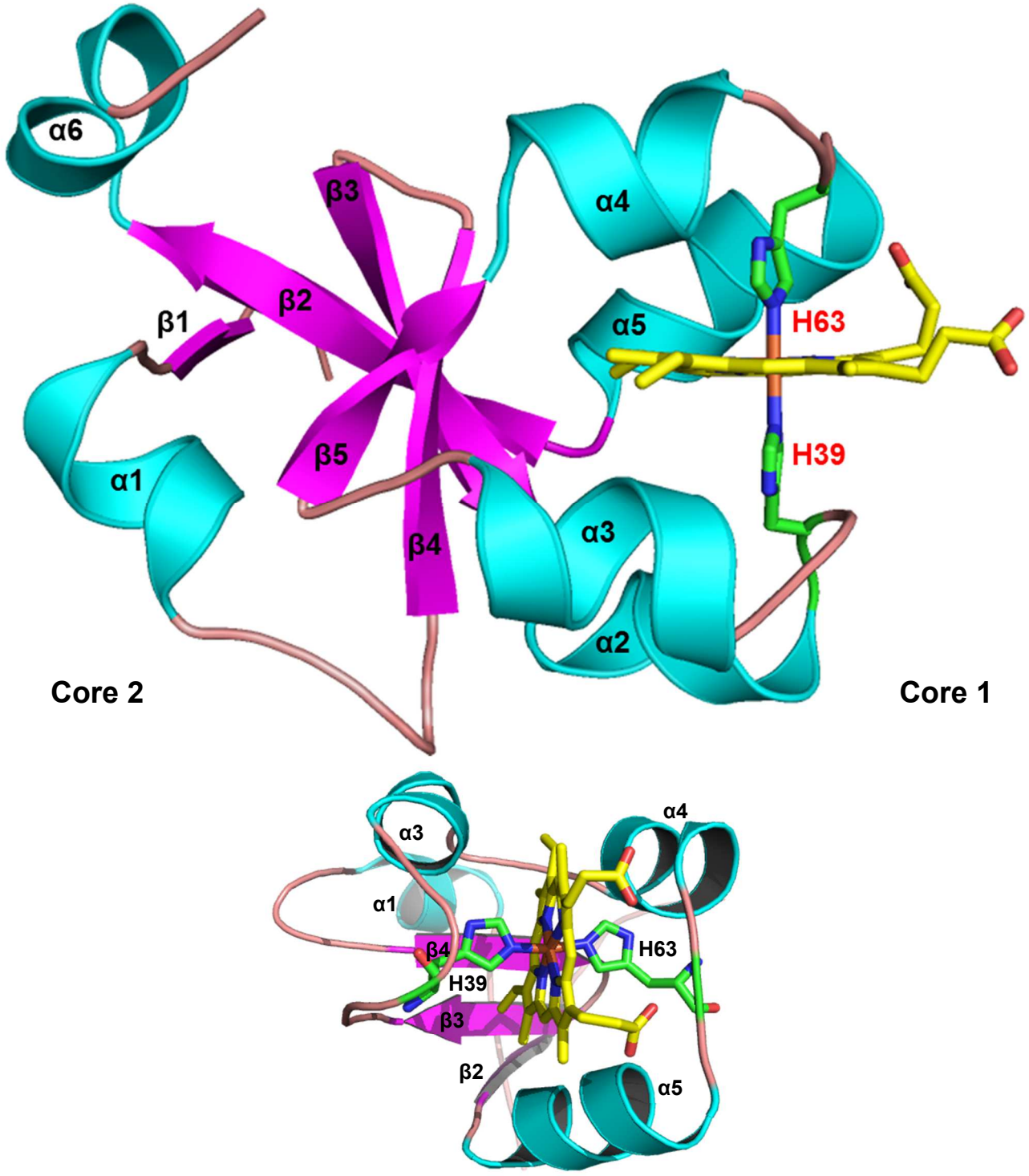

Figure 3: Structure of one subunit of the **(a)** bovine microsomal cytochrome *b*5 (1cyo.pdb) and **(b)** rat mitochondrial cytochrome *b*5 (1b5m.pdb), homologs of the Giardia proteins. Alpha-helices are shown as cyan ribbons, beta strands as magenta arrows and loops are salmon. The heme and the two histidine axial ligands are shown in yellow and green ball and stick model, respectively (Mathews *et al.* 1979; Rodriguez-Maranon *et al.* 1996)

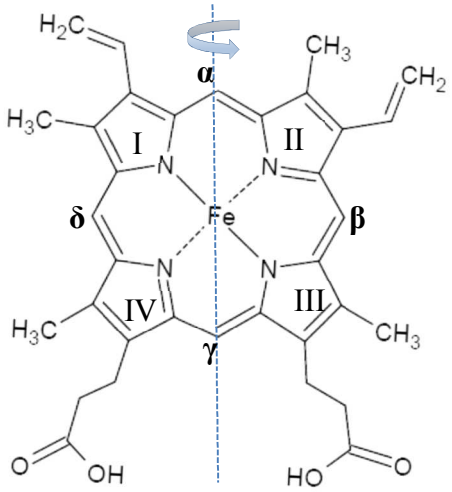

Figure 4: Heme *b* orientation in cytochrome b_5 differ by 180° rotation about the α and γ carbons. If the His39 coordinates the iron from above, then the form as shown is referred to as form A and is predominantly found in microsomal cytochrome *b*5 (9:1 Walker *et al.* 1988) and form after rotation is referred to as form B and is predominantly found in mitochondrial cytochrome *b*5 (Silchenko *et al.* 2000). The ratio of both forms vary depending on the species that the protein is isolated from.

Although x-ray crystallography shows that microsomal and outer mitochondrial cytochrome b_5 have identical folds (Durley and Mathews 1996 and Rodríguez-Marañón *et al.* 1996) and share similar UV-Vis and 1H NMR spectroscopic properties (Rivera *et al.* 1994), there are differences in their biophysical properties. The sequence identity and similarity between these two isoforms is 58% and 78%, respectively (Altuve *et al.* 2001). As it possesses more hydrophobic residues within the heme pocket, with more van der Waals contacts to the cofactor, outer mitochondrial cytochrome b_5 binds its heme more strongly than does the microsomal protein (Altuve *et al.* 2004). The mitochondrial protein is also more stable (Silchenko *et al.* 2000) and has a more negative reduction potential (Rivera *et al.* 1994).

3.1.2: Apocytochrome b_5

The protein with heme bound to it is known as holocytochrome b_5 (holo-CYT*b*5), while a protein devoid of heme is known as apocytochrome b_5 (apo-CYT*b*5). Apo-CYT*b*5 has similar structure as holo-CYTb_5 in core 2, but the structure of heme-binding core 1 is less compact and less stable in solution than the holo-CYT*b*5 (Huntley and Strittmatter 1972; Moore and Lecomte 1990). The final CYT*b*5 fold is dependent upon the binding of heme, thus the absence of the heme in the apo-CYT*b*5 results in an unstructured α-bundle, whereas the β-barrel maintains its organized native structure (Falzone *et al.* 2001). Despite the differences, apo-CYT*b*5 largely maintains the secondary structure of the holoprotein (Moore and Lecomte 1990), and it can be a good model for studies where the heme poses an issue or to study effects of heme.

Studies of the apo-CYT*b*5 included determining the structure and stability of the apoprotein itself (Falzone *et al.* 1996), the structural changes that result from heme-binding

(Falzone *et al.* 2001; Mukhopadhyay and Lecomte 2004), and the heme association and dissociation constants (Vergéres *et al.* 1993). The apo-CYT*b*5 is partially disordered without the heme and is refolded upon heme incorporation (Bhattacharya *et al.* 1999). Study by Ihara *et al*. (2000) demonstrated that when the heme is incorporated into the apo-CYT*b*5, the fluctuating His63 loop has a greater affinity for the heme and coordinates the heme before the His39 loop. This suggested that there are more hydrophobic interactions between the His63 loop and the heme than the His39 loop.

In majority of the studies using apo-proteins, the apo-CYT*b*5 serves as the starting material (Landfried *et al.* 2007) for either the reconstitution of heme or replacement of heme with modified prosthetic group, such as isotopically-labelled heme (Rivera and Walker 1995), or protoporphyrin IX containing other metal, for example Mn(III) (Gruenke *et al.* 1997). Experiments on manganese-substituted cytochrome *b*5 originally suggested that the partially disordered apo-CYT*b*5 can fulfill roles in the cell that are unrelated to the heme group, such as stimulation of cytochrome P450, as will be discussed later (Schenkman and Jansson 2003). Kotrbová *et al*. (2009) further showed that the heme is not required for CYT*b*5 to stimulate CYP450 (CYP3A4) using heterologously expressed of the rabbit apo-CYT*b*5 protein in *E. coli*.

3.2: Functions of cytochrome *b*5

Cytochrome b_5 primarily function as a ubiquitous one-electron carrier that transfers electrons, usually from NAD(P)H *via* a reductase to a variety of enzymes that require redox chemistry to perform a broad spectrum of physiological functions (Figure 5). Below are described several of the most well known roles of these proteins. Table 1 provides a complete summary of these and other roles.

3.2.1: Microsomal cytochrome b_5

Microsomal cytochrome b_5 (CYT*b*5A) has been extensively characterized and has been shown to participate in a multitude of biosynthetic and biotransformation reactions, such as plasmalogen biosynthesis, cholesterol biosynthesis, hydroxylation of N-acetyl-neuraminic acid, fatty acid desaturation and stimulation or inhibition of cytochrome P450-dependent microsomal monooxygenase (MMO) reactions. The MMO enzymes are responsible for the oxygenation of hydrophobic endogenous and exogenous compounds, such as fatty acids, steroid hormones, vitamin D_3, xenobiotics, pharmaceuticals, and toxic compounds. The mechanism by which cytochrome b_5 acts on cytochrome P450 depends on the type of P450 isozyme, the type of substrate and the concentration of cytochrome b_5 (Schenkman and Jansson 2003). One proposed mechanism is that CYT*b*5A provides the second (rate limiting) of the two electrons to MMO that is required for reducing diatomic atmospheric oxygen (Vergéres and Waskell 1995). Cytochrome *b*5 can have both a stimulatory and an inhibitory effect on CYP450 and it has no effect on the enzyme if these two opposite effects are equal (Im and Waskell 2011). The effect of CYT*b*5A on CYP450 is dependent upon the molar ratio of CYT*b*5A to CYP450 reductase. At low CYT*b*5A concentrations (molar ratio < 1), CYT*b*5A stimulates monooxygenase activity by increasing the rate of catalysis, which improves reaction efficiency and thus decrease the production of byproducts, such as reactive oxygen species (ROS). At high CYT*b*5A concentration (molar ratio >1), cytochrome *b*5 binds to the CYP450 reductase site on CYP450 which prevents the first electron from being transferred from CYP450 reductase to CYP450 thereby preventing CYP450 reduction and inhibiting enzyme activity. Another proposed mechanism is that CYT*b*5A-cytochrome P450 reductase complex formation

permits two electrons to be transferred to cytochrome P450 in one-step. Lastly, CYT*b*5A can also influence cytochrome P450 activity through allosteric effects that do not involve electron transfer (Schenkman and Jansson 2003).

3.2.2: Mitochondrial cytochrome b_5

In comparison to microsomal cytochrome b_5, there is little known about the cytochrome b_5 of outer mitochondrial membrane (CYT*b*5B). Similar to microsomal cytochrome b_5, CYT*b*5B also interacts with mitochondrial cytochrome P450 either as the transferer of a second electron, or by inducing conformational changes in the P450 enzyme upon formation of the CYT*b*5B-cytochrome P450 complex (Ogishima *et al.* 2003). The mitochondrial monooxygenases specialize in the oxidation of endogenous substrates such as cholesterol, and play a crucial role as stimulators of gonadal steroid (testosterone) synthesis mediated by cytochrome P450-17α (Davydov 2001; Soucy and Luu 2002). CYT*b*5B and its reductase are also involved in detoxification reactions through reduction of N-hydroxylated compounds, such as amidoxime, in association with a molybdenum enzyme, known as mitochondrial amidoxime reducing component (mARC). CYT*b*5B has a role in the reduction of ascorbate radical, semidehydroascorbate, (Ito 1981; Nishino and Ito 1986) and this isoform is overexpressed in bone marrow cells of malignant Hodgkin lymphomas (Murphy *et al.* 2010).

3.2.3: Soluble cytochrome b_5

Soluble cytochrome b_5 in erythrocytes of animals serves as an intermediate electron transfer protein in the NADH-dependent reduction of methemoglobin and methmyoglobin to form hemoglobin and myoglobin, which restores the oxygen-binding activity of these

proteins (Hegesh *et al.* 1986). In protobacterium *Ectothiorhodospira shaposhnikovii*, soluble cytochromes b_5 functions in photosynthetic energy production (Schenkman and Jansson 2003). A unique example of soluble cytochrome b_5 in animals is N-acetylneuraminic acid hydroxylase for the biosynthesis of a type of sialic acid, called N-glycolylneuraminic acid (Kawano *et al*. 1994). This type of sialic acid is not normally found in humans, but makes up 3% of sialic acid in human colon cancer (Takematsu *et al*. 1994).

3.2.4: Multidomain enzymes with cytochrome b_5 modules

Cytochrome b_5 frequently occur as a domain within various fusion enzymes, such as flavocytochrome b_2 (yeast L-lactate dehydrogenase), sulfite oxidase (Guiard and Lederer 1977) and nitrate reductase (Dunn *et al.* 1998). Furthermore, many types of fatty acid desaturases, which introduce *cis*-double bonds into acyl chains, contain a cytochrome b_5 module.

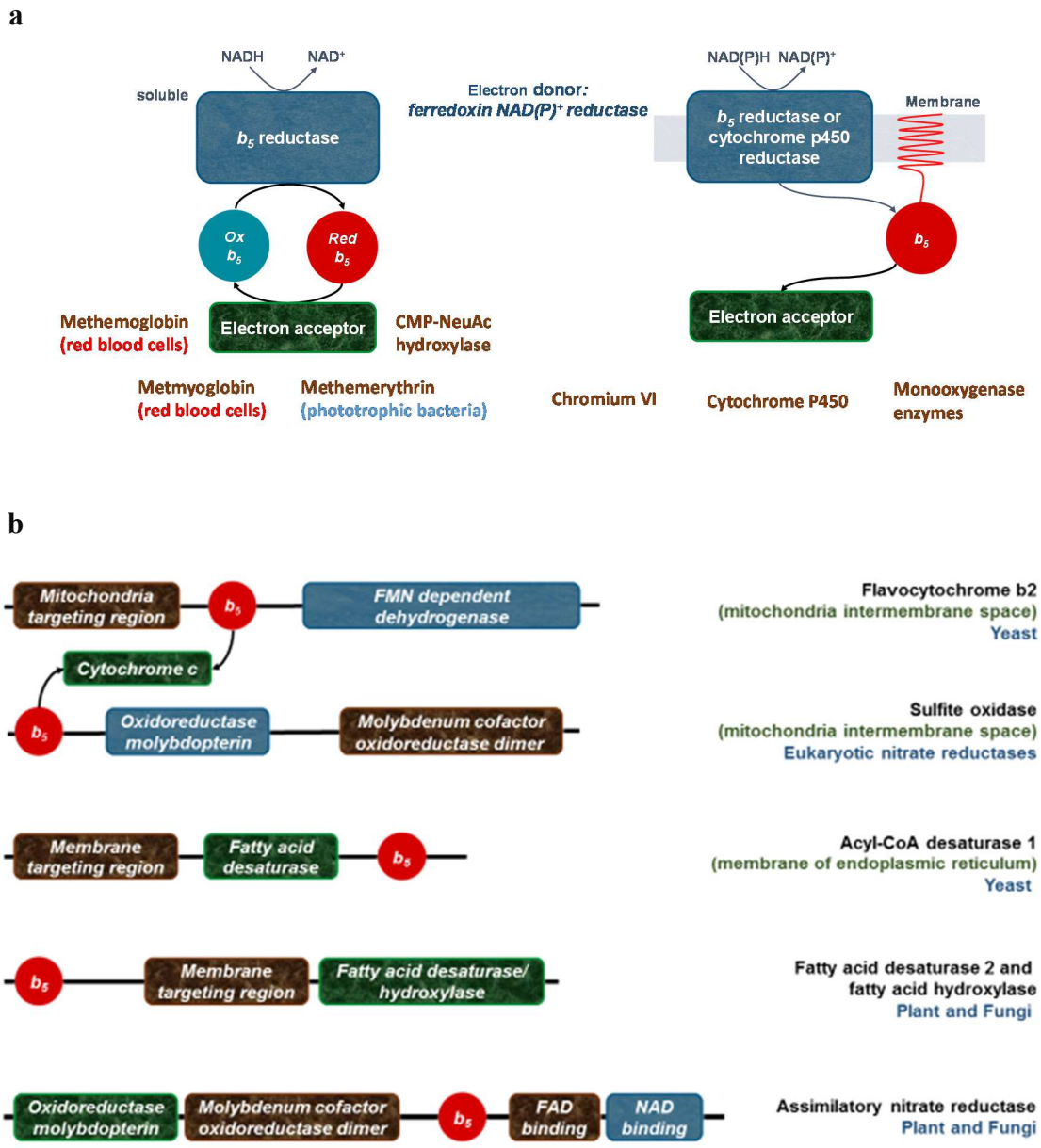

Figure 5: (a) Roles of cytochrome b_5: Soluble (left) and membrane-bound (right) cytochromes *b*5 act as electron shuttles accepting electrons from reductase and donating them to oxygen atom of various oxygenases. However, these reducing and oxidizing partners are not found in gCYT*b*5, thus the protein's role in *Giardia lamblia* is unknown. (b) Cytochrome b_5: as a subunit of other proteins

Table 1. Function of cytochrome b_5 proteins

Function	Electron donor (reductase, R)	Electron acceptor	Role of cytochrome b_5
Microsomal cytochrome b_5 (membrane bound)			
Biosynthesis of plasmalogen	NAD(P)H-b_5 R	plasmenylethanol-amine Δ^1-desaturase	Donates electron to form a double bond into carbons α, β to the ether linkage of the phospholipid to make a vinyl-ether group, which has an antioxidant role
Biosynthesis of cholesterol precursors	NADH-b_5 R	4-Methyl sterol oxidase	Provides electron to 4-methyl sterol oxidase for oxidation of lanosterol methyl group to a steroid -4α-oic acid
		Lathosterol Δ5-desaturase	Forms a double bond in C-30 of lathosterol to make dehydrocholesterol
Cytochrome P450 reduction for functions such as drug metabolism	NADPH-P450 R	P450 (various enzymes)	When b_5 provides the second electron to P450, the catalysis of P450 is enhanced 10-100 fold. However, at high concentrations of b_5, catalysis is inhibited as b_5 competes with P450 reductase binding site for transfer of first electron
Cr(VI) to Cr(III) reduction	NADPH-P450 R	chromium(VI)	b_5 either directly reduces Cr(VI) or it directly reduces Fe(III) to Fe(II) which can reduce Cr(VI) and Cr(V)
Adrenal androgen synthesis regulation mediated by P450	b_5 does not transfer electron directly		b_5 increases product formation through allosteric mechanism resulting in enhanced interaction and electron transfer between NADPH-P450 R and P450 17α/17,20-lyase
Androgen synthesis regulation mediated by 3βHSD	b_5 does not transfer electron directly		b_5 allosterically increases the efficiency of a non-P450 enzyme, 3βHSD, by increasing its affinity for its cofactor NAD^+

Function	Electron donor (reductase, R)	Electron acceptor	Role of cytochrome b_5
Outer mitochondrial cytochrome b_5 (OMb_5)			
Regulation of gonadal steroidogenesis mediated by P450	NADPH-P450 R	P450	OMb_5 may increases 17, 20-lyase activity either through allosteric conformational changes of P450 upon complexing with b_5 or through more efficient transfer of the second electron needed by the P450 enzyme.
Detoxification and drug metabolism through N-reductive pathway	NADH-b_5 R	Mitochondrial amidoxime reducing component (mARC)	*b*5 accepts electrons from b_5-R and passes them via its heme to the Moco of mARC, N-reductive system
Reduction of semidehydroascorbate			mediates the regeneration of ascorbate from the ascorbate radical
Soluble cytochrome b_5			
Reduction of methemoglobin and metmyoglobin in erythrocytes	NADH b_5 oxidoreductase	Methemoglobin and metmyoglobin reductase	Electrons are transferred from NADH-dependent b_5 -R to b_5 which reduces the non-functioning ferric methemoglobin back to its functional oxygen-binding, ferrous form
Biosynthesis of *N*-glycolylneuraminic sialic acid	NADH dependent b_5 and reducing factors in liver cytosol	monooxygenase component of CMP-NeuAc hydroxylase	The monoxygenase component of CMP-*N*-acetylneuraminic acid (CMP-NeuAc) hydroxylase binds CMP-NeuAc and reductively activates oxygen with the electrons it receives from NADH through the *b*5 reductase and *b*5 to produce CPM-N-glycolylneuraminic acid

Function	Electron donor (reductase, R)	Electron acceptor	Role of cytochrome b_5
cytochrome b_5 modules within multidomain enzymes			
Monounsaturated fatty acid desaturation (ER membrane)	NADPH-P450 R desaturases	Stearoyl coenzyme A desaturase	N-terminal component of the stearyl-CoA desaturase, that utilizes oxygen and electrons from reduced b_5 to catalyze double bond insertion into a spectrum of fatty acyl-CoA substrates including palmitoyl-CoA and stearoyl-CoA.
Polyunsaturated fatty acid desaturation (ER membrane)	NADH- b_5 reductase	Fatty acid desaturases	These desaturase use electrons from the b_5 domain to convert a single bond between carbon atoms in a saturated fatty acyl chain to a double bond to make polyunsaturated fatty acid (PUFA)
fatty acid hydroxylase	ceramide very long chain fatty acid	fatty acid components of ceramides	Hydroxylates the very long chain (saturated) fatty acids of sphingolipid and ceramides
Flavocytochrome *b*2 (lactate dehydrogenase (Mitochondria intermembrane)	flavin FMN dependent (flavocytochrome b_2)	cytochrome *c* oxidoreductase (flavocytochrome b_2)	FMN
Sulfite oxidation (Mitochondria intermembrane)	Molybdenum pterin (sulfite oxidase)	Cytochrome *c* (sulfite oxidase)	Sulfite + O_2 + H_2O ↔ sulfate + H_2O_2. Molybdenum cofactor
Nitrate reduction (plant and fungi)	NADH dependent FAD (nitrate reductase)	Molybdenum pterin (nitrate reductase)	Accepts electrons from duroquinol (NADH to FAD) and transfers them to molybdopterin, which transfers the electron to nitrate to reduce it to nitrite NH_3+2H_2O+ 6 O ferredoxin↔NO_3+6 R ferredoxin + 7H^+

Cytochrome b_5 reductase (b_5 R), cytochrome P450 reductase (P450 R), 3βhydroxysteroid dehydrogenase (3βHSD)

4: *Recombinant Proteins*

Because of the universality of the genetic code, recombinant DNA technology can be used to overexpress a protein of interest in *E. coli*, encoded by a gene from a different organism. One consideration in recombinant protein expression is the control of this process to optimize expression levels. In the widely used pET series of expression vectors, transcription of the target gene is controlled by engineering the vector such that it has components derived from both bacteria (the *lac* repressor system), and bacteriophage (phage T7 RNA polymerase). In pET vectors, the T7 promotor region is upstream of the target gene to be expressed. This region is recognized by the T7 RNA polymerase, which is encoded by a gene that is incorporated into the lysogenized host bacteria's genome by the T7 phage during infection to promote the propagation of the viral proteins. *E. coli* strains that are lysogens of bacteriophage λDE3 carry the T7 RNA polymerase gene under transcriptional control of the *lac* operator. The pET system uses this gene to regulate transcription of the gene for the recombinant protein of interest, once its expression has been activated by the addition of a lactose analog, IPTG, to the bacterial culture. The high levels of T7 polymerase and its specificity for its promoter drive overexpression of the protein of interest encoded on the pET vector.

The pET14b vector specifically carries an N-terminal His-Tag sequence, which is used to purify the recombinant protein using affinity chromatography. This vector also encodes a thrombin site that can be used to cleave the tag off following purification.

5: *UV-Visible Spectroscopy of heme proteins*

Ultraviolet-visible spectroscopy is electronic spectroscopy that records the absorption of UV and visible light radiation in the electromagnetic spectrum by a chromophore. This absorption of the electromagnetic radiation at specific wavelengths arises from electronic transitions in a molecule due to excitation of an electron from a lower energy state to a higher energy state (Holler *et al.* 2007). The energy required for various electronic transitions differs according to the strength of a chemical bond and thus depends on the molecular structure of compound being analyzed (Figure 6). The UV region (180 to 400 nm) corresponds to higher energy transitions than the visible region, which absorbs from 400 nm to 780 nm. Aromatic compounds absorb at 280 nm due to $\pi \rightarrow \pi^*$ transitions of electrons in aromatic ring. Most proteins contain the aromatic amino acids phenylalanine, tryptophan, and tyrosine and thus will absorb near 280 nm. Heme proteins such as cytochrome b_5 have additional characteristic UV/Visible spectra resulting from the presence of this cofactor. The heme is composed of a porphyrin ring, which is aromatic in nature and thus has extensive delocalization of π-orbital electrons. These $\pi \rightarrow \pi^*$ transitions in porphyrin ring result in an intense Soret (γ) band and weaker alpha (α) and beta (β) bands observed in the visible region. The position of these absorbance bands is sensitive to oxidation, coordination and spin state of the heme iron, and the local heme environment.

Heme can be quantified by UV-visible spectroscopy. When treated with alkaline pyridine, heme proteins are unfolded and the free heme forms a complex with pyridine. The reduced heme-pyridine complex has an extinction coefficient of 32.4 $mM^{-1}cm^{-1}$ (Paul *et al.* 1953). This provides a means to measure the fraction of purified protein that has heme bound to it, as the heme content of heme proteins is often substoichiometric.

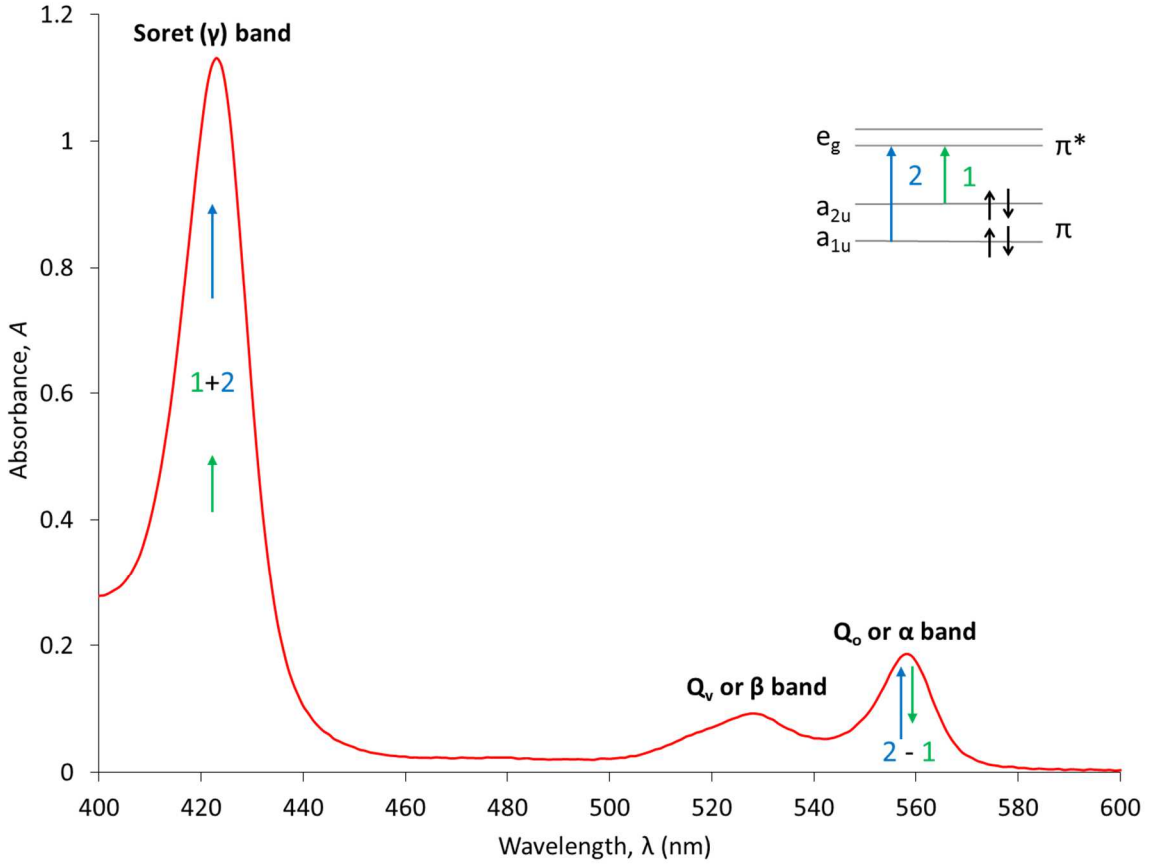

Figure 6: Visible region of a UV-Visible spectra of Giardia cytochrome *b*$_5$.
The excitation of an electron from a lower energy state to a higher energy state results in absorption bands at certain wavelengths. The delocalization of π-orbital electrons in porphyrin ring of the heme results in a Soret (γ, 420 nm), an alpha (α, 560 nm) and a beta (β, 530 nm) band.

6: *Electron transfer in biological systems*

Electron transfer, or the act of moving an electron from one molecule to another, is central to most biochemical pathways, including photosynthesis and oxidative phosphorylation (Kennepohl and Solomon 2003). Consequently, there has been considerable research dedicated to understanding the fundamental principles surrounding the process of adding and removing electrons from chemical species, especially biological redox centers such as cytochromes.

There are three types of oxidation-reduction reactions observed in biological systems (Gary and Ellis 1994). The first type involves redox reactions of protein side chains, such as the oxidation of two cysteine residues to form a disulfide bond. The second case involves variety of redox-active organic molecules. These include the nicotinamide adenine dinucleotide cofactors (NAD^+, $NADP^+$) that transfer electrons in pairs, and the flavins (FMN, FAD) and quinones (coenzyme Q) that transfer electrons singly or in pairs. The third type of biological electron transfer uses redox-active metals such as iron (Fe) or copper (Cu). Such metalloproteins can act as electron shuttles (cytochrome b_5, cytochrome *c*, ferredoxins), transporters of O_2 (hemoglobin, hemocyanin) and as redox catalysts (monooxygenases and dioxygenases).

Electron transfer between two redox-active transition metal coordination complexes can be classified into two main types of reaction mechanisms (Fenton 2008). The inner sphere electron transfer mechanism proceeds though a bridged intermediate in which a ligand with two lone pairs is transitorily shared between the coordination spheres of the reactants. The bridging ligand is directly bonded to the inner coordination sphere of both metal complexes and the electrons are transferred from one sphere to another. In many

reactions, the transfer of electrons is also associated with transfer of bridging ligand group from oxidant to reductant.

Currently, there are no known inner sphere electron transfer reactions that involve a pair of metalloproteins (Fenton 2008). The redox active sites in metalloproteins are often buried within bulky proteins that present an intense steric barrier to the formation of a transition state where the bridging ligand needs to bind directly to the coordination spheres of two redox centres. Inner sphere reactions cannot occur without the formation of this intermediate and thus we have not encountered such mechanism in biological systems. In addition, this mechanism requires the electron to reside on the ligand for a short time, leading to formation of ligand radical.

In the outer sphere mechanism, the coordination spheres of the oxidant and reductant remain intact during electron transfer without any exchange of ligands. In this reaction, the outer or solvent coordination sphere of the metal centre is involved in transferring electrons (Roat-Malone 2007). The simplest (and fastest) electron transfer reactions are outer sphere, because the reaction proceeds without any bond breakage or reformation.

Outer sphere electron transfer occurs most often in biology and can be classified as intramolecular and intermolecular (Fenton 2008). Intramolecular electron transfer occurs at fixed sites within a single protein, whereas an intermolecular electron transfer occurs between sites on different proteins (Scott *et al*. 1985). The intermolecular electron transfer leads to the electron-transfer chains, where a series of consecutive electron-transfer reactions occur between pairs of proteins. In these reactions, electrons are transferred between metal sites that are arranged either within a protein or within a complex of

proteins. These electrons may need to travel distances of up to 30 Å at reasonable rates (>10 sec^{-1}) through intervening peptides for long-range electron transfer.

An intermolecular reaction between two different species consists of several steps, which starts with the two redox partners approaching one another and forming a precursor complex.

$$A_{ox} + B_{red} \leftrightarrow [A_{ox}B_{red}] \rightarrow [A_{red}B_{ox}] \leftrightarrow A_{red} + B_{ox} \quad \textbf{(1)}$$

where $[A_{ox}B_{red}]$ and $[A_{red}B_{ox}]$ are the precursor and successor complexes, respectively. A simplified case of the above that is useful in explaining electron transfer rates is electron self-exchange, in which the donor and acceptor are the same molecule, differing only in oxidation state. In an efficient self-exchange intramolecular electron transfer reaction, the energies of donor and acceptor orbitals, bond length and bond angle do not change (Roat-Malone 2007).

$$A_{ox} + A_{red} \rightarrow A_{red^*} + A_{ox^*} \quad (2)$$

These rates of outer sphere electron transfer reactions, including those of metalloproteins are often consistent with a theory proposed by Rudolph Marcus (Marcus and Suttin 1985). According to Marcus theory, the rate constant of reaction (k_{21}) between two species correlates with equilibrium constant for the electron transfer reaction K and the electron self-exchange rate constants of the reactants (k_{11} and k_{22}) as follows:

$$(k_{21})^2 = k_{11} \bullet k_{22} \bullet K \bullet f \quad (3)$$

where $f \sim 1$, $k_{11}.k_{22}$ represents the intrinsic barrier to electron transfer and K is the measure of overall free energy $\Delta G°$of the reaction, which can be determined by measurement of the electrochemical driving force (reduction potential) of the reaction. The correlation between second order rate constants predicted by this theory and those obtained experimentally are

usually in agreement for small inorganic electron complexes, and many electron transfer proteins as well. One prediction made by Marcus theory is that each electron transfer reaction will have an optimal driving force. Interestingly, if the free energy of this reaction is more favorable than this optimal driving force then the rate of reaction decreases rather than increases. This inverted region has been observed in experiments for both metalloproteins and small molecule reactions .

Rapid electron transfer rates and partner selectivity are critically dependent on the structure of the redox protein (Adman 1979). One of the most influential factors is the distance between electron transfer sites, with the electron transfer rate decreasing exponentially with increasing distance between sites. In general this leads to the observation that rapid electron transfer is limited to intersite distances of 10 Å or less. Other factors that influence electron transfer rates include the nature of the intervening media and the orientation of donor and acceptor sites (Vergères and Waskell 1995). These factors can cause the electron transfer rates of different types of electron transfer protein to vary by many orders of magnitude (Lippard and Berg 1994).

The oxidation-state dependent conformational differences in protein structure are also important in the determining electron transfer rates. As the equilibrium conformations of the oxidized and reduced states are usually different, the Franck-Condon principle has two implications for biological electron transfer. First, that conformational changes must occur prior to electron transfer; second, that electron transfer rates are fast when these conformational differences are small (Roat-Malone 2007). It has been observed that for most electron transfer metalloproteins the conformational differences between oxidized and reduced states are slight (Adman 1979).

An electron transfer protein is also structured so that it is stable in its environment, is able to recognize its specific electron transfer partners, and tunes its reduction potential to provide the required driving force (Adman 1979). The stability of the protein results from its overall structure that is resistant to proteolysis, unfolding, and is compatible with membrane or cellular fluids. Selectivity towards electron transfer partners is determined by surface complementarity between the sites of contact, for example by complementary charge interactions of surface residues. The tuning of the redox potential of the metal is shaped by its protein environment. For heme proteins, this includes the type of axial ligands and the polarity of the heme binding pocket, with a polar environment favoring the oxidized state (Fe^{3+}; +1 net charge on heme) over the reduced state (Fe^{2+}; 0 net charge on heme).

7: *Electrochemistry*

Cytochrome *b*5 is an electron transport protein, and the tendency of the protein to either accept or release electrons and thereby be reduced or oxidized is measured through its reduction-oxidation (redox) potential. Redox potentials are determined using electrochemical techniques, where electrical quantities, such as potential or current, are manipulated then measured and related to chemical parameters of a system.

Dynamic electrochemical techniques are used to monitor the transfer of electrons across the interface between an electrode (electronic) and electrolyte solution (ionic) during a redox half-reaction of an electroactive species, A:

$$A^{+}_{Oxidized} + e^{-} \leftrightarrow A_{Reduced} \quad (4)$$

This half-reaction at the electrode will occur when the conditions are thermodynamically or kinetically favorable to promote the transfer of electrons from or to the working

electrode. The relationship between the concentration of electroactive species and Gibb's free energy change (ΔG, J.mol-1) for an equilibrium reaction is as follows

$$\boldsymbol{\Delta G = \Delta G^{\circ} + (RT) ln \frac{[oxidized]}{[reduced]}} \quad (5)$$

where ΔG° is standard Gibb's free energy change ($J.mol^{-1}$), R is the universal gas constant (8.314 $J.K^{-1}mol^{-1}$) and T is absolute temperature in Kelvin (K). Gibb's free energy change of the oxidation-reduction equilibrium is related directly to the cell potential as follows:

$$\boldsymbol{\Delta G = -nFE} \quad (6)$$

where n is the number of electrons transferred in the reaction, E is the electrode potential (volts, V), and F is the is the charge on a mole of electron or Faraday constant (96 487 Coulombs). Under standard state conditions with the reactants and products having unit activity, this equation can be written as:

$$\boldsymbol{\Delta G^{\circ} = -nFE^{\circ}} \quad (7)$$

where E° is the standard electrode potential in Volts or millivolts. The standard reduction potential corresponds to the electrical potential at which the concentrations of oxidized and reduced states of the redox-active molecule are equivalent. According to equation 7, in order for the reaction to be spontaneous (a negative free energy change) in the direction written, the cell potential must be positive.

A thermodynamically favorable electrochemical reaction occurs when a change in applied electrode potential results in a reversible, kinetically fast electron exchange. If the electron transfer reaction is favorable, then the potential of the electrode is related to the concentration of the electroactive species at the surface of the electrode, according to the Nernst equation (8):

$$\boldsymbol{E = E^{\circ} + \left(\frac{RT}{nF}\right) ln \frac{[oxidized]}{[reduced]}} \quad (8)$$

Potential is a measure of the energy that is available to drive a charge and is measured in units of volts, where 1 V = 1 joules/coulombs (J/C). Since potential is a relative term, the applied potential cannot be measured directly and requires the establishment of a reference point. In a potentiostatic measurement, this is accomplished by using a two-electrode system of a working and a reference electrode. The working electrode is where the redox process occurs while the reference electrode maintains a constant potential under different experimental conditions. The potential is measured as the energy difference between these two electrodes.

In theory, any stable electrochemical reaction with a well-known potential can be used as a reference electrode. The internationally accepted reference electrode is the standard/normal hydrogen electrode (SHE or NHE) consisting of a platinum wire in 1 M HCl solution, in equilibrium with H_2 gas and an assigned potential of 0 V. While conceptually useful, this electrode is cumbersome in practice and is not typically used in experiments. Instead, the silver-silver chloride electrode (Ag/AgCl/KCl, $E°$=197 mV *vs* SHE) or the saturated calomel electrode, or SCE (Hg/Hg_2Cl_2/KCl, $E°$=242 mV vs SHE) are used. Both are compact, inexpensive, and stable.

By convention, redox half-reactions are written as reduction. Thus, a positive redox potential indicates that the half reaction has a greater tendency to accept electron and be reduced, relative to the SHE. Conversely, a negative reduction potential indicates that the analyte prefers the oxidized state and tends to donate electrons as compared to SHE. As the applied potential of a working electrode is made more positive, electrons flow from the analyte (oxidation) to the electrode (reduction), which results in an oxidation current. A

more negative potential applied to the working electrode results in a flow of electrons from this electrode to the analyte and produces a reduction current.

For a simple electron transfer, the pathway of the electrode reaction involves (1) the mass transport of electroactive species to the electrode surface, (2) the electron transfer across the interface and (3) the transfer of products back to bulk solution. For a Nernstian reaction, the electroactive species can undergo a kinetically fast electron transfer, such that rate of reaction is controlled only by the rate at which that electroactive species reaches the electrode surface (Wang 2000). That is, Nernstian reversible reactions are limited only by mass transport to the electrode surface.

Mass transport to the electrode occurs by three different modes: diffusion, convection and migration. Diffusion is a spontaneous movement of electroactive species from regions of high concentration to regions lower concentration in response to a concentration gradient (Wang 2000). Migration is the movement of charged electroactive species in response to an electrical field created by the electrode. Convection occurs when electroactive species are transported to the electrode by bulk physical movement, such as stirring of solution and rotation or vibration of electrode (Wang 2000).

Another fundamental concept of electrochemistry at electrode-solution interface is the electrical double layer. The double layer is a formation of around 10 nm of charged zone at the electrode-solution interface that counteracts the excess charge at the electrode (Wang 2000). The counter layer is made of ions with charge opposite to the electrode such that the overall charge at the interface is neutral. For example, a negative electrode attracts a layer of positive ions in the solution adjacent to the electrode (Figure 7). This double layer creates a surface potential that decreases as one moves away from the electrode.

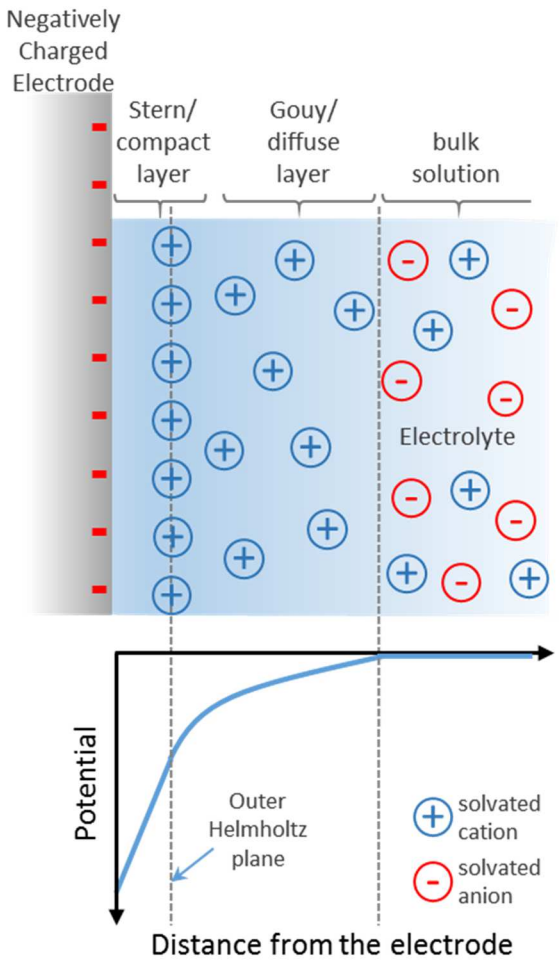

Figure 7: The potential-distance profile across the electrical double layer.
The formation of double layer results in a surface potential between the electrode and electrolyte. This potential decreases linearly in the Stern layer from the electrode to the outer Helmholtz plane and exponentially in the diffuse layer until it approaches zero at the bulk solution.

7.1: Cyclic voltammetry

Cyclic voltammetry (CV) is the most commonly used technique to determine reduction potentials of redox complexes, including many proteins. This technique involves varying the applied potential of the working electrode in a linear manner with a potentiostat, while the current that results from electron transfer between electrode and protein is monitored using an ammeter. The potential acts as an electron pressure that forces the protein to gain or lose an electron, and the current shows the rate at which electrons move across the electrode-solution interface (Wang 2000).

The current resulting from the change in oxidation state of the electroactive species follows Faraday's Law (reaction of n moles of substance results in a change of n x F coulombs) and is a direct measure of the rate of the redox reaction (Wang 2000). A cyclic voltammogram is a plot of current signal versus the excitation potential whose shape and magnitude varies with the technique used in electrode reaction (Wang 2000).

A sample cyclic voltammetry waveform and voltammogram for one-electron reversible reaction is shown in Figure 8 and 9, respectively. This experiment begins with the protein in the oxidized state and the potential of the working electrode positive relative to the reduction potential of the protein (Rafferty 1992). Since no electrochemical reaction occurs at this potential, there is no current flow observed (a). As the applied potential is lowered in a linear manner, it approaches the reduction potential of the protein, and some of the protein near the electrode gets reduced. The transfer of electrons from the electrode to the oxidized protein results in a cathodic current (i_c) flow (b) and the concentration of oxidized protein decreases according to Nernst equation. At an applied potential equal to the $E°'$ of the protein, the ratio of oxidized to reduced protein is equal to one. When the

applied potential is just past the reduction potential, more protein is reduced around the working electrode and the cathodic current increases rapidly until all the protein near the working electrode is reduced (c). At this point the cathodic current is at a maximum and a peak current at I_{pc} and potential at E_{pc} forms. Beyond this point, further reduction of protein is limited by diffusion of oxidized protein to the electrode from the bulk solution, and as a result, the current drops to 'diffusion limited current' (d).

When the scan direction is switched to positive potential for the reverse scan, initially there is little current observed because the applied potential is too negative to induce re-oxidation. As the potential approaches the reduction potential, the protein that was reduced in the forward scan is now re-oxidized and an anodic current (I_c) is observed (f). When the applied potential passes the reduction potential of the protein, all the protein near the electrode is oxidized (g) and the current peaks (I_{pa}) at the peak anodic potential (E_{pa}). The current then decays as oxidation is limited by diffusion and eventually drops to 0 when no electrochemical reaction occur.

The reduction potential can be calculated from the position of the anodic and cathodic peak potential:

$$\boldsymbol{E^{\circ}} = \frac{\boldsymbol{E_{pa}} + \boldsymbol{E_{pc}}}{\mathbf{2}} \tag{9}$$

For a symmetrical cyclic volammogram the electrochemical reaction between the protein and electrode must be rapid and reversible. An electrochemically reversible reaction occurs when the protein can undergo a fast electron transfer in response to the change of potential at the electrode surface such that the Nernst equation is followed. If this is the case, then the Faradaic current depends only on the rate of mass transfer to the electrode surface. Cyclic voltammetry experiments are set such that only diffusion is involved in mass

transport (Rafferty 1992). Convection is avoided by not stirring the solution during the reaction and migration is prevented by using supporting electrolytes in solution.

Cyclic voltammetry usually uses a three-electrode system to avoid current passing through the reference electrode, which would otherwise alter its composition and potential (Wang 2000). In a three-electrode system, a counter electrode is include along with the working and reference electrodes so that the current passes only between the first two while the applied potential remains constant between the reference and the working electrodes. An inert metal, such as platinum is most often used as the counter electrode.

The measured current in a cyclic voltammogram is a combination of both the faradaic current, due to transfer of electrons between the protein and the working electrode, and the non-faradaic background current. The non-faradaic current results from charging of the electric double layer that occurs when a potential is applied across it.

In cyclic voltammetry, the direct transfer of electrons between the electrode surface and metalloprotein is made possible through modification of the electrode surface. Prior to the 1980s, direct voltammetric studies of redox proteins was not possible due to adsorption and denaturation of proteins at the electrode surface, and, in some cases unfavorable electrostatic repulsion between protein and electrode (Wu and Hu 2007). Surface modifications of the electrode surface make the electrode more hydrophilic and promote interaction between the active site of protein and the electrode. Such surface modifiers themselves are not redox-active. Surface use functional groups capable of hydrogen bonding and favorable electrostatic interactions to reversibly bind the protein on the electrode surface in an orientation suitable for electron transfer. For example, when a monolayer of bipyridine is adsorbed on an electrode, the bipyridine molecules hydrogen

bond to the lysine residues near the active site of the protein. This results in protein being held close to the protein in an orientation that promotes rapid electron transfer (Lippard and Berg 1994). A drawback of these modifications is that these functional groups may interact with the redox centre and possibly alter the electrochemical potential of the protein (Aono *et al.* 2010). Surface modifications, while essential for electrodes such as gold electrode, is not required for indium tin oxide which will be used in this study.

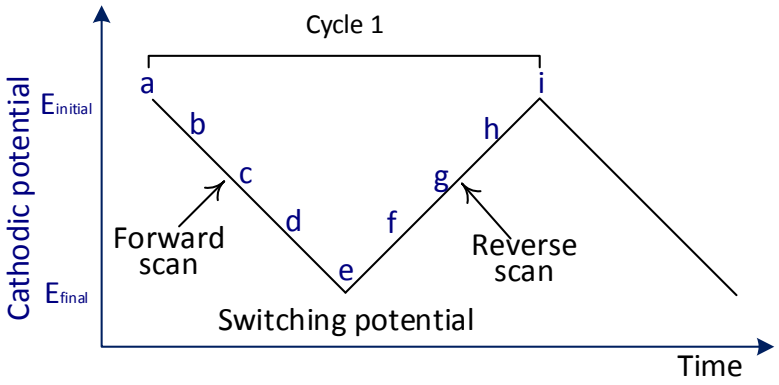

Figure 8: A cyclic voltammetry potential excitation signal with switching potentials

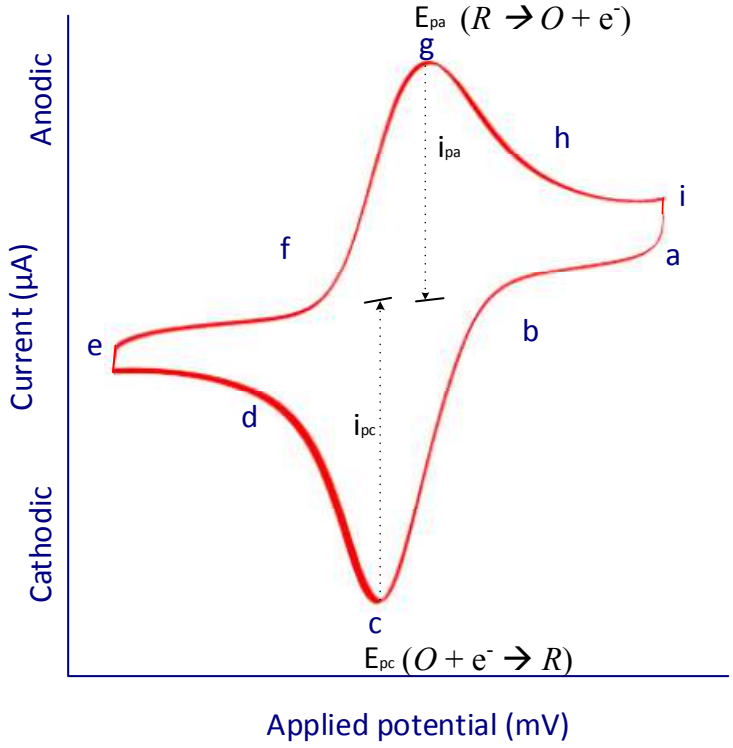

Figure 9: Cyclic voltammogram showing the current response to the potential excitation signal in Figure 8. The i_{pc} and i_{pa} refer to peak cathodic and ionic current, respectively, while E_{pc} and E_{pc} refer to the applied potential corresponding to the respective peak current.

7.2: Spectroelectrochemistry

Voltammetric techniques determine reduction potentials using electrical parameter of current flow as a function of potential and are excellent for electrochemical measurements, but provide limited structural information (Wang 2000) Spectroelectrochemistry (SEC) goes beyond that as it combines reaction-oriented electrochemistry with species-focused spectroscopy allowing the measurement of both electrical and physical properties of an electroactive species simultaneously (Bard and Faulkner 2001). Integration of UV-Visible spectroscopy with electrochemistry is one such classical technique. Since the oxidized and reduced species of cytochrome b_5 have sufficiently different spectra in UV-Visible region, this is an ideal technique to measure its reduction potential.

In UV-Vis spectroelectrochemistry, a potentiostat controls the cell potential of the electrochemical cell through the working electrode, while the resulting change in absorbance due to the ratio of the oxidized and reduced states of the protein are measured spectrophotometrically. As the potential is changed, this ratio is altered, with detectable changes in the spectrum. A Nernst plot of applied potential versus the logarithm of the ratio of oxidized to reduced states, derived from the spectrophotometric changes, yields the reduction potential of the protein.

As working electrode is in the light path of the spectrophotometer, it must be transparent as well as electrically conductive. Such optically transparent electrodes (OTE) allows partial transmission of light through their surface and solution. Mini-grid electrodes are a type of OTE that consist of thin wires of a chemically inert metal, such as platinum or gold, woven into a micromesh containing small holes (10-30 μM) to allow partial light

transmission. Commercially available honeycomb electrodes are an improvement of the mini-grid electrodes where the electrode is a ceramic substrate with channels (125 μm) whose interior walls are coated with metal (gold or platinum). These electrodes have a longer path length (1.7 mm) and give larger absorbance, which allows sensitive monitoring of weakly absorbing species. These also include a counter electrode patterned onto the ceramic support, which eliminates the need for separate counter electrode. These electrodes are inserted into a thin layer quartz cell, which is optically transparent. The cell consisting of electroactive species, reference electrode and working electrode are placed in spectrophotometer (Figure 10).

One issue that arises with protein electrochemistry at electrode surfaces is that heme proteins usually have their redox site buried deep within them. In this situation, proteins will not readily transfer electrons with a metal electrode even under favorable conditions due to steric and electrostatic effects, so that the attainment of equilibrium at each applied potential becomes impractically slow (Bard and Faulkner 2001). In spectroelectrochemistry this is counteracted by using small inorganic mediators, which are redox-active molecules that shuttle electrons between the electrodes and the protein. Mediators hasten the attainment of equilibrium between the electrode and the protein, which allows determination of redox potential of proteins using this technique on a reasonable time scale of several hours for a complete experiment (Wang 2000).

Ideally, mediators should not absorb light in the same wavelength range of the protein. For rapid electron transfer their reduction potential should be known and be close to the anticipated potential of protein of interest, and they should not react with the protein in a way that alters the reduction potential of the protein. In addition, these mediators

should have stable oxidized and reduced forms, fast electron transfer and should be soluble at the pH of electrochemical cell.

Unlike cyclic voltammetry, in spectroelectrochemistry there is typically no *direct* electron transfer between the electrode surface and the protein, as it is the mediators shuttle electrons between the two. It is important to note here that the reduction potential of the same protein obtained using different methods are not always identical. This is because interactions between the protein and surface modifiers used in cyclic voltammetry may affect its reduction potential (Bott 1999).

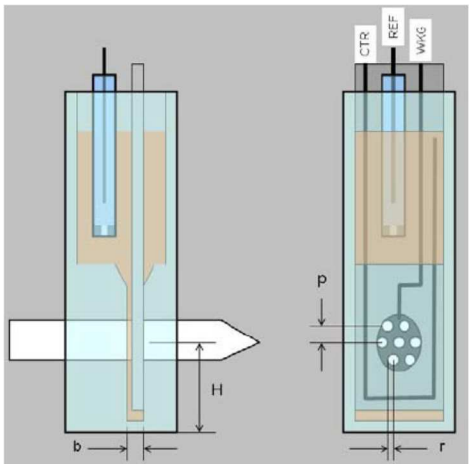

Figure 10: An electrochemical cell with a honeycomb electrode in a quartz slotted cell used in spectroelectrochemistry. The working (WKG) and counter (CTR) electrodes are integrated into a ceramic plate, while the gel reference (REF) electrode is inserted separately. The dimension of path length (b) is ~1.7 mm, the hole radius of channels (r) is ~125 μm and the standard beam height (H) is 15 mm. This diagram is obtained from Pine Research Instrumentation spectroelectrochemistry kit manual (2012).

8: *Electrochemical properties of cytochrome b_5*

The reduction potential of mammalian cytochromes b_5 varies over a wide range of nearly 120 mV (Table 2). This variation is not only observed between cytochromes b_5 from different organisms, but even within the same species when isolated from different cell types (mitosomal vs. mitochondrial). These potentials also differ depending upon the type of experiment used to determine the potential (Aono *et al.* 2010), temperature (Reid *et al.* 1982) and ionic strength (Rivera *et al.* 1994).

The earliest reported reduction potential measurements for cytochrome b_5 were done on the microsomal protein isolated from rabbit, which has a potential of +13 mV (Iyanagi 1977; all potentials relative to the SHE). In comparison the reduction potential of rat mitochondrial cytochrome b_5, is -102 mV (Rivera *et al.* 1994).

Many factors influence the reduction potentials of cytochromes, including the identity of the axial ligands, the orientation of the ligands relative to the heme plane, the dielectric constant of the medium surrounding the heme, and steric effects on the heme (Qian *et al.* 2002). Since all cytochromes b_5 share the same porphyrin prosthetic group (Lee *et al.* 1991) and are coordinated non-covalently by the same histidine axial ligands (Reedy and Gibney 2004), the differences in their reduction potential must result from the heme's interaction with the protein chain. These factors include the orientation of the heme within the protein (Walker *et al.* 1988), the hydrophobicity of the heme environment (Mauk and Moore 1997), the electrostatic potential contributed by surface charges (Qian *et al.* 2002), accessibility of the heme to solvent (Paoli *et al.* 2002) and steric constraints resulting in distortion of heme (Olea *et al.* 2010).

Table 2. Reduction potentials of mammalian cytochromes b_5

Source organism	Potential (mV vs SHE)	Type of electrochemistry	Electrode modification/ Promoters/Mediators	References
Trypsin-digested microsomal cytochrome b_5 (hepatic)				
rabbit	**13**	direct potentiometry with dithionite	toluidine blue (2 μM) indigodisulfonate (2 μM)	Iyanagi 1977
bovine	**5.1±0.1**	SEC gold (500-line/in) OTTLE	$Ru(NH_3)_6^{2+/3+}$ (12 μM)	Reid *et al.* 1982
bovine	**-1.9±1.6**	SEC gold minigrid (100-line/in) OTTLE	$Ru(NH_3)_6^{2+/3+}$ (0.2 mM) $K_3Fe(CN)_6$ (0.2 mM) methyl viologen (1 mM)	Walker *et al.* 1988
bovine (recombinant)	**3±0.1**	SEC electroformed gold (500-line/in) OTTLE	$Ru(NH_3)_6^{2+/3+}$ (12 μM)	Funk *et al.* 1990
bovine (recombinant)	**0±2**	CV gold electrode	β-mercaptopropionic acid modified 0.2 mM $Cr(NH_3)_6^{3+}$	Rivera *et al.* 1994
bovine (recombinant)	**2**	SEC gold minigrid (400-line/in) OTTLE	$Ru(NH_3)_6^{2+/3+}$ (10 μM)	Yao *et al.* 1997
bovine (recombinant)	**-10±3**	DPV gold disk electrode (2 mm)	cysteine modified No promoters	Xue *et al.* 1999
bovine (recombinant)	**-1.2 ±3 10.7±3***	DPV gold electrode	cysteine modified *4 mM Mg^{2+}	Qian *et al.* 2002
bovine (recombinant)	**5.5±1.8**	redox potentiometry with dithionite and ferricyanide	1 μM of 16 mediators**	Parthasarathy *et al.* 2011
rat	**5±1**	spectrophotometrically by periodic exposures to xenon arc lamp (1-5 s)	methylene blue (5 μM) indigodisulfonate (2 μM) dithionite crystals	Martinis *et al.* 1989
rat	**-7±1**	DPV gold electrode	cysteine modified	Rodgers and Silgar 1991
rat (recombinant)	**1.3±0.7**	redox potentiometry with dithionite(4 mM) and ferricyanide (1 mM)	1 μM of 16 mediators**	Parthasarathy *et al.* 2011
recombinant outer mitochondrial membrane cytochrome b_5				
rat	**-102±2**	SEC gold minigrid 200 wires/inch OTTLE	$Ru(NH_3)_6^{2+/3+}$ (0.4 mM) methyl viologen (1 mM)	Rivera *et al.* 1994
rat	**-78[a] -43[b] -8[c] 8d**	CV gold electrode 1-mm	modified with β-mercaptopropionic acid [a]0.2 mM $Cr(NH_3)_6^{3+}$	Rivera *et al.* 1994
rat	**-102**	SEC	0.30 mM $[Ru(NH_3)_6]Cl_3$,	Rivera *et al.* 1998

Source organism	Potential (mV vs SHE)	Type of electrochemistry	Electrode modification/ Promoters/Mediators	References
	-70[e] **-40**[f]	gold minigrid (200 wires/in)	1.41 mM methyl viologen polylysine	
rat	**-72**[e] **-63**[f]	CV 1 mm diameter gold disk	modified with β-mercaptopropionic acid	Rivera *et al.* 1998
rat	**-27**	CV glassy carbon electrode	modified with a thin film of the cationic surfactant DDAB at 22°C	
rat	**-102**	SEC platinum-foil working electrode	200 μM $[Ru(NH_3)_6]Cl_3$ 25 μM 2,5-dihydroxy-*p*-benzoquinone and 25 μM anthraquinone-2,6-disulfonate	Wirtz *et al.* 2000
rat	**-43**[b] **-26**[c,d]	CV with indium-doped tin oxide (ITO) semiconductor films electrode	poly-L-lysine	Wirtz *et al.* 2000
human testis (synthetic gene)	**-40**	SEC titrations with dithionite gold Electrode	25 μM of 9 mediators* 100 μM of $[Ru(NH_3)_6]Cl_3$ and methyl viologen	Altuve *et al.* 2004
rat	**-54.8±1.3**	redox potentiometry with dithionite(4 mM) and ferricyanide (1 mM)	1 μM of 16 mediators**	Parthasarathy *et al.* 2011
human	**-53.8±1.2**			
Erythrocyte soluble cytochrome b_5				
human	**-2**	redox potentiometry with dithionite and ferricyanide Platinum/Silver chloride	1 μM methylene blue and 0.1 μM thionine, indigodisulphonate, and indigotetrasulphonate	Abe and Sugita 1979
human (recombinant)	**-9±2**	direct electrochemistry gold electrode	modified with the peptide KCTCCA	Lloyd *et al.* 1994
human (recombinant)	**4±1**	redox potentiometry with dithionite and ferricyanide	1 μM of 16 mediators**	Parthasarathy *et al.* 2011

SEC= spectroelectrochemistry
CV= cyclic voltammetry
DPV= differential pulse voltammetry
Poly-L-lysine/b_5 = [b]0.5, [c]1.0, [d]2.0
Poly-L-lysine MW = [e]3970, [f]9000
* and **: duroquinone, 1,2-naphthoquinone, 5,8-dihydroxy-1,4-naphthoquinone, 2-hydroxy-1,4-naphthoquinone, 2,5-dihydroxy-1-4 benzoquinone, 9,10-anthraquinone-2,6-disulfonic acid
*only: anthraquinone-1,5-disulfonic acid, Toluylene blue, pentaaminechlororuthenium (III) chloride
** only: 5- hydroxyl-1,4-naphthoquinone, 1,4-naphthoquinone, 2,6-dimethylbenzoquinone, 2-methyl-1,4-benzoquinone, anthraquinone-2-sulfonic acid, 1,2-naphthoquinone-4- sulfonic acid, pyocyanin, phenazine methosulfate, benzyl viologen

9: *Electrospray mass spectrometry (ESI-MS)*

Electrospray (ES) is the dispersion of a liquid into small charged droplets by electrostatic fields. Electrospray ionization (ESI) is a technique that uses electrospray to ionize intact large molecules, such as proteins. Using ESI as an ionization source in mass spectrometry (MS) generates multiply-charged ($z>>1$) ions. Multiple charging of ions enables the mass to charge (*m/z*) ratios of large molecules to be small enough for molecular weight detection by limited *m/z* range mass analyzers (Konermann *et al.* 2012).

An electrospray ionization mass spectrometer is composed of three main components: an ESI source, a mass analyzer, and a detector. The analyte is introduced into the electrospray ionization source where intact protonated or deprotonated molecules are produced. These molecules pass through several compartments that are connected through skimmers, focusing lenses and multipoles from the ionization source at atmospheric pressure to the mass analyzer at vacuum ($\sim 10^{-6}$ Torr). Once the ionized analytes reach the mass analyzer they are sorted and separated according to their mass to charge ratio, *m/z*. In a tandem mass spectrometer selected ions may be fragmented and further analyzed before they are detected. The detector then measures the abundance of ions at each *m/z* ratio, which is then transmitted to a data-processing system that produces a mass spectrum.

9.1: Electrospray ionization source

Electrospray ionization is a complex process that can be divided into two main phases, the formation of charged droplets and formation of gas-phase ions. The formation of charged droplets is based on aerosol science and, because it is a much older technique, its mechanisms are well understood. Whereas, the mechanism of how gas-phased ions are produced from the charged droplets is not very clear and several theories exist on this topic.

9.1.1: Formation of charged droplets

In electrospray ionization, an analyte sample is mixed in a suitable polar solvent, such as water, methanol, acetonitrile or dimethylsulfoxide, and is pumped into either a metallic capillary tube or a hypodermic needle. An electrospray is produced under atmospheric pressure, by applying a strong electric field (10^6 Vm^{-1}) to the sample passing through the capillary in a continuous stream at the flow rate of 1 to 10 $\mu Lmin^{-1}$. The electric field is generated by applying high voltage of around 2 to 6 kV at the capillary tube relative to the counter electrode located 0.3 to 2.0 cm from the tip of the capillary tube. A gas, mostly dry nitrogen, is injected coaxially at low flow rates around the capillary to allow the dispersion of the flow to be limited in space for better nebulization and to direct the spray towards the mass spectrometer.

This electrostatic field results in an electrochemical reaction at the metal/solution interface between the solvent and the capillary causing an electron flow to or from the capillary. In the positive-ion mode, an oxidation of solvent occurs, ions are charged *via* protonation of the analyte and a protonated molecule $(M+nH)^{n+}$ is detected; while in the negative ion mode a reduction of the solvent occurs, the ions are charged via deprotonation of the analyte and deprotonated molecule $(M-nH)^{n-}$ is detected. These redox reactions provide either positive (added protons) or negative (abstracted protons), droplets in solution depending on the capillary electrode polarity. The high voltage capillary repels these ions and thus accumulation of a net positive or a net negative charge occur at the surface of the liquid sample that emerges from the end of the capillary tip. The pressure from the accumulation of like-charges at the tip in the strong electric field causes the emerging sample to form a meniscus and then elongate to a point that the surface tension

of the solvent breaks to form a 'Taylor cone' from which a mist of highly-charged droplets emerge (Figure 11, Wu *et al.* 2012).

The effluent from the Taylor cone emerges as a fine spray of charged droplets, with radii about a micrometer, into a chamber that is at atmospheric pressure. These droplets experience Coulombic repulsion forces between the like charges on the surface and are thus driven away from each other. The solvent is rapidly evaporated from the charged droplets through a heated capillary or through the flow of counter-current dry gas, such as nitrogen, in the direction opposite to the passage of the droplets (Figure 12). As the solvent evaporates, the droplets shrink and the ions within them move closer together increasing the charge per unit volume. The droplet size decreases until it reaches the Rayleigh limit where the repelling Coulombic forces between the ions overcome the liquid surface tension and results in a jet fission or Coulombic explosion. The explosion disintegrates the parent droplet into smaller, highly charged progeny droplets. The progeny droplets shrink further by solvent evaporation, and continue to undergo cascade of these explosions until the highly charged, solvent-free analyte droplets are produced with radii of only a few nanometers (Banerjee and Mazumdar 2012 and Hoffman and Stroobant 2007).

9.1.2: Formation of gas-phase ions

The mechanism of gas-phase ion production from small highly charged liquid droplets is still not very well understood. There have been several hypothesis based on experimental observations, but no model is unambiguously accepted. Most researchers in the field of ESI tend to agree with one of the two proposed mechanisms, the charge residue model (CRM) for globular molecules and the ion evaporation model (IEM) for low molecular weight analytes. In the CRM, the solvent evaporation from the droplets leads to

several Coulombic explosions that ultimately produce small droplets of 1-nm radius containing one analyte molecule that retains the droplets' surface charge and becomes an ion (Dole 1968). The IEM also presumes the CRM scenario of producing small highly charged droplets by solvent evaporation and Coulombic explosion, but it does not require that the droplet size be reduced until it only has one analyte molecule (Iribarne and Thomson 1976). Alternatively, it uses the fact that as the solvent evaporates the charge density on the surface of the droplet increases, producing a strong electric field. Eventually, the combination of a small radius of curvature (R<10 nm) and a high charge density at the droplet's surface results in an electric field that is strong enough to overcome the solvation forces holding the ion to the droplet and subsequently pull the ion from the surface into the ambient gas. There is a newer proposed charged ejection model (CEM) that postulates that the hydrophobic nature of unfolded proteins or disordered polymer chains makes the interior of droplet unfavorable for them (Konermann *et al.* 2013). This causes these polymers to immediately migrate towards the surface of the charged droplet, until they are sequentially ejected from the droplet into the vapor phase. A cartoon summary of the process is presented in Figure 13.

Z-spray and orthogonal spray sources are modifications of the ion trajectories from the linear ESI source that prevent clogging of heated capillary tubes and skimmers due to non-volatile material and neutral molecules.

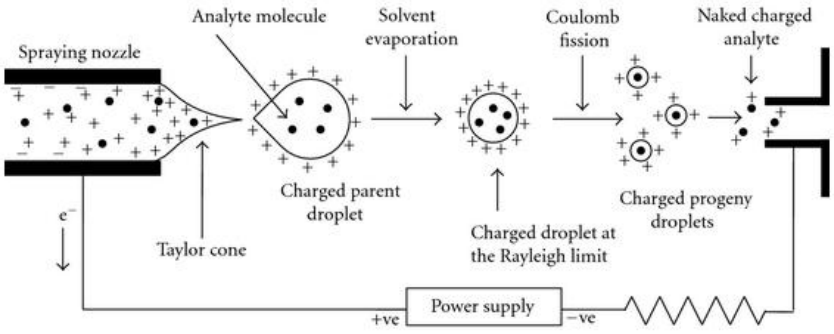

Figure 11: Diagram of the steps involved in creation of charged analyte in electrospray ionization source operated in positive ion mode. Image is reproduced from Banerjee and Mazumdar (2012)

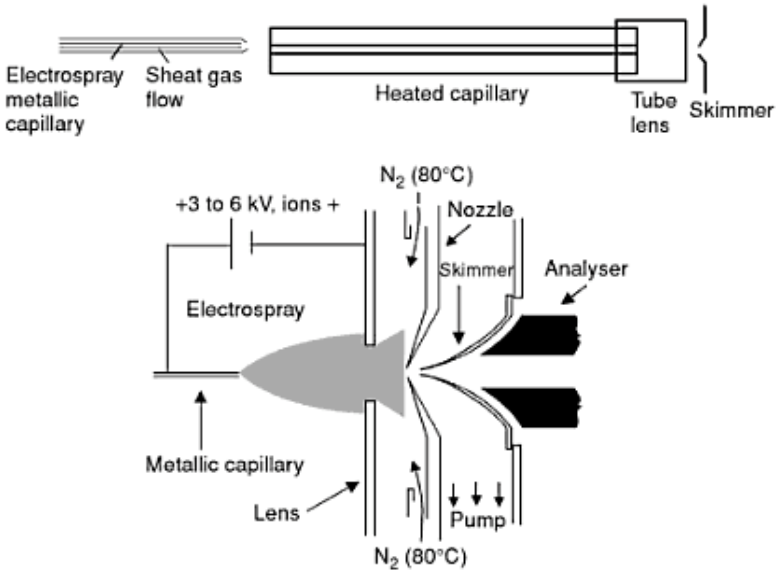

Figure 12. Illustration of electrospray ionization sources (a) the top ESI uses a heated capillary for desolvation, while **(b)** the bottom ESI uses heated nitrogen gas for desolvation. (Reprinted from Hoffman and Stroobant 2007)

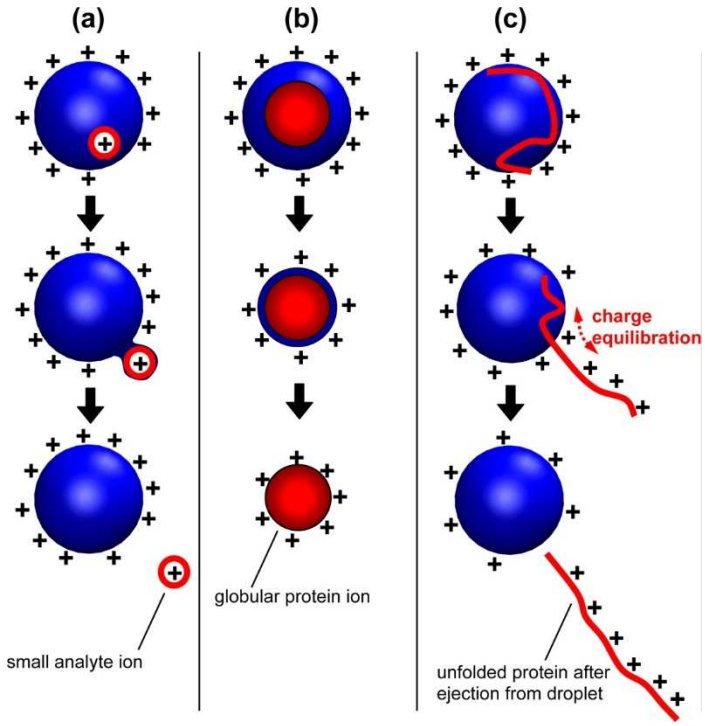

Figure 13: Summary of mechanisms of formation of gas phase ions from the charged droplets (a) IEM: small ion ejection from a charged droplet. **(b)** CRM: release of a globular protein into the gas phase. **(c)** CEM: ejection of an unfolded protein. (Reprinted from Konermann *et al.* 2012)

9.2: Mass analyzers

Electrospray ionization source can be coupled to different types of mass analyzers for protein analysis. These include quadrupole mass filter, ion trap, and time-of-flight (TOF) mass analyzers. The type of mass analyzer chosen depends on the type of application and its requirement for mass range, detection limit, sensitivity, resolution, and scan rate.

The most common mass analyzer coupled to an ESI source is quadrupole mass filter because it is easy to interface it with a high-pressure source and also because the limited mass range disadvantage associated with a quadrupole instrument is overcome by multiple charging of an electrospray ion. A quadrupole is a mass filter that separates ions by means of a time-varying oscillating electric field generated between four metal rods, which only allow ions with a desirable *m/z* ratio to have a stable trajectory and reach the detector. Most quadrupole MS used for protein analysis are triple quadrupole instruments that are made up of three sections: a mass separating quadrupole, where precursor ions of a specific *m/z* are selected; a central quadrupole or multipole cell, where ions are fragmented in the presence of an inert gas by collision-induced dissociation (CID); a final quadrupole mass filter, where the fragmented product ions are scanned or separated.

Quadrupole mass spectrometers have a mass accuracy of 0.1 to 1 Daltons (Da), and are relatively inexpensive and easy to use. A triple quadrupole MS can isolate a peptide and obtain a mass spectrum of fragments in multiple scan modes. However, quadrupoles do have a low unit mass resolution and this is why the triple quadrupole is often accompanied with a time of flight analyzer, where the separation section of the third quadrupole is replaced with a TOF. This instrument provides combines the high mass accuracy of a quadrupole with the high resolution of a TOF analyzer.

9.3: Detectors

Once the ion passes through the mass analyzer it is then detected and transformed into signals by a detector. Detectors generate an electric current from the incident ions that is proportional its abundance. There are several different types of detectors that are available and the type of detector chosen depends on the application and the instrument for which it will be used.

The electron multiplier (EM) is an ion detector in which the ions from the analyzer are accelerated to high velocities using a high-voltage conversion dynode. The dynodes have a high potential that are opposite to the charge on the detected ion. Thus, when an ion, electron or neutron hits the conversion dynode it causes the emission of electrons from the outer layers of the striking atom. The number of secondary electrons released varies based on the type, energy and angle of the incident particle as well as the characteristic of incident surface. These emitted electrons are then amplified in the electron multiplier by a cascade effect to produce an electronic current. This current, when applied to a resistance, produces a voltage that is fed through an analog-to-digital converter to obtain the ion abundance. There are many different types of electron multipliers, such as discrete dynode, continuous dynode, channel plate, microchannel plate and multichannel plate.

9.4: ESI-MS spectra

When a pure protein is analyzed on an ESI, all peaks in the ESI mass spectrum represent the intact molecular species with variable charging, such that between a minimum and maximum number of charges per ion, every possible charge state is present in the mass spectrum. The mass spectrum has a sequence of peaks, and each peak differs from the adjacent peak by one charge, as shown in Figure 14. The distribution of peaks has a similar

pattern to a Boltzman distribution and the number of charge states increases with increasing molecular weight of sample analyzed, with the maximum allowed charge state, n_{max} equal to 0.077 $MW^{1/2}$). In addition, to the molecular ion peaks there are also solvent peaks.

The molecular mass of a species can be determined from an ESI spectrum through software provided with the instrument that uses mathematical algorithms based on charge deconvolution theory. This calculates the molecular weight from each multiply-charged ion, and then averages these values across all charged states. This leads to mass accuracies of ± 0.01% or a one Da error at a molecular weight of 10 000 Da, even on mass spectrometers with modest mass resolving capabilities (Aebersold and Mann 2003).

Electrospray mass spectrometry can rapidly determine an accurate mass of a protein, which is very useful for their identification. It has been used to differentiate molecules of similar mass that could not be differentiated by other methods. One example is of human hemoglobin, where there are many variants of β-chain polypeptide, mostly due to a single amino acid substitutions resulting from single base substitution in the DNA coding sequence. ESI-MS is able to identify many of these variants based on molecular weight information (Lacan *et al.* 2005).

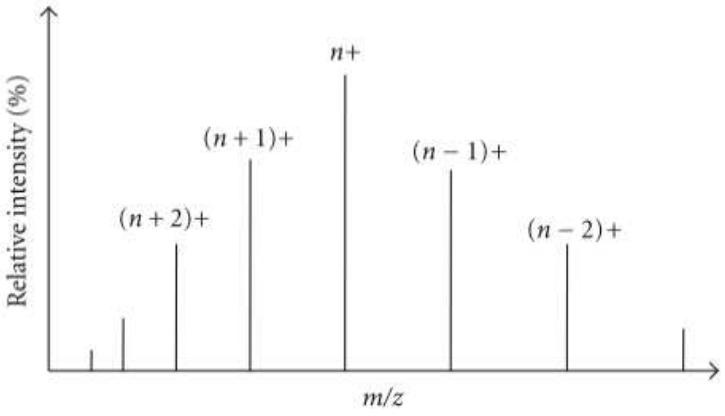

Figure 14: A sketch of a theoretical ESI-MS mass spectrum in positive mode (Reprinted from Banerjee and Mazumdar 2012).

10: *Research objectives*

The main objective of this research was to determine whether the *Giardia lamblia* cytochrome b_5 gene encodes a functional protein and if so, to characterize some of its basic properties and suggest possible roles for it. In brief, the cytochrome b_5 coding region was amplified from Giardia genomic DNA and cloned into an *E. coli* expression vector from which recombinant protein was expressed. Giardia cytochrome b_5 was expressed with heme bound to it, has spectroscopic characteristics similar to other b_5-type cytochromes, and has an unusually low reduction potential. Moreover, homology modelling of the protein provides some information on the likely structure of this protein in the active site and the reason for this low reduction potential. This research is a significant step towards identifying the roles of heme proteins in an organism that was long thought to lack such proteins.

MATERIALS AND METHODS

1: *Homology modelling*

Swiss Model (Arnold *et al.* 2006) was used to generate homology structures of the cytochrome b_5 sequence from *Giardia lamblia* assemblage A isolate WB: gCYTb_5-I (UniprotKB: A8B968). For the initial modelling trials, no input sequence was specified for the template from which the model structures were obtained; these trials identified the heme domain of *Saccharomyces* flavocytochrome b_2 (1kbi.pdb) as a template for gCYTb_5-I. In subsequent trials, the cytochrome b_5 domain of CYB5R4 was specified as the template for modelling. Structural figures were prepared using MacPyMOL (Delano Scientific). Secondary structure predictions of the non-conserved flanking sequences were performed with the program GOR4 (Combet *et al.* 2000). Isoelectric points were estimated from protein sequences with the program ProteinParam (Gasteiger *et al.* 2005).

2: *Cloning of the full length Giardia cytochrome b_5 gene*

Two primers (Appendix I) were designed for PCR-amplification of the coding sequence for Giardia cytochrome b_5 gene (Gene ID: GL50803_9089) based on the genomic DNA sequences of *Giardia lamblia* (GiardiaDB). The forward primer possessed a *NdeI* restriction enzyme site (underlined), extra nucleotides (lower case) and initiation codon (bold):

5' gtagaa <u>CAT **ATG**</u> AGT GAA CAT CAT GGT CGC CCA TCT GG 3'

The reverse primer possessed a *BamHI* restriction enzyme site (underlined), extra nucleotides (lower case) and termination codon (bold):

5' tagaat <u>GGA TCC</u> **TTA** GGC CGG CGA CCC TCT TCT AAG 3'.

PCR conditions for this amplification are given in Appendix. The PCR product was blunt-end cloned into the vector pJET1.2 (Fermentas). The blunting reaction consisted of 245 ng of PCR product, 1μL DNA blunting enzyme, 2X reaction buffer and nuclease-free water for a total reaction volume of 20 μL (Appendix III). The mixture was vortexed briefly, centrifuged for 5 seconds, incubated at 70°C for 5 minutes and then briefly chilled on ice. The ligation reaction was set up such that 1 μL of T4 DNA ligase and 82.5 ng of pJET1.2/blunt cloning vector was added to the blunting reaction mixture. This mixture was vortexed briefly, centrifuged for 5 seconds and then incubated at 22°C for 30 minutes.

The ligation product was transformed into electrocompetent *E. coli* strains (either DH5α or JM109). For each transformation a 100 μL aliquot of ice-cold competent cells was placed in a pre-chilled 0.2 cm-gap electroporation cuvette, followed by ~10 ng of ligation product. Electroporation was performed with the following settings: voltage, 2.5 kV; resistance, 129 Ohm; capacitance, 50 μFarads. The resulting pulse time was between 4 and 5 milliseconds. After electroporation, each the cells were immediately transferred to 400 μL of LB in a 15 mL culture tubes. This culture was incubated at 37°C with shaking for 1 hour. 250 μL of culture was spread onto a LB plate with 0.1 mg/mL of ampicillin. The plates were incubated at 37°C overnight.

Transformants bearing the desired insert were identified by colony PCR screening. Four colonies from each plate were picked and cultured in a microfuge tube with 50 μL of LB broth at 37°C for 1 hour. A master plate was also prepared with the same selected colonies and incubated overnight at 37°C. PCR screenings were performed by preparing a master mix consisting of 0.25 μM Cyto*b*5 forward and reverse primers, 100mM dNTPs, 1 unit of Taq polymerase (Bioshop), 2 mM $MgCl_2$ and 1x Taq Buffer. 49 μL of master mix

was placed in each PCR tube and 1 µL of bacterial culture was added to each tube to obtain a final PCR volume of 50 µL. Once the PCR reaction was completed, 15 µL of each reaction was checked on 1.2% agarose gel.

One clone that was positive in the PCR screening was picked from the master plate and inoculated into 10 mL of LB containing 0.1 mg/mL Ampicillin. The culture was incubated at 37°C for 16 hours in a 100-mL Erlenmeyer flask. The overnight culture was used to prepare a glycerol stock by combining 500 µL of culture with 500 µL of 50% glycerol. The bacterial cells were harvested in a 15 mL tube by centrifugation at 4000 x *g* for 10 minutes at 4°C. All traces of the supernatant were removed from the bacterial cell pellet. The recombinant plasmid DNA was isolated by Plasmid DNA purification using QIAprep Spin Miniprep Kit Microfuge protocol by Qiagen. The plasmid was eluted in 50 µL EB buffer. The initial restriction enzyme digestion of the expression vector clones was performed to verify the presence of insert of the expected size.

Cloning vector pJET1.2-gCYTb_5-I was digested for three hours in a 40 µL reaction mixture containing 10 µg of vector, 40 units each of *NdeI* and *BamH1*, and 4 µL of 10X *BamH1* buffer. After the digestion, 3 µL of product was electrophoresed on a 1.2% agarose gel to ensure that the digestion was complete and the gCYTb_5-I-coding insert had been released. Once this had been verified the rest of the digest was electrophoresed under identical conditions. The gel was stained with ethidium bromide and DNA bands were observed under UV-transillumination. The 420 bp band corresponding to the gCYTb_5-I insert was cut out from the gel using a utility knife. The coding insert was extracted from the gel using a QIAquick gel extraction kit and was eluted in 50 µL of 10mM Tris-HCl, pH 8.5.

3: *Preparation of the expression vector pET14b-gCYTb5-I*

To prepare the host vector, 4.75 µg of pET14b vector (Appendix II) was digested with 30 units of *NdeI* in a 70 µL reaction mixture at 37°C for 2 hours, followed by digestion with 30 units of *BamH1* and a further 10 units of *NdeI* for 3 hrs**.** The digest was heat inactivated at 65°C for 20 minutes. A small portion of the product was electrophoresed in 0.8% agarose gel alongside uncut pET14b to check that the digestion was complete. A second preparatory scale gel was used to purify the balance of the cut vector, which was extracted from the gel slices with a Qiagen QIAquick gel extraction kit. The vector was eluted with 30 µL of 10 mM Tris-HCl, pH 8.5 buffer.

The linearized pET14b was dephosphorylated to remove phosphate groups from 5' end of the DNA to prevent self-ligation of residual vector that had been cut with only one enzyme. A 50 µL reaction mixture was made with 8 ng/µL of double digested pET14b, 1 unit of shrimp alkaline phosphatase and 5 µL 10X shrimp alkaline phosphatase buffer. The reaction was incubated at 37°C for 60 minutes followed by enzyme inactivation at 65°C for 20 minutes.

To ligate the gCYTb_5-I insert to the doubly-digested vector, 12.3 fmol of cut vector was combined with gCYTb_5-I insert at 1:0 (control), 1:5 and 1:10 vector to insert ratios. The total reaction volume for each ligation was 25 µL and contained of 4µL 1x ligation buffer and 320 units of T4 DNA ligase. The ligation reaction was incubate at 22°C for 1 hour followed by 16°C overnight.

The 3 µL of each ligation reaction was added to 50 µL of commercially prepared competent *E. coli* strain DH5α cells thawed on ice. The mixture was incubated on ice for 30 minutes, heat shocked at 42°C for 30 seconds, followed by incubation on ice for 5

minutes. The cells were added to 950 µL of SOC medium and culture outgrowth occurred at 37°C with shaking at 220 rpm for 1 hour. 100 µL and 200 µL of each culture spread onto warm LB plate with 0.1 mg/mL of ampicillin. These plates were then incubated at 37°C overnight. From these plates 24 colonies were selected for PCR screening as described above. The forward primer used for PCR screening were a primer corresponding to the T7 promoter region of the pET14b vector. The gCYTb_5-I//BamHI-1b primer was used as the reverse primer. PCR reactions were screened by running 15 µL of reaction product on a 1.2% agarose gel. A total of 11 clones bearing the desired insert were obtained. Of these, four clones were selected for plasmid preparation and storage as frozen glycerol stocks. Glycerol stocks were prepared from 500 µL freshly saturated overnight culture and 500 µL of 50% glycerol followed by storage at -80°C. The bacterial cells were harvested in 15 mL Falcon tubes by centrifugation at 4000 *g*. Plasmid DNA was isolated by Plasmid DNA purification using QIAprep Spin Miniprep Kit Microfuge protocol by Qiagen. The plasmid was eluted in 50 µL ml 10mM Tris-HCl buffer.

Restriction enzyme digestion of the expression vector was performed to ensure that the insert of the expected size were present in selected clones. The double digestion consisted of 500 ng of pET14-gCYTb_5-I, 14 units of NdeI and BamH1, 2µL of 10x NEB2 Buffer to a final volume of 20 µL. A second digest was done with to linearize the vector with BamH1 alone. Double digested, linearized and uncut vector were all electrophoresed on a 1.2% agarose. One of the positive clones with the correct sized insert and vector was selected for DNA sequencing with the T7 forward primer at Natural Resources DNA Profiling and Forensic Centre (Trent University, Peterborough, ON; ABI3730 DNA Analyzer).

4: *Preparation of truncated cytochrome b_5 inserts*

There were three truncated versions of cytochrome b_5 prepared over the course of this project: core heme-binding domain gCYT*b*5-1$_{(32-107)}$ (with both N and C-terminal truncations), N-terminal truncated gCYT*b*5-1$_{(32-131)}$ and C-terminal truncated gCYT*b*5-1$_{(1-107)}$ (Appendix V, VI, VII). The primer set for the PCR amplification of each version is shown below:

Core heme-binding domain gCYTb_5-1(32-107)
forward: 5'ggcattgg CATATG TAC ACG GCT AAT CAG GTT TAT GAG CAT CGT 3'
reverse: 5'tagact GGATCC TTA TCC CTG AAG CAT TCC TAT GTG CAA GGG 3'

N-terminal truncated gCYTb_5(32-131)
forward:5' ggcattgg CATATG TAC ACG GCT AAT CAG GTT TAT GAG CAT CGT 3'
reverse: 5' agatac GGATCC TTA cGC gGG CGA CCC TCT TCT AA 3'

C-terminal truncated gCYTb_5(1-107)
forward: 5' tagcattag CAT ATG AGT GAA CAC CAC GGT CGC CCA TCT 3'
reverse: 5' tagact GGATCC TTA TCC CTG AAG CAT TCC TAT GTG CAA GGG 3'

The pET14b-gCYTb_5-I$_{(1-131)}$ plasmid was used as the template for the PCR amplification of these expression vectors (Appendix VIII). The PCR products were electrophoresed on a 1.2% agarose gel and imaged under UV light. The DNA bands on the gel corresponding to gCYTb_5-I insert were extracted using QIAquick Gel Extraction Kit (Qiagen) and was eluted in 20 µL of EB buffer. Each purified PCR products (1 µg) was digested with *Nde* I and *Bam* HI 37ºC for 3 hours, enzymes were heat inactivated at 65°C for 20 minutes and kept at 25ºC for 15 minutes. The digested product was purified using the QIAquick PCR Purification Kit (Qiagen) according to the manufacturer's instructions and eluted in 50 µl of EB. These truncated inserts were ligated into the *Nde* I and *Bam* HI sites within dephosphorylated pET14b to produce the expression vector pET14b-gCYTb_5-I$_{(32-107)}$, pET14b-gCYTb_5-I$_{(32-131)}$ and pET14b-gCYTb_5-I$_{(1-107)}$. The protocol for the

subsequent expression and purification was similar to that described for the full length protein. The truncated protein sequencing was done at MOBIX at McMaster University, Hamilton, ON.

5: *Expression and purification of recombinant gCYTb$_5$-I*

The expression vector pET14b-gCYT*b$_5$*-I was transformed into electrocompetent BL21(DE3) cells. For each transformation 100 µL aliquot of thawed, iced-cold competent cells was placed in an electroporation cuvette and 2 µL of 5 ng/µL vector was added to this cuvette. Electroporation conditions were set as described in section 2: and transformants were immediately transferred to 400 µL of LB media in a 15 mL culture tube. This culture was incubated at 37^{o}C with shaking for 1 hour. Of the cell suspension, 50 µL and 100 µL were spread onto a LB plate with 0.1 mg/mL of ampicillin and incubated at 37°C overnight.

To test different expression conditions and their effect on protein yield, small-scale expressions (250 mL) were done. One propagated colony was picked with an autoclaved toothpick and cultivated in 2 mL LB broth with 0.1 mg/mL of ampicillin at 37°C for 18 hours. The overnight culture was harvested by microcentrifuging 1 mL of culture in a microfuge tube at 12 000 rpm for 1 minute. The recovered pellets were resuspended in 500 µL of Terrific broth and inoculated into 50 mL Terrific broth with 0.l mg/mL ampicillin in a 250 mL flask. One flask was incubated for 48 hours at 30°C. Another flask other was grown at 37°C until an OD_{600} of 0.5-1.0 was reached, at which point protein expression was induced with 1mM IPTG followed by incubation at 30°C overnight. The cultures were harvested by centrifugation at 16 200*g* for 20 minutes, and if the pellet was red then a large-scale culture (>1L) was made of the selected clone.

For large-scale preparations, transformation was performed as described above. A single colony was selected from a freshly prepared plate and inoculated in 5 mL of LB broth with 0.1 mg/mL Ampicillin. The inoculum was incubated at 37°C overnight with shaking at 220 rpm. A glycerol stock was made by microcentrifuging 1 mL of the overnight culture, resuspending the pellet in 500 µL of LB broth and 500 µL of 50% glycerol and storing the stock at -80°C.

The remaining 4 mL of saturated small scale culture was microcentrifuged in four microfuge tubes, the supernatant was decanted and each pellet was resuspended in 1 mL of Terrific Broth. Each 1 mL suspension was used to inoculate a 2-liter culture flask containing 400 mL Terrific Broth with 0.1 mg/mL of Ampicillin, which was then incubated at 30°C for 48 hours without IPTG induction. The cells were harvested by centrifugation at 5000 *g* for 15 minutes. The supernatant was decanted and the cell pellets were stored at -80 °C for future use. Overexpression of the cytochrome was indicated by a ruby-red cell pellet.

To purify the protein, cell pellets were thawed at room temperature, weighed, and resuspended in 4 volumes (v/w) of Thermo Scientific Pierce B-Per Reagent with 100 µg/ml of lysozyme, 1 mM TCEP (reducing agent), and 1 mM each of the protease inhibitors PMSF and captopril. The cell suspension was incubated for 15 minutes at room temperature, then centrifuged at 15 000 *g* for 15 minutes to separate soluble proteins (including the cytochrome) from the insoluble proteins and cell debris, and the supernatant was stored for purification. If the pellet obtained after lysis and centrifugation were still pink it was re-extracted by with 10 mL of B-PER Reagent and lysozyme (100 µg/mL). The supernatants were combined and applied to a 5 mL His-Pur column charged with Co^{2+}

(Thermo Scientific Pierce) for isolation of the polyhistidine-tagged cytochrome. The column was prepared with 50 mL of equilibration buffer (50 mM sodium phosphate, 300 mM sodium chloride, 1 mM imidazole; pH 7.4) at a flow rate of 5 mL per minute, delivered by a peristaltic pump. The protein supernatant was mixed 1:1 with equilibration buffer, and applied to the column at a flow rate of 1 mL per minute such that total volume loaded did not exceed 200 mg of protein. Cytochrome was detected as a pinkish-red band at the top of column. After loading, the column was washed with 25 mL of equilibration buffer, followed by 50 mL of wash buffer (50 mM sodium phosphate, 300 mM sodium chloride, 10 mM imidazole; pH 7.4) at flow rate of 5 mL per minute. The protein was eluted with 50 mL elution buffer (50 mM sodium phosphate, 300 mM sodium chloride, 500 mM imidazole; pH 7.4) at flow rate of 1 mL per minute.

5.1: SDS-PAGE for qualitative assessment of purity and molecular weight

Protein sample for SDS-PAGE were prepared by mixing 2.5 µL of 10X sample loading buffer with 25 µL of the respective protein fractions, heating the sample at 90 °C for 5 minutes and microcentrifugation for 1 minute. 20 µL of each fraction loaded on an 14% SDS-PAGE gel (prepared in lab) with the New England Biolab's (NEB) 10 to 250 kDa protein ladder. Electrophoresis was done in 1x Tris-Glycine buffer in a vertical gel box at 150 V for 1 hour. The gel was stained with Coomassie Brilliant Blue dye using a microwave protocol and was destained overnight in destaining solution containing ethanol, water and acetic acid (5:5:1).

6: *Size exclusion chromatography*

Size exclusion chromatography (SEC) was performed on a Superdex™ 200 (GE Life Sciences) 10 x 300 mm high resolution gel filtration column run on a Varian Prostar high performance liquid chromatography (HPLC) system. The molecular weight standards used for column calibration consisted of the following proteins: thyroglobulin (Mr 670,000), bovine gamma globulin (Mr 158,000), chicken ovalbumin (Mr 44,000), equine myoglobin (Mr 17,000), and vitamin B12 (Mr 1,350) (Bio-Rad Gel Filtration Standard).

7: *Mass spectrometry*

Mass spectrometry was performed on a Quattro™ LC-MS/MS triple-stage quadrupole mass spectrometer (Waters/Micromass) with a hexapole collision cell and an electrospray (Z-spray) atmospheric pressure ionisation (API) source. The MassLynx NT™ software system was used to control the instrument, acquire data and analyze results. The experiments were performed under the supervision of Dr. Ray March at the Water Quality centre, Trent University, Peterborough, ON, Canada.

For ESI-MS analysis, the full-length gCYTb_5-I was desalted using a chromatography column composed of 5 mL of Bio-Gel® P-6DG desalting gel in a 1.0 x 10 cm Econo-Column®. Once desalted, the protein was concentrated and exchanged into 20 mM ammonium acetate buffer (pH 7) using an Amicon Ultrafiltration unit with a molecular weight cut-off of 10 kDa.

The desalted gCYTb_5 was mixed 1:1 with methanol to a concentration of 50 µM and was injected into the probe by direct infusion at 10 µL min-1 using a model 11 syringe pump (Harvard Apparatus). The sample from the infusion pump entered through the electrospray metallic capillary, which was set at a voltage of 3.5 kV, and was converted to

an electrospray. The source block temperature was 80°C, while the desolvation gas heater, which was used to heat nitrogen gas to evaporate methanol from sample, was set at 60° C. The voltages for sample cone and extraction lens cone were 100 V and 4 V, respectively. The mass range of *m/z* 1200–2500 was recorded with unit mass resolution in both negative and positive ion mode. The cone was optimized for maximum sensitivity by varying the cone voltage from 40 to 160 V.

8: *Spectroscopic Analysis of Cytochrome b_5*

8.1: UV-visible spectroscopy of Giardia Cytochrome *b_5*

The oxidized and reduced spectra for cytochrome b_5 were obtained by using a Cary 400 Bio UV-visible spectrophotometer. The baseline was recorded by scanning 50 mM sodium phosphate buffer (pH 7.4) in a 1 mL quartz cuvette from 700 nm to 200 nm. Cytochrome *b*5 was added to cuvette and an oxidized spectrum was recorded. Then, a few milligrams of sodium dithionite was added to the sample cuvette and reduced spectrum was obtained. Sodium dithionite reduction has the following half reaction:

$$2\ SO_3^{2-} + 2\ H_2O + 2\ e^- \rightarrow S_2O_4^{2-} + 4OH^- \qquad E° = -1.12\ V \tag{10}$$

where dithionite, $S_2O_4^{2-}$, is oxidized to sulfite SO_3^{2-}.

8.2: Resonance Raman Spectroscopy

Resonance Raman spectroscopy was performed by Dr. Rafferty at Université Laval in the laboratory of our collaborator Dr. Manon Couture. The protein samples for the Raman experiments were used at a 67 μM concentration based on heme content and were buffered in 0.1 M sodium phosphate buffer, pH 7.5. The ferrous state reduced protein

samples were prepared by injecting a small amount of a freshly prepared sodium dithionite solution to argon-equilibrated protein samples in tightly sealed Raman cells.

9: *Heme extraction of Giardia Cytochrome b_5*

To test whether the heme in cytochrome b_5 was bound covalently or non-covalently, a concentrated cytochrome solution was treated with acid butanone (Teale 1959). In a microfuge tube, 500 µL of 0.1 M HCl was added to 100 µL of cytochrome b_5. The solution was chilled on ice then combined with 500 µL of ice-cold butanone. The mixture was shaken, microcentrifuged and allowed to stand for a few seconds to separate the top organic layer from the bottom aqueous layer. The organic phase was red, indicating the presence of heme and demonstrating that heme was non-covalently bound to the protein, which remains in the aqueous phase.

10: *Quantification of Giardia Cytochrome b_5 protein*

The concentration of protein was determined by Bradford Assay, which relies on Coomassie Blue dye undergoing a shift in maximum absorbance from 465 nm to 595 nm upon binding of protein. The assay used a 0.10 mg/mL bovine serum albumin (BSA) stock solution to make 1.2 mL standards with 0, 2, 4, 6, 8, 10, 12, 14, 16, 18 and 20 µg of BSA in 1.0 mL Bradford Dye Reagent and water. A Cary 400 Bio UV-visible spectrometer was first zeroed at 595 nm with a blank sample in quartz cuvette and then absorbance of each of standards in increasing concentration was recorded ensuring cuvette was cleaned each time. A standard curve was prepared by plotting A_{595} versus mass of protein (µg). A cytochrome b_5 sample was prepared by mixing 100 µL of diluted protein with 100 µL of water and 1.00 mL of Bradford dye reagent. The absorbance of each sample was recorded

only if this value fell into the standard curve. If it did not then the protein was diluted by a known amount and the experiment repeated.

11: *Quantification of Heme in Giardia Cytochrome b_5*

The amount of heme present in a sample of cytochrome b_5 was quantified by reduced pyridine hemochrome assay, in which the protein is denatured under alkaline conditions and the released heme forms a complex with pyridine that has a characteristic spectrum upon reduction with sodium dithionite. A baseline of alkaline pyridine was obtained from 700 nm to 250 nm in a quartz cuvette with 1 mL of 20% pyridine in 0.2 M NaOH. The ferric pyridine complex spectrum was obtained by adding 35.7 ng of cytochrome to this cuvette with gentle mixing. To obtain the pyridine hemochromogen a few milligrams of sodium dithionite on tip of spatula was added to the sample and the spectrum was recorded. The difference in absorption at 557 nm relative to 575 nm ($\Delta A_{557\text{-}575}$) was calculated from the graph and heme concentration was determined using an extinction coefficient ($\varepsilon_{557\text{-}575}$) for the pyridine-heme complex of 32.4 $mM^{-1}cm^{-1}$ (Paul *et al.* 1953). From the results of the Bradford assay for protein and the pyridine hemochrome assay, the stoichiometry of heme binding to the recombinant cytochrome could be determined.

12: *Thermostability measurements of Giardia Cytochrome b_5*

Temperature dependence measurements were performed using Cary 400 Bio UV-visible spectrophotometer (Varian) equipped with thermostattable temperature-controlled multicell holder (±0.05 °C, Peltier). The sample contained ~30 μM full-length cytochrome b_5 in 20 mM potassium phosphate, in a 3-mL quartz cuvette equipped with a magnetic

stirrer. The cuvette and sample at 4°C was used as a baseline for the UV-visible spectrum between 700 nm and 280 nm. The temperature in the spectrophotometer was increased linearly at a rate of 1°C/minute for the first experiment and 0.25°C/minute for the second experiment. The absorbance was recorded at each temperature to determine at which temperature cytochrome b_5 starts to denature, as indicated by an increase in light scattering due to formation of protein aggregates.

13: *pH dependence of the UV-visible spectrum of Giardia Cytochrome b_5*

Potassium phosphate buffers (Ionic strength =20 mM) of pH 5.0, 6.0, 7.0, 7.4, 8.0 and 9.0 and 10 were prepared. A concentrated stock solution of full-length cytochrome b_5 (pH 7.4) was diluted to 30 μM to prepare 5-mL of solution at each pH. The sample was placed in a 1-mL quartz cuvette and the UV visible spectrum between 700 nm and 280 nm was recorded using the Cary 400 Bio UV visible spectrophotometer (Varian) after taking an initial baseline with buffer at pH 7.4.

14: *Giardia cytochrome b_5 electrochemical measurements*

14.1: Cyclic voltammetry

Cyclic voltammetry (CV) experiments on gCYTb_5-I were performed in the laboratory of Grant Mauk at the University of British Columbia using a custom-made indium tin oxide (ITO) working electrode. ITO-coated glass was purchased from Donnelly Applied Films (Longmont, CO, USA.) and cleaned by ultrasonication in acetone (10 minutes), atmospheric plasma treatment (10 minutes), followed by soaking in 1M KOH (5 minutes), and rinsing with ultra-pure water. CV was performed with an Autolab PGSTAT12 potentiostat-galvanostat (Eco Chemie, Utrecht, Netherlands). A platinum wire

and saturated calomel electrode (SCE) were employed as the counter and reference electrodes, respectively. All measurements were performed at a scan rate of 100 mV/sec, and the potentials were referenced to the standard hydrogen electrode (SHE).

14.2: Spectroelectrochemistry

14.2.1: Instrument setup

A spectroelectrochemistry package was newly purchased from Pine Research Instruments (Durham, NC) to conduct these experiments. Each electrode card contained a built-in honeycomb working electrode with gold-coated channels (125 μm hole radius) and a patterned counter electrode adjacent to the working electrode (Figure 15a). The reference electrode (3.5 mm diameter, 60 mm length) was an Ag/AgCl type in saturated KCl gel with a ceramic fritted tip. A special cuvette cap was used to securely hold the electrode card and reference electrode in a quartz slotted thin-layer cell (1.7 mm optical path length). The electrode card and the reference electrode were electronically connected *via* a mini-USB cable to a WaveNow portable USB potentiostat/galvanostat (Pine Research) from which the applied potential was controlled through AfterMath Instrument control and data analysis software. The cuvette was mounted on an Ocean optics CUV-UV spectrometer cuvette holder which was connected by fiber optic cables to the Ocean optics USB2000+ spectrometer connected to a mini deuterium-tungsten-halogen light source (DT-MINI-2-GS, Figure 15b). The UV-visible spectra were obtained through OceanView operating software.

Once the instrument had been setup, it was tested by spectroelectrochemical experiments on the ferricyanide/ferrocyanide couple until agreement with literature values was obtained. To restore functionality to the working electrodes after prolonged use,

electrodes were cleaned chemically using Piranha Solution (concentrated H_2SO_4: 30% H_2O_2 3:1 v/v). They were electrochemically cleaned twice throughout this study. Electrochemical cleaning entails continuous and repetitive voltammetric cycling of gold honeycomb electrode in a 0.5 M H_2SO_4 electrolyte at a 500 mV/s sweep rate. This cycling is repeated until a voltammogram that can retrace the voltammogram of the previous cycle is obtained, which can take anywhere from 2 to 10 minutes.

14.2.2: Spectroelectrochemistry using potential-step experiments

Prior to the experiment, nitrogen gas was passed through the quartz cell and bubbled under the solution of phosphate buffer (μ=20 mM, pH 7.4) and mediator for approximately 20 minutes to deoxygenate them. The cell was filled with buffer and mediator solution using a Hamilton gas tight syringe, the electrodes were inserted into the cell and a baseline UV/Vis absorption spectrum was recorded. Once the baseline light and dark spectra were obtained, gCYT*b*5 was added to the cell with a syringe to a final concentration of 30 μM through a port hole in the cuvette cap. The channels of the honeycomb electrode were then prefilled with electrolyte solution and inserted back into the cell. This system containing the protein and mediators (750 μL) was blanketed by a continuous flow of nitrogen gas throughout the experiment to prevent autoxidation.

The honeycomb and reference electrodes were then connected to the potentiostat and a spectrum was obtained without any applied potential. The potential was then set at -500 mV *vs* Ag/AgCl for 20 minutes and a spectrum of the reduced gCYT*b*5 was obtained. The gCYT*b*5 solution was then oxidized at 500 mV *vs* Ag/AgCl for 20 minutes to obtain an oxidized spectrum. This was followed by another electrochemical reduction for 20 minutes at -500 mV *vs* Ag/AgCl to complete an oxidation-reduction cycle and ensure that

reduction spectra were similar. Once the protein was fully reduced the potential was increased at 25 mV increments up to -300 mV *vs* Ag/AgCl and then increased by 50 mV increments until the protein was completely oxidized (-100 mV *vs* Ag/AgCl). The solution was allowed to come to equilibrium for approximately 10 minutes after each change in applied potential and then a UV-Vis absorption spectrum was recorded. All measurements were performed at room temperature between 20-22°C.

14.2.3: Mediators

Spectroelectrochemical experiments used 6 μM of hexaammineruthenium(III) chloride ($E°$= 50 mV *vs.* SHE) and 3 μM naphthoquinone ($E°$= -137 *vs.* SHE) as mediators. Some experiments were performed with only one of the two mediators. We selected these mediators because they have insignificant absorbances over the wavelength of interest and their reduction potentials are close to those recorded for other cytochrome b_5 (Reid *et al.* 1982; Altruve *et al.* 2004).

14.2.4: Determination of redox potential using potential-step experiments

Ideally, in a thin layer cell (OTTLE), bulk electrolysis occurs within a few seconds and thus the oxidized and reduced form of analyte reaches equilibrium a described by the Nernst equation with each applied potential. Changing the applied potential of the working electrode through the potentiostat results in changes the ratio of the oxidized and reduced states of the redox couple, which corresponds to absorption changes for an optically active protein. The absorption of oxidized and reduced species at equilibrium is monitored for each of the different potentials. Figure 16 shows spectra of cytochrome b_5 for the fully reduced species (A_R), fully oxidized species (A_o) and an intermediate state containing both

oxidation states (A_E). These absorbencies can be used to calculate the fraction of oxidized [O] and reduced [R] species and their corresponding absorption ratio at point E of the experiment, as follows:

$$[\boldsymbol{O}] = \frac{\boldsymbol{A_E - A_R}}{\boldsymbol{A_o - A_R}}, \qquad [\boldsymbol{R}] = \frac{\boldsymbol{A_O - A_E}}{\boldsymbol{A_o - A_R}} \qquad \text{and} \qquad \frac{[\boldsymbol{O}]}{[\boldsymbol{R}]} = \frac{\boldsymbol{A_E - A_R}}{\boldsymbol{A_O - A_E}} \tag{11}$$

Through the application of Beer's law ($\boldsymbol{A=\varepsilon cl}$), the absorption ratio of oxidized to reduced species at a particular wavelength is correlated to their concentration ratio, $\frac{[\boldsymbol{O}]}{[\boldsymbol{R}]}$, at each applied potential. The data is then analyzed using the Nernst equation:

$$\boldsymbol{E} = \frac{\mathbf{RT}}{\boldsymbol{nF}} \boldsymbol{log}\left(\frac{[\boldsymbol{O}]}{[\boldsymbol{R}]}\right) + \boldsymbol{E}^{\circ} \tag{10}$$

where E is the applied potential of the working electrode (mV) and $E°$ is formal redox potential (mV). R, T, n, and F are the gas constant, temperature, stoichiometry of electrons transferred, and Faraday's constant, respectively; at 298K these values combine to yield a slope of 59 mV. The logarithm of the concentration ratio is plotted against the applied electrode potential, which results in a straight plot with the y-intercept equal to the midpoint reduction potential of the cell, if the protein exhibits Nernstian response. This midpoint potential measured against the Ag/AgCl reference is then converted to the standard reduction potential versus the SHE by the addition of 197 mV.

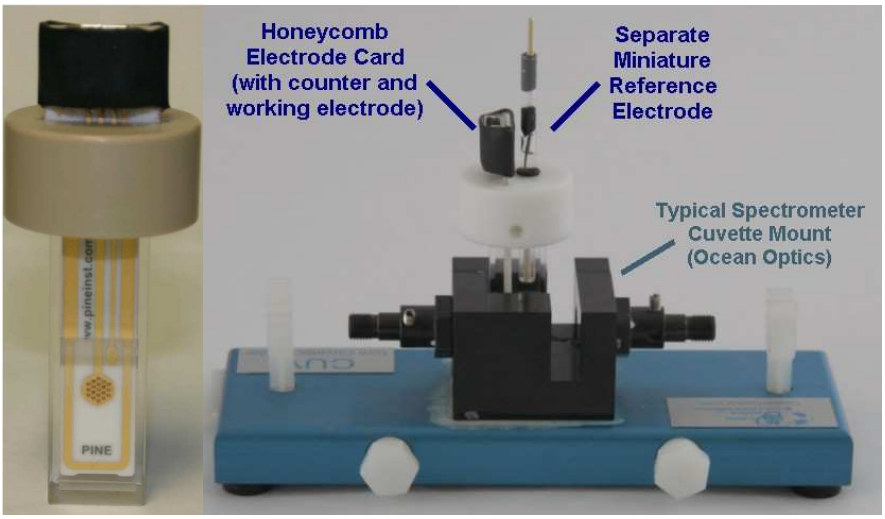

Figure 15: Spectroelectrochemistry setup (a) Cell used for spectroelectrochemistry measurements with honeycomb electrode (b) Cell placed in the spectrometer with working and reference electrodes in place

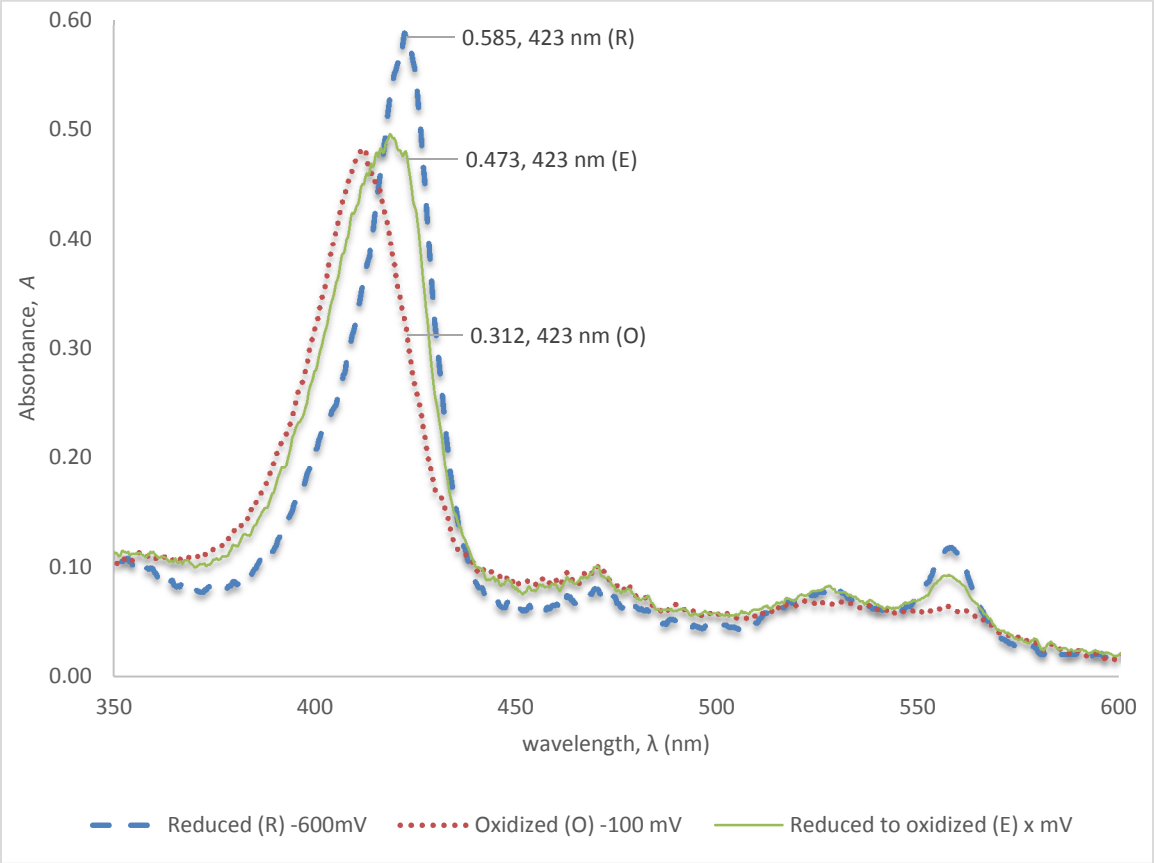

Figure 16: Sample spectra of cytochrome b_5 showing the absorbencies at 423 nm for a fully reduced protein (R), fully oxidized protein (O) and a protein being oxidized (E) at a specific applied potential (mV vs. Ag/AgCl) during spectrochemical experiment.

15: *NMR*

15.1: 1D ^{1}H NMR experiments

The 1D ^{1}H NMR experiment was performed on unlabeled full-length cytochrome b_5 expressed as described before. The sample was prepared to a concentration of 1-2 mM in 100% D_2O in a volume of 250 µL. The protein used for this experiment had been through a freeze thaw cycle and some of the protein precipitated during the buffer exchange and concentration process. The ^{1}H NMR spectrum was recorded on the NMR spectrometer at the Department of Biochemistry and Molecular and the Centre for Blood Research, University of British Columbia, Vancouver, BC, Canada.

15.2: HSQC NMR experiments

15.2.1: HSQC NMR protein expression

The isotope-labelled cytochrome b_5 used for HSQC NMR experiments was expressed by growing gCYTb_5-I transformed *E. coli* strain BL21(DE3) cells on minimal media supplemented with glycerol, α-aminolevulinic acid and ferric chloride (M9-GAFe) in the presence of ampicillin (100 µg/mL). The M9 salt solution had ^{15}N-labelled ammonium chloride added to a concentration of 1 g/L (Appendix IX). The starter culture was prepared by growing freshly transformed cells in 2 mL LB at 37°C for 8 hours then using the pellet from the 2 mL culture to inoculate 50 mL of LB with ampicillin (100 µg/mL) and letting this culture grow overnight at 37°C. This starter culture was used to inoculate 500 mL of M9-GAFe media and these cells were grown in aerobic conditions at 37°C until the OD_{600} was 0.5. If the culture was to be induced for protein expression then 1 mM of IPTG was added to the culture at this cell density. All cell cultures were grown at

30°C from this point forward; for 24 hours if induced with IPTG, or 48 hours without induction. The cells were harvested by centrifugation and the resulting pellet was frozen at -80°C. Protein was purified as described above. The protein yield of these preparations varied between 2 to 4 mg per litre of culture.

15.3: HSQC NMR sample preparation

^{15}N-enriched gCYTb_5-I was first prepared in 50 mM phosphate buffer (pH 7.4) to a concentration of 136 μM utilizing an Amicon ultrafiltration membrane. However, the sample was aggregated during NMR experiments under these conditions, thus before NMR, the ^{15}N-labelled gCYTb_5-I sample was run through a Superdex 75 size exclusion column. The fractions corresponding to MW of cytochrome b_5 (15 kDa) were exchanged into phosphate-buffered saline (pH 7.7) and concentrated to 300 μL in a Shigemi NMR sample tube to a final concentration of ~ 100 μM.

The NMR experiments were performed at a temperature of 30°C on a Varian Inova 500 MHz NMR spectrometer equipped with a cold probe at the laboratory of Logan Donaldson, York University. One experiment was run overnight at 256 scans/FID.

RESULTS AND DISCUSSIONS

Giardia lamblia encodes several putative heme-binding proteins, of which three have high sequence similarity to the cytochrome b_5 family. These have not been characterized in Giardia, and nothing is known of their function. One isotype of this protein, gCYT*b*5-I, was expressed as a recombinant histidine-tagged protein in *E. coli*. We characterized this protein using bioinformatics, UV-Visible spectroscopy, Resonance Raman spectroscopy, mass spectrometry, NMR spectroscopy, size exclusion chromatography, cyclic voltammetry, and spectroelectrochemistry.

1: *Protein sequence and structure*

A BLASTp search on the National Center for Bioinformatics (NCBI) server using the predicted amino acid sequence of gCYTb_5-I indicated that the core of the protein (residues 30 to 109) matched the profile of the cytochrome b_5 family (Altschul *et al*. 1997). The sequences with highest identity were the b_5-domains of human NADH: cytochrome b_5 oxidoreductase (34%), yeast flavocytochrome b_2 (41%), *Ostreococcus tauri* virus 2 (33%), outer mitochondrial membrane cytochrome b_5 [rat (36%) human (34%)], *Ectothiorhodospira shaposhnikovii* cytochrome b_{558} (43%), mammalian microsomal cytochrome b_5 (rat 38% bovine 32%), *Ascaris suum* cytochrome b_5 (37%), and house fly cytochrome b_5 (26%). Moreover, there were additional sequences with higher sequence identities in the non-redundant database; however, most of those proteins were annotated as uncharacterized. Consequently, our analyses were restricted to matches of known cytochromes b_5.

The multiple sequence alignment (MSA) was created using MAFFT with the BLASTp sequences that had the highest identity to gCYTb_5 and lowest E- value

(Figure 17). The noncovalently bound heme was predicted to interact with 15 residues by the utilities RaptorX Binding (Källberg *et al.* 2012), I-TASSER (Zhang 2008) and 3DLigandSite (Waas *et al* 2010), as displayed in Table 3. The strongest interaction is the coordination bond between the the heme iron and conserved histidine ligands of gCYT*b*5-I, His^{65} and His^{88} (corresponding to His^{39} and His^{63} of bovine cytochrome b_5), both located in helix-loop-helix motifs. Giardia is one of the few cytochromes where the highly conserved HPGG loop motif between helices α2 and α3 is replaced by HPAG. The second VGHS loop motif between helices α4 and α5 is VAHS in Giardia. The substitution of glycine with alanine can result in a considerable loss in conformational flexibility of backbone. Furthermore, the proximity of the substitution to the histidine ligand and heme probably has unique structural and functional implications.

Among the interesting residues found in Giardia are two cysteine residues at position 47 and 84 (gCYTb_5-I numbering). Giardia shares the Cys^{47} residue with *E. shaposhnikovii* cytochrome b_{558}, *O. tauri* virus 2 and Arabidopsis (plant) cytochrome b_5, but it is not found in other species at that position. The only other species in our alignment with two cysteine residues are *A. summ* and *E. shaposhnikovi* b_{558}. In both these proteins the two cysteines form disulfide bridges; Cys^{47} binds with Cys^{76} in *E. shaposhnikovi* b_{558} (Kostanjevecki *et al.* 1999) and Cys^{24} with Cys^{107} in *A. summ* (Yokota *et al.* 2006) raising the possibility that gCYTb_5-I also contains a disulfide bond. The gCYTb_5-I Cys^{84}, corresponding to bovine cytochrome b_5 position 58, is also interesting because it is at a highly conserved location where almost all other species have phenylalanine. The phenyl ring of Phe^{58} (84) stacks with the imidazole ring of His^{63} (88) and the porphyrin ring of the heme (Shan *et al.* 2005). There are rare substitutions by large aromatic or hydrophobic

residues such as tryptophan in *E. shaposhnikovi* b_{558} (Kostanjevecki *et al.* 1999) or leucine in *A. summ* (Yokota *et al*. 2006), but in Giardia we have a small hydrophilic cysteine.

Another noticeable difference between gCYT*b*5-I and others is the lack of acidic residues around the heme edge that are found in microsomal versions of this protein. These negatively charged carboxyl residues form complementary electrostatic interactions with positively charged basic residues on redox partners, such as methemoglobin, cytochrome P450, cytochrome *c* or NADH cytochrome b_5/P450 reductase (Rodgers and Sligar 1991; Mayer *et al.* 1993; Vergéres *et al*. 1993; Schenkman and Jansson 2003). The lack of such residues in gCYT*b*5-I may effect its choice of redox partners, its method of interaction with those partners as well as its reduction potential. The bacterial protein *E. shaposhnikovi* b_{558} also shares this unique charge distribution with gCYT*b*5-I (Kostanjevecki *et al.* 1999).

Table 3: Heme binding site prediction for gCYTb_5-I using I-TASSER and 3DLigandSite (Waas *et al.* 2010 and Zhang 2008)

Giardia residues		**Corresponding Bovine residues**	
51	TYR	25	LEU
61	TYR	35	PHE
65	**HIS**	**39**	**HIS**
66	PRO	40	PRO
67	ALA	41	GLY
71	ILE	45	VAL
72	LEU	46	LEU
75	PHE	49	GLN
84	CYS	58	PHE
87	ALA	62	GLY
88	**HIS**	**63**	**HIS**
89	SER	64	SER
90	TRP	65	THR
93	ILE	68	ALA
97	ILE	72	SER

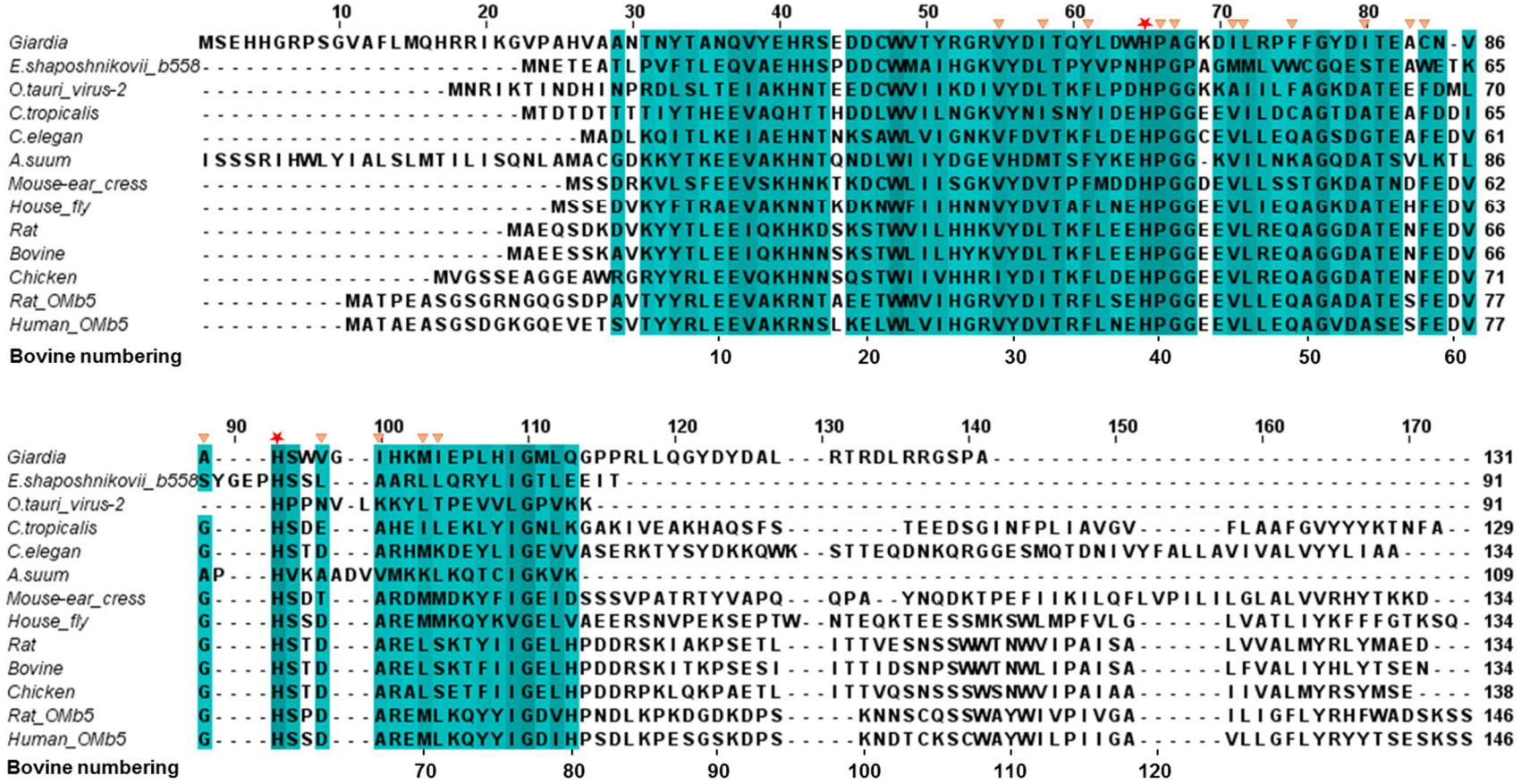

Figure 17: Alignment of amino acid sequence of *Giardia lamblia* cytochrome b_5 against cytochrome b_5 from different species. Aqua green is conserved core region, ✶ point to the conserved histidine residues and ▼ represents the heme-binding residue in *Giardia lamblia* as predicted by RaptorX Binding (Källberg *et al.* 2012). This alignment was done using MAFFT multiple sequence alignment software version 7 (Katoh *et al.* 2013) and edited using Jalview version (Waterhouse *et al.* 2009).

1.1: Homology modelling of gCYT*b*$_5$-I structure

Multiple sequence analysis is limited in that it only considers sequence similarity, whereas protein function is also a consequence of protein fold. In the absence of a structural obtained by x-ray crystallography or NMR, homology modelling can be used to determine the secondary structure of a protein whose primary sequence is more than 30% identical to proteins with known structures.

When the non-restrictive mode on Swiss Model was used for homology modelling, gCYT*b*$_5$-I was automatically modeled to the heme-binding domain of *Saccharomyces* flavocytochrome b_2 (1kbi.pdb, sequence identity 42%). This model did not include the heme cofactor because Swiss Model requires all the residues interacting with the ligand to be fully conserved between model and template in order for the ligand to be included (Arnold *et al.* 2006). This lack of heme slightly restricted our ability to examine heme-protein interactions. To obtain a model with heme bound to it, the modelling was repeated in Swiss Model automatic mode with the template specified as human NADH cytochrome b_5 oxidoreductase 4 (CYTB5R4, 31f5.pdb, sequence identity 34%). The final model was generated with a heme coordinated by H65 and H88 (Figure 18). The superimposition of the two models of the template shows that their folds are similar (Figure 19). The presence of heme in one model and not the other one was due to the stringent requirements of the program for ligand inclusion.

Analysis of the structure of gCYT*b*5 revealed significant details that were not apparent from sequence alone. For example, the structural model made it clear that our suspicion about gCYT*b*$_5$-I forming a disulfide bond, similar to *A. summ* and *E. shaposhnikovi* b_{558}, is unlikely because the two cysteines are far apart (Figure 20).

However, the proximity of the Cys^{84} (Phe^{58} in bovine) to the heme does raise the possibility of a thioether linkage between the heme and the cysteine residue. This possibility was further supported when a study by Barker *et al.* (1993) demonstrated that the replacement of Asn^{57} with Cys^{57} within the heme-binding pocket of bovine liver cytochrome b_5 by site-directed mutagenesis resulted in a covalent attachment of the cysteine residue to the heme. This finding prompted us to do a precautionary test to determine whether the heme was covalently or non-covalently bound to the protein. A portion of the purified protein was treated with acid-butanone, and after the acid-induced denaturation the heme was extractable with 2-butanone. This clearly demonstrated that the heme is noncovalently bound to gCYTb_5-I and that the cysteine is neither involved in a thioether linkage with the heme nor does it form a disulfide bond.

Another reason that the position Cys^{84} was important because it is at a highly conserved location in the heme binding pocket where almost all other species have phenylalanine, and has been subjected to mutational studies (Shan *et al*. 2005). As shown in Figure 21, in bovine microsomal b_5 the benzene ring of Phe^{58} stacks with the imidazole ring of His^{63} in a face-to-face π-stacking mode and with the porphyrin ring of the heme in the edge-to-face T-stacking mode (Shan *et al*. 2005). These stacking interactions are not observed in homology model of gCYTb_5 because there are no aromatic side chains in cysteine residue that replaces the phenylalanine. Previous mutational studies on bovine microsomal b_5 have shown that mutating phenylalanine to a similar residue, such as tyrosine has no effect on the structure of the protein (Shan *et al*. 2005). However, when a residue different in size and properties, such as tryptophan, replaces the same residue the stacking interactions are weakened which results in a less stable protein (Shan *et al*. 2005).

Future mutational studies where the cysteine in gCYT*b*$_5$-I is mutated to phenylalanine can reveal important details about the tertiary structure and function of this protein.

Cytochrome b_5 also forms an aromatic network with axial ligand His^{39}, Phe^{35} and Tyr^{74}, as shown for bovine microsomal b_5 in Figure 21. In gCYTb_5, the histidine ligand remains unchanged, but Tyr^{61} and Leu^{107} replace Phe^{35} and Tyr^{74}, respectively (Figure 21). The structural model of gCYTb_5-I shows that the residue Tyr^{61} is in a similar position and orientation as Phe^{35} of bovine b_5 with the phenol ring of Tyr^{61} pointing to the plane of the heme similar to the phenyl ring of Phe^{35}. The structural similarity between these two residues allows the stacking interactions to be preserved and causes no apparent structural changes. However, the hydroxyl group of tyrosine makes the residue polar and reactive, which could cause functional changes in the active site that result in a modified reduction potential (Yao *et al*. 1997). The last member of the aromatic network, Tyr^{74} corresponds to an aliphatic Leu^{107} in gCYTb_5-I. The leucine residue is unlike the tyrosine and may cause tertiary structure changes in gCYTb_5-I, but the homology model shows that the residue is far from the heme group and is not likely to have major functional implications. A study done on rat microsomal cytochrome *b*5 with Tyr^{74} was mutated to Lys^{74} demonstrated that tyrosine is not essential for electron transfer and does not determine reduction potential or spectroscopic properties, rather it functions to shield the heme from the solvent and enhances its association with the protein (Vergéres *et al*. 1993).

Homology modeling was limiting because it did not allow us to model the amino and carboxy extensions of gCYT*b*5-I; as these sequences are not conserved there are no homologs to model these parts of the protein. The current models also give limited information about the heme-ligand orientation within the protein, which is important for

determining reduction potential of the protein. Hence, homology modelling is not a replacement of experimentally determined structures through crystallography or NMR spectroscopy. However, while we wait for these structures to be determined comparative models can guide us into doing meaningful mutational studies and future work on this protein.

a)

```
34.1% identity in 82 aa overlap (34-115:58-139); score:  214 E(10000): 1.4e-14

gCYTb5-I 34   TANQVYEHRSEDDCWVTYRGRVYDITQYLDWHPAGKDILRPFFGYDITEACNVAHSWVGI 93
CYB5R    58   TEEELKKHNKKDDCWICIRGFVYNVSPYMEYHPGGEDELMRAAGSDGTELFDQVHRWVNY 117

gCYTb5-I 94   HKMIEPLHIGMLQGPPRLLQGY 115
CYB5R    118  ESMLKECLVGRMAIKPAVLKDY 139
```

b)

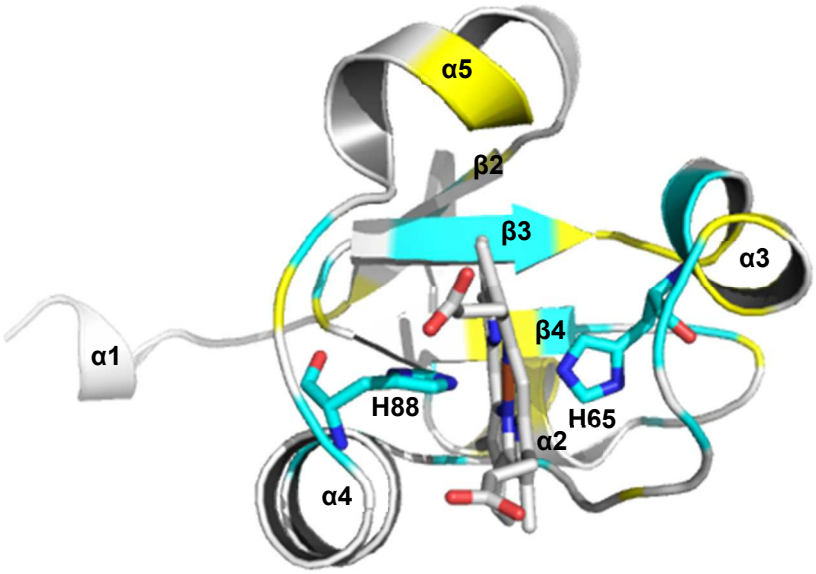

Figure 18: Structural comparison of gCYT*b*$_5$-I to the heme-binding domain of human NADPH cytochrome *b*$_5$ oxidoreductase 4 (CYB5R4; UniProtKB Q7L1T6, 3lf5.pdb).
(a) Sequence alignment, with identical and conservative residues highlighted in cyan and yellow respectively. The axial histidine ligands are in bold.
(b) Homology model structure of gCYT*b*$_5$-I, based on the structure of CYB5R4, with residues coloured as in a).

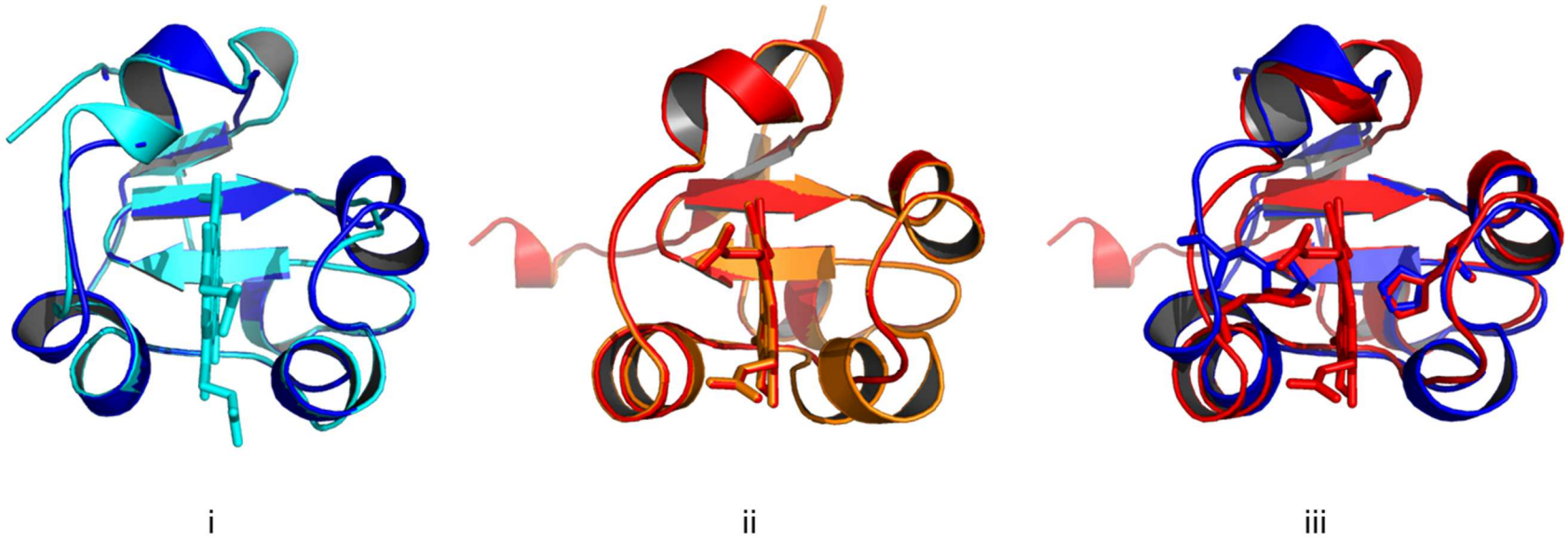

Figure 19: **Superimpositions of templates and model structures of gCYT*b*$_5$-I.**
i) 1kbi.pdb (cyan) and the gCYT*B*$_5$-I structure modelled to this template (blue).
ii) 3lf5.pdb (orange) and the gCYT*b*$_5$-I structure modelled to this template (red)
iii) The two gCYT*b*$_5$-I model structures, colored as above.

.

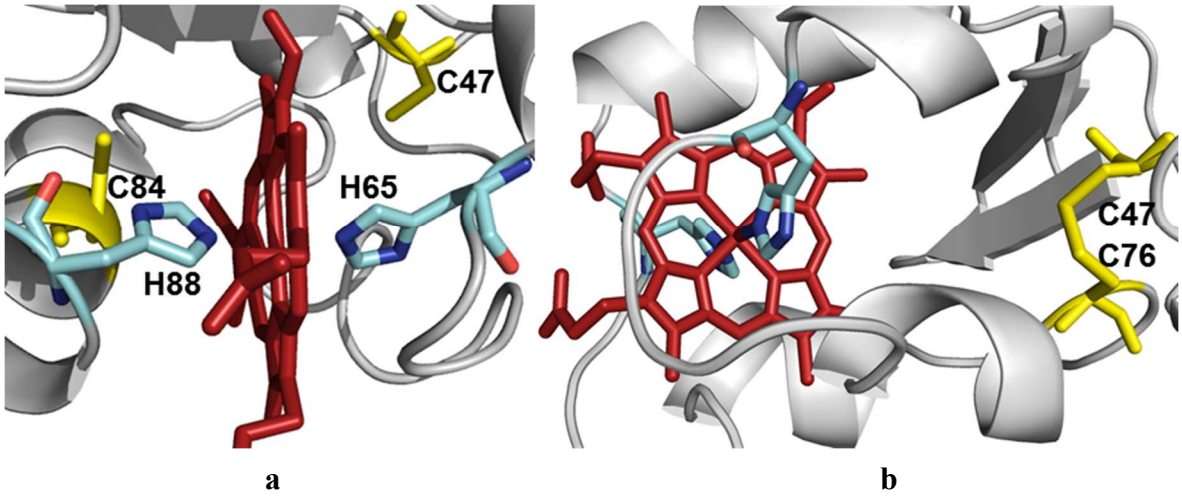

Figure 20: Comparison of cysteine residue found in gCYTb_5 and *E. shaposhnikovi* b_{558} **(a)** The position of C47 residue to C84 makes a disulfide bond unlikely, but the proximity of C84 to the heme creates a possibility of a thioether bond between C84 and the heme. **(b)** In *E. shaposhnikovi* b_{558} the two cysteines in close proximity form a disulfide bridges.

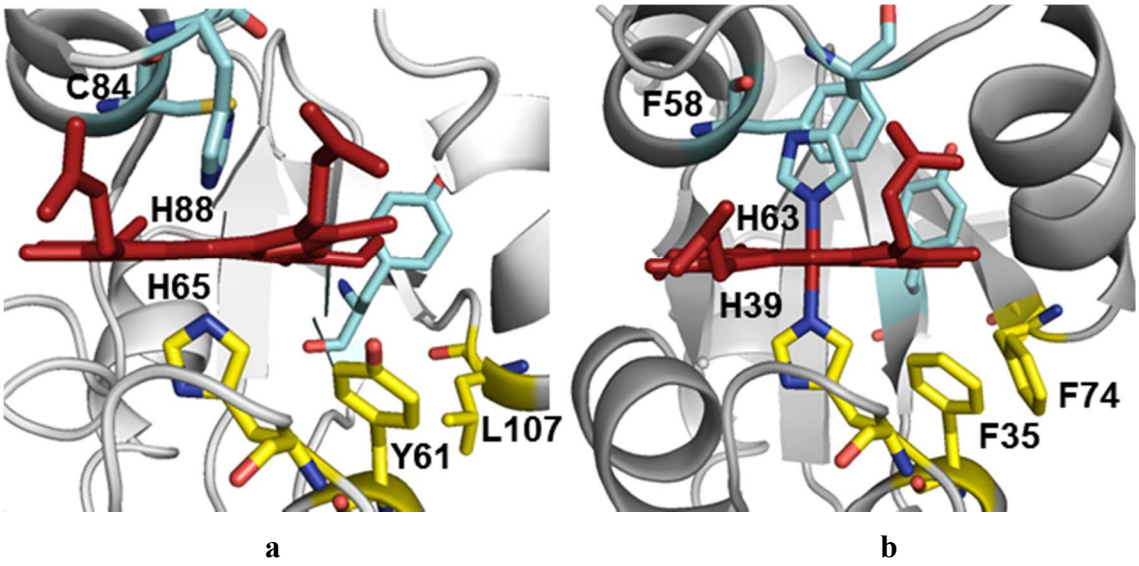

Figure 21: **Structural differences between gCYTb_5-I and microsomal cytochrome b_5 (1cyo.pdb).** The two aromatic network of amino acid one compromised of Phe^{35}, His^{39} and Phe^{74} the and second of Phe^{58} and His^{63} in microsomal cytochrome b_5 **(a)** is replaced by Tyr^{61}, His^{65} and Leu^{107} and Cys^{84} and His^{88} in gCYTb_5-I **(b)**.

2: *Cloning and expression of gCYTb$_5$-I*

2.1: Construction of pET14b-gCYT*b$_5$*-I expression vector

The full length cytochrome *b*5-I gene (GL50803_9089) was PCR amplified from genomic DNA of Giardia isolate WB with gene specific primers Cyto*b$_5$*/*Nde*I-1a and Cyto*b$_5$*/*Bam*HI-1b with T_{m1} of 60°C and T_{m2} of 64°C, as described in methods. This yielded a successful PCR reaction, as the amplification product appeared as a band around 420 bp, which corresponds to the size of the full length CYT*b*5-I gene and additional nucleotides of the primer (

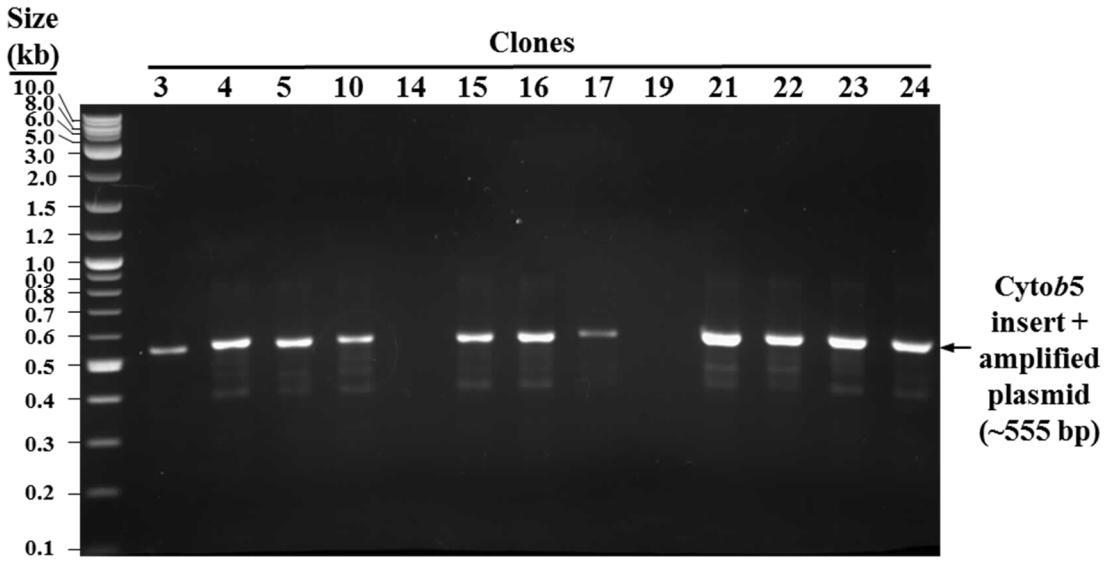

Figure **22**A). The cloning of CYT*b*5-I amplicon into a blunt vector, pJET1.2, and its subsequent transformation into DH5α cells yielded 74 scattered colonies. Four of these colonies were picked for PCR screening using primers to amplify gCYT*b*5-I gene. The insert of the expected size (~420 bp), was detected in only one colony (clone 10), which was cultured and its plasmid was extracted. Cohesive ends on gCYT*b*5-I were generated by digesting recombinant pJET1.2/CYT*b*5 with *Nde*I and *Bam*HI and extracting the double

digested product from electrophoresed gel. This digested product was then ligated to double-digested pET14b vector to generate pET14b-gCYTb_5-I expression vector.

Transformation of this recombinant plasmid into NEB DH5-α cells (transformation efficiency of 3.61 x 10^8 cfu/µg) yielded a lawn of colonies, 13 of which were randomly selected for PCR screening. Since the PCR was done using T7 as a forward primer and gCYT*b*5-I/BamHI-1b as reverse primer, the amplification product included both the cytochrome b_5 gene (420 bp) and the T7 promoter region (135 bp) so the expected size of the positive insert band was 555 bp (

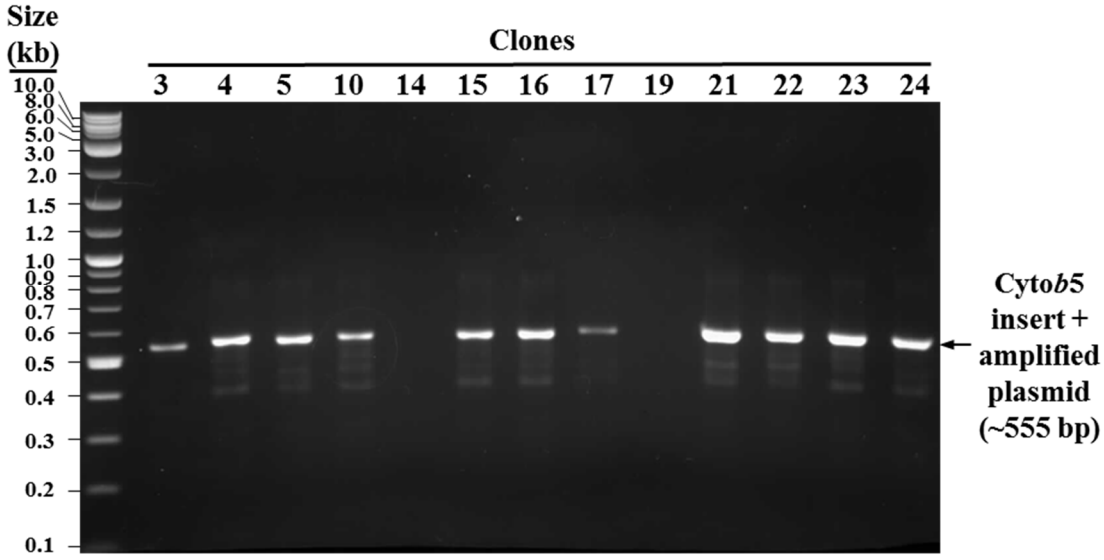

Figure **22**C). The gCYT*b*5-I insert was detected in eleven colonies, four of which were selected for propagation and plasmid purification. Restriction enzyme digestion was performed on the recombinant plasmid from clones 16, 17, 21 and 23 to ensure the vector

and insert of the expected size were present in the selected clones (

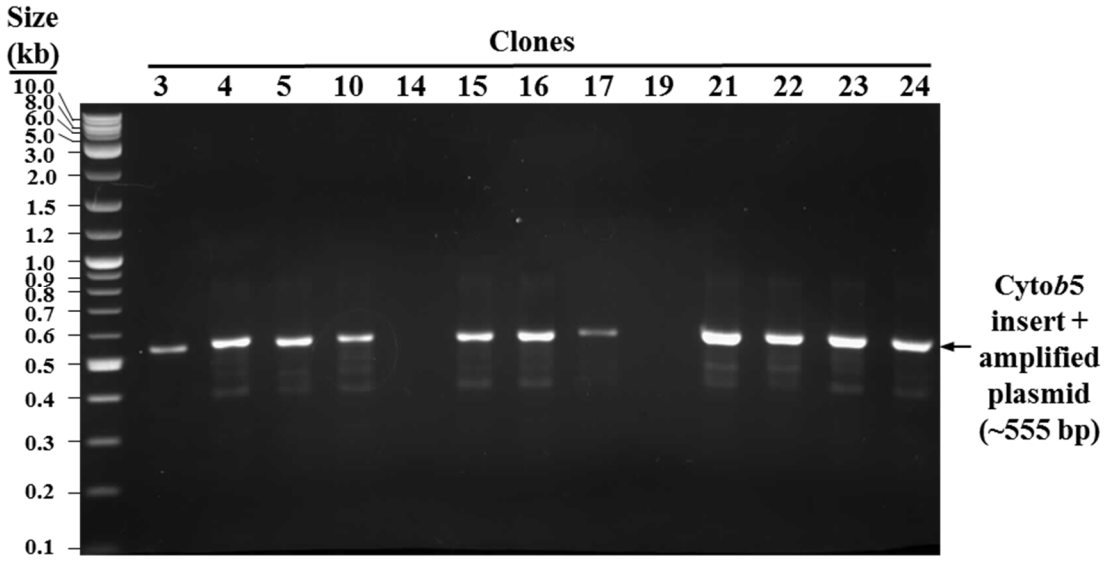

Figure **22**B). Clone 21 was selected for DNA sequencing because it gave the highest plasmid DNA yield in NEB-5α culture and tested positive for both the PCR screening and *Nde*I/*Bam*HI digestion. The results from the sequencing indicate that the cytochrome b_5 gene was successfully inserted into the vector. Similar procedure was followed for truncated protein and its PCR amplification and restriction enzyme digest are shown in Figure 23A and 25, respectively.

The pET14b vector specifically carries an N-terminal His-Tag sequence, which is used to purify the recombinant protein using affinity chromatography. This vector also encodes a thrombin site that can be used to cleave the tag off following purification. However, we did not cleave this tag off because molecular modelling and dynamic stimulations on cytochrome b_5 with and without the histidine tag have demonstrated that the $(His)_6$-CYT*b*5 has similar properties and function to isolated CYT*b*5 (Lin *et al.* 2009). Experimental results from this modelling shows that N-terminal $(His)_6$-tag does not alter the heme active site as the $(His)_6$-tag adopts a helical conformation that packs against the

bottom hydrophobic core of cytochrome b_5 and does not interact with the heme binding hydrophobic core (Lin *et al.* 2009).

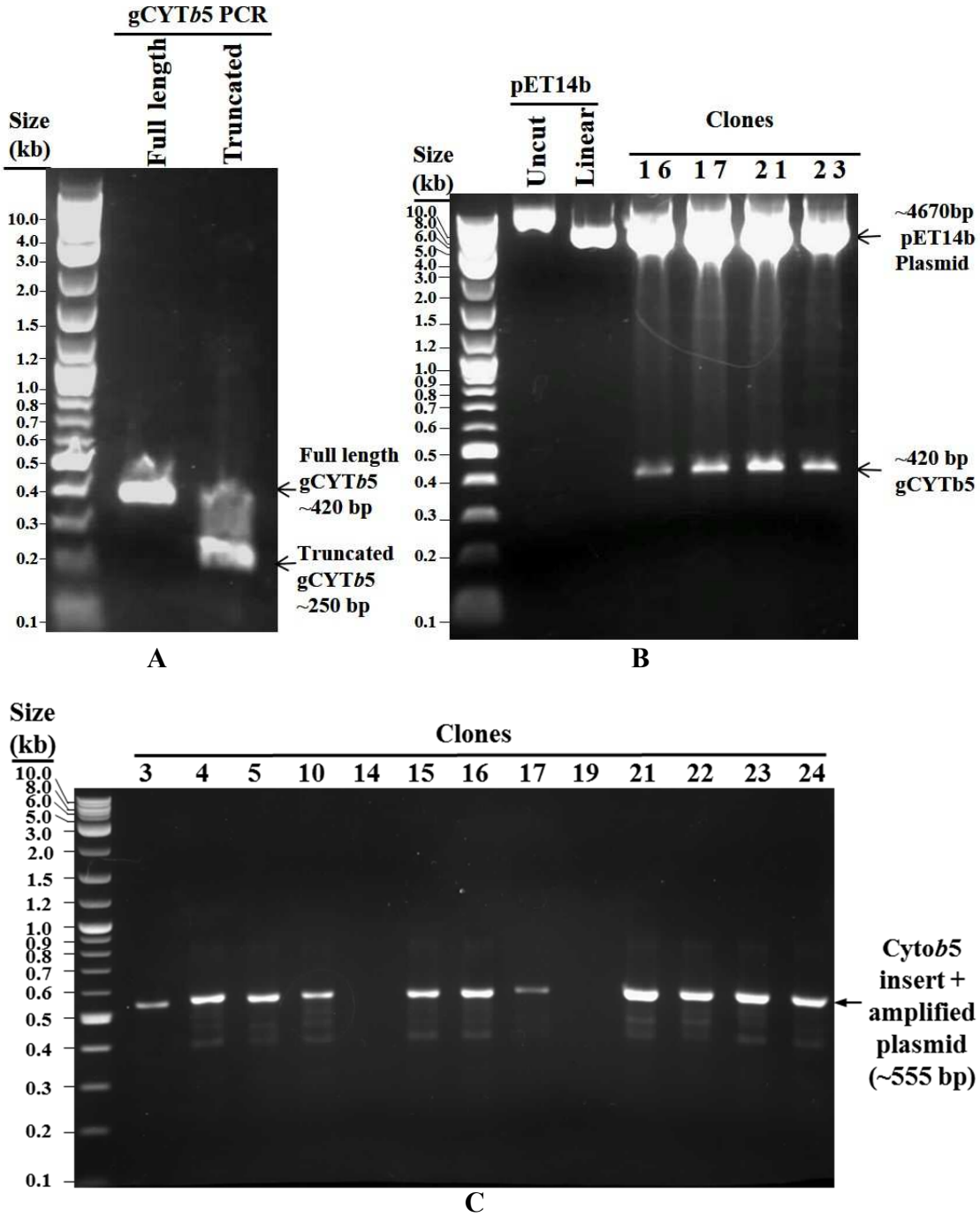

Figure 22: A) PCR products amplified from Giardia genomic DNA using primers for full length or truncated gCYT*b*5 **B)** *Nde*I/*Bam*HI digestion of pET14b-CYT*b*5 plasmid DNA isolated from four bacterial transformants. Each clone contains two bands: one corresponding to full-length cytochrome *b*5 insert at ~420 bp and a second band representing the linearized pET14b plasmid at ~4670 bp **C)** PCR screening of pET14b/gCYT*b*5 clones transformed into DH5-α cells. Clones were amplified using T7 forward primer and CYT*b*5/*Bam*HI-1b reverse primer. Positive clones were around 555 bp in size.

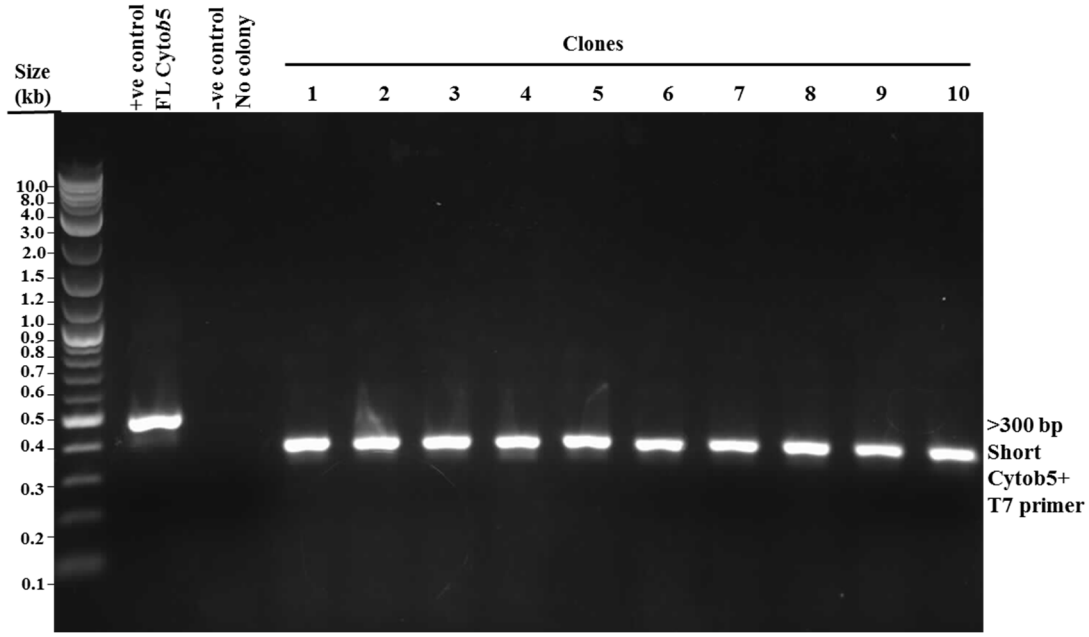

Figure 23: PCR screening of pET14b/gCYT*b*5 clones transformed into DH5-α cells. Clones were amplified using T7 forward primer and CYT*b*5/*Bam*HI-2b reverse primer. Positive clones were around 300 bp in size.

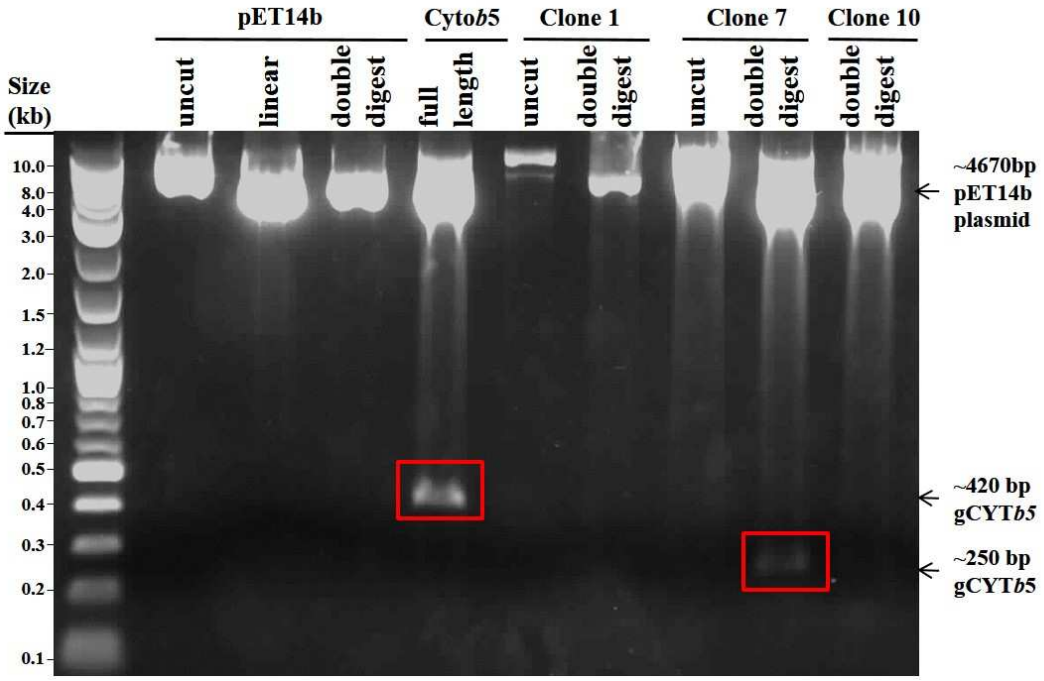

Figure 24: *Nde*I/*Bam*HI digestion of three pET14b-truncated CYT*b*5 clones that tested positive for truncated cytochrome *b*5 insert by PCR screening. Clone 7 contains two bands: one corresponding to truncated cytochrome b_5 insert at ~250 bp and a second band representing the linearized pET14b plasmid at ~4670 bp

2.2: Expression and purification of gCYT*b*5-I

Transformation of *E. coli* BL21(DE3) with pET14b vector containing the gene for gCYT*b*5-I resulted in high expression of heme-bound recombinant protein as indicated by the pink color of bacterial pallets. To optimize the expression of the gCYT*b*5-I, several small-scale cultures of transformed cells were subjected to different growth conditions and the color of their bacterial pellets were observed. A time course experiment for optimal incubation time revealed that the optimal yield for gCYT*b*5-I cultures was observed after 24 hours of incubation. Incubation of protein for less than 24 hours results in lower yield, while incubation for longer time (32 or 48 hours) results in accumulation of degraded recombinant protein. The proteins were also subjected to growth at 22°C (room temperature), 30°C and 37°C and it was observed that 30°C was optimal for growth of

cultures in Terrific broth, while 37°C was suitable for overnight growth of starter cultures in LB broth.

Through these small-scale expression experiments it was observed that cultures that were grown at 30°C without IPTG induction for 20 to 24 hours produced small sized and deep pink pellets, while the cultures that were induced with IPTG produced a larger pellets that were mostly beige. It seems that IPTG induction triggered the protein to be expressed in inclusion bodies that made it difficult to purify the protein. It was also observed that addition of heme precursor, δ-aminolevulenic acid (ALA), was not necessary for holocytochrome b_5 formation, as basal heme production was sufficient without it and its addition did not increase protein yield. Thus, further protein expressions were performed without IPTG induction or ALA addition.

The full-length version of gCYTb_5-I was expressed in parallel to the core lacking the amino and carboxy-terminal extensions (Figure 25). A similar pattern was noticed for the truncated protein, where the best expression was observed when bacteria were not induced with IPTG. However, in comparison to the full-length protein the truncated protein was expressed with less heme bound and thus the addition of ALA was more important for expression of truncated protein than for the full length version. The best time to introduce ALA into cultures was when the 1-L culture was inoculated with the pellets from overnight 50-mL culture.

The full-length protein was expressed at a much higher proportion than the truncated protein (Figure 26). The average yield for the full-length protein was approximately 30 to 35 mg of recombinant protein per litre of culture, as calculated by

Bradford protein assay (BSA). The truncated protein had much lower yields of around 7 mg per litre of culture as measured by NanoDrop.

The His_6-tagged gCYT*b*5-I was purified by affinity chromatography on cobalt columns. The purified His_6-tagged gCYTb_5-I was soluble and had a molecular weight of ~17 kDa for the full-length gCYT*b*5, and ~11 kDa for the truncated gCYT*b*5, as shown in SDS-PAGE gels (Figure 26). Several washes were performed to remove most of the endogenous bacterial proteins; however, the eluted fractions contain a number of additional proteins, many of which are of a higher molecular weight than the recombinant protein. Most prominent of these were proteins with bands around ~25 kDa and ~70 kDa. These bands may result from the nonspecific binding of untagged protein, such as a cellular protein with several histidine residues, to the IMAC matrix and then coeluting with the gCYTb_5. Another possibility is nonspecific hydrophobic interactions or disulfide bond formation between gCYT*b*5-I and other proteins that leads to coelution and subsequent contamination. There is also an additional band in the full-length protein around 35 kDa, which may represent dimers of gCYT*b*5-I. The presence of low molecular weight bands around 15-kDa can possibly be cytochrome *b*5 with its histidine tags cleaved.

It is also evident that the truncated protein is more contaminated than the full-length protein, which indicates that IMAC may not be sufficient as the only purification method for the truncated protein. It has been previously reported in literature that nonspecific binding of endogenous proteins to the IMAC column is more likely for tagged proteins expressed at low levels, as more sites are available on the resin for weakly-interacting proteins to bind. Therefore, for the truncated gCYT*b*5 it is necessary to use the

polyhistidine tag in conjunction with an additional purification techniques, such as size exclusion chromatography.

The polyhistidine tag was left intact after purification and all characterizations were done with the tag. This was because relative to the protein, the size and charge of the His_6-tag moiety are smaller and do not affect protein activity or redox properties.

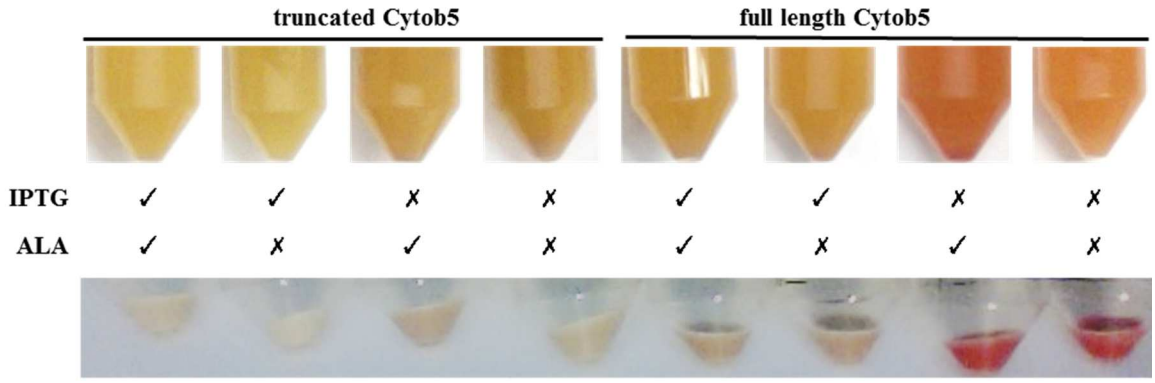

Figure 25. Cell culture and pellets of truncated vs. full-length cytochrome b_5 expressed in presence or absence of IPTG and/or ALA.

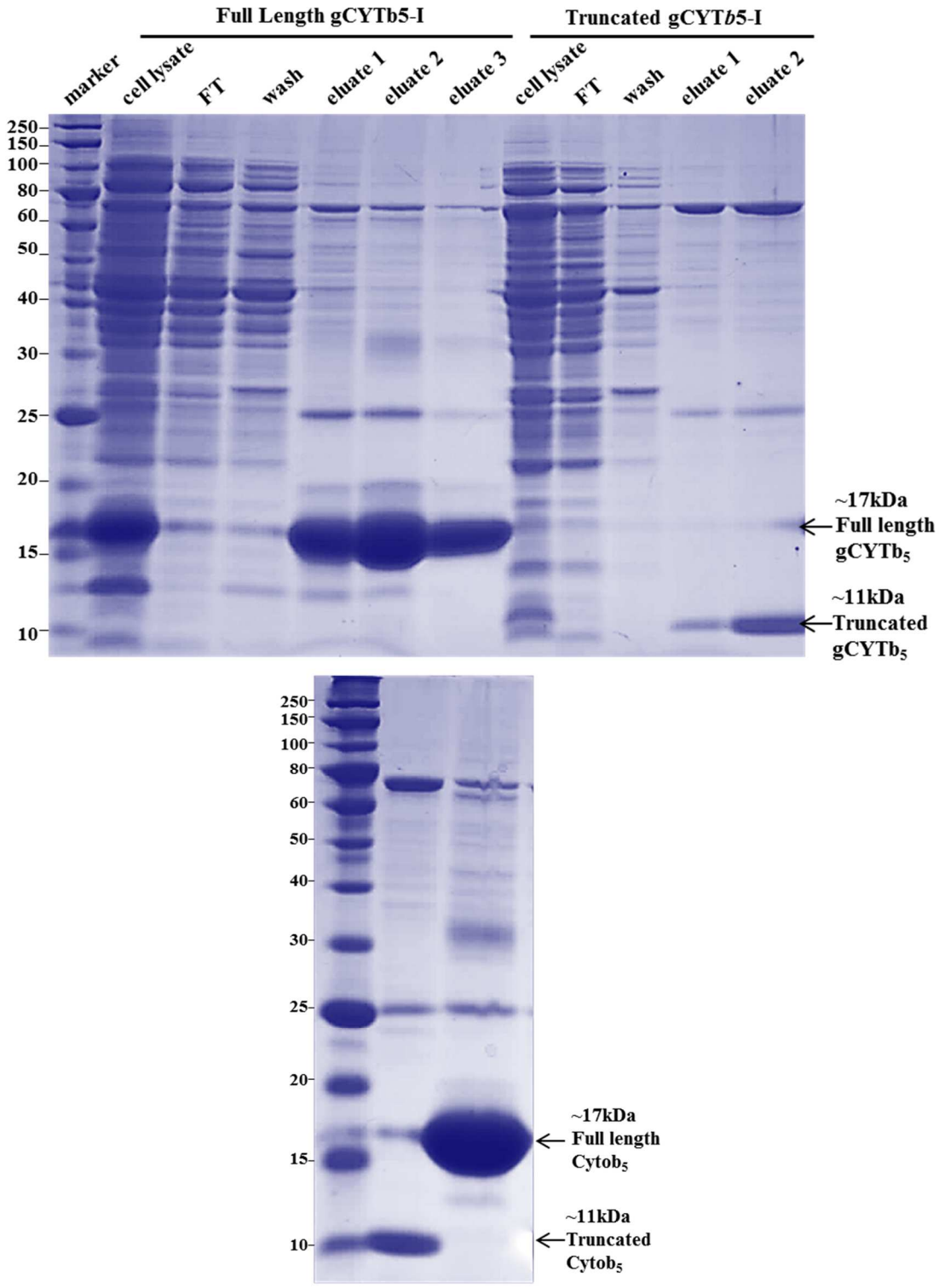

Figure 26: SDS-PAGE analysis of 17-kDa and 11-kDa His_6-tagged gCYT*b*5-I purification using a Co^{2+}–carboxylmethylaspartate (Co^{2+}-CMA) matrix. Shown are the fractions obtained at each step of protein purification: cell lysate, the flow through (FT), the wash material, and the eluate from the column. The 15% gel was visualized by Coomassie staining.

3: *Size exclusion chromatography*

Size exclusion chromatography (SEC) was performed on gCYTb_5-I to determine the protein's quaternary structure. In particular, SEC can discriminate between monomers and dimers. As seen in Figure 27 there is only one peak observed for the cytochrome b_5, indicating that the protein is indeed a monomer. SEC also confirms that the mass of gCYTb_5-I is around 17-kDa since the protein elutes near the same point as the size standard, equine myoglobin, which has a molecular weight of 17 kDa.

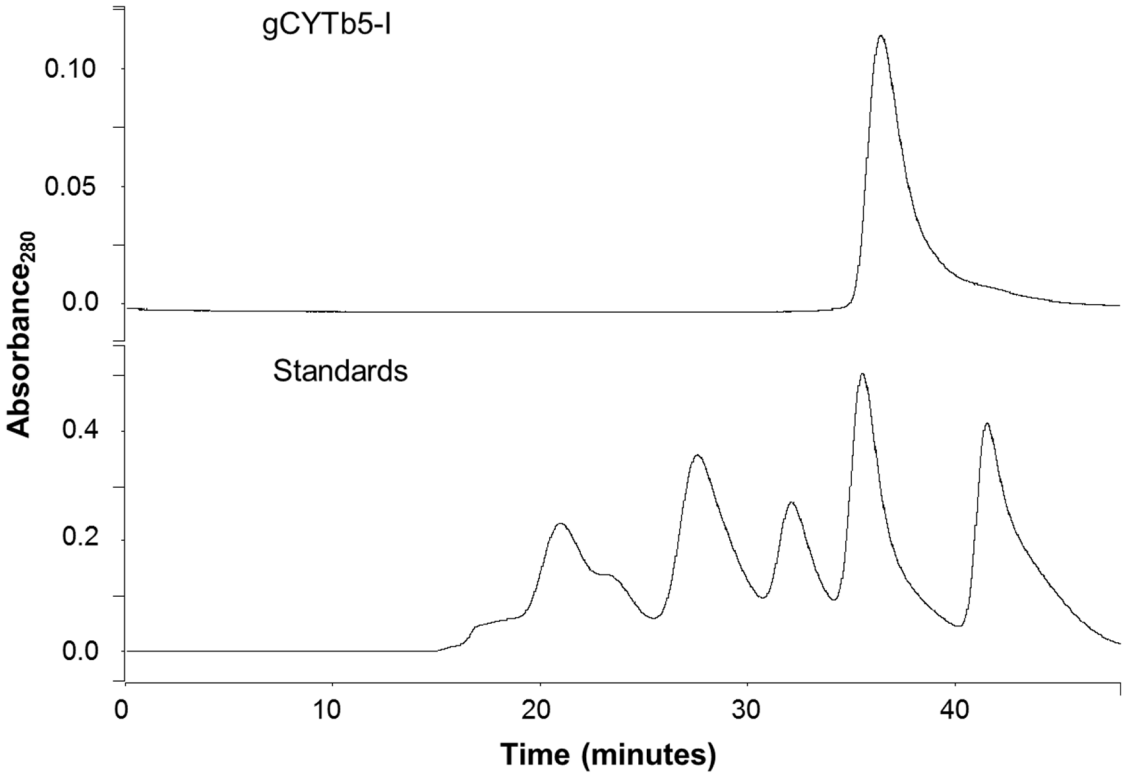

Figure 27. Size exclusion chromatogram of gCYT*b*5-I on Superdex 200 (top). Bio-Rad calibration standards (below). From the left, thyroglobulin (M_r 670,000), bovine gamma globulin (M_r 158,000), chicken ovalbumin (M_r 44,000), equine myoglobin (M_r 17,000), and vitamin B12 (M_r 1,350) (Bio-Rad Gel Filtration Standard).

4: *Mass spectrometry*

The mass spectrum of gCYTb_5-I in the positive mode consists of protonated molecular ions in a distribution from 8+ to 14+ charge states with the maximum intensity at 11+ charge state (*m/z*=1568). Calculating the mass from these peaks result in an average mass of 17187 Da which is expected as the mass obtained from the sequence of the gCYT*b*5 is 17250 Da and SDS-PAGE is around 17 kDa. In the average mass spectra (Figure 28), there is also a peak at 15735 Da, which represents gCYTb_5-I without the histidine tag (15087 Da). The protein was subjected to negative ion mass spectrometry and a similar charge state distribution was obtained with mass of around 17201 Da (Figure 29).

The mass spectrum in Figure 30 detects apo-protein at a low pH (2.8) where the protein appears to a mixture of folded and unfolded states as shown by the many high charge states in the range 16+ to 20+. In this experiment, the cone voltage (CV) was varied from 40 V to 70 V and finally to 100 V. It was observed that the most intense peaks were 20+ to 11+, 16+ to 10+ and 13+ to 7+ charge states, respectively. This pattern shows that an increase in CV results in the charge state distribution (CSD) more closely resembling the CSD of native gCYTb_5-I (pH=7.0). One explanation for this pattern, based on relative sensitivity, is that at a low CV of 40 V, the low charge folded peak are accompanied by a tail of high mass peaks which can be attributed to the formation of solvent clusters. As the CV increases, the heating source causes the solvent to be dissociated from the protein and thus there is a reduction in the high mass tail along with an increase in peak intensity. Another explanation is based on cone voltage induced in-source dissociation, where the cone voltage is used to induce proton stripping to restore proteins to their native state.

$$[Protein + nH]n^{+} \rightarrow [Protein + (n\text{-}1)H](n\text{-}1)^{+} + H^{+} \qquad (12)$$

Table 4. Sample calculation for mass of His-tagged Giardia cytochrome b_5 from mass spectrometry.

Positive Ion mode		
Charge state	**Peak (*m/z*)**	**Unprotonated mass (Da)**
10	1724.1	17219
11	1568.1	17210
12	1434.7	17161
13	1325.1	17156
Average mass (Da)		**17187**

Negative Ion mode		
Charge state	**Peak (m/z)**	**Unprotonated mass (Da)**
8	2154.3	17226
9	1914.9	17225
10	1724.1	17331
11	1568.1	16862
12	1434.7	17347
13	1325.1	17213
Average mass (Da)		**17201**

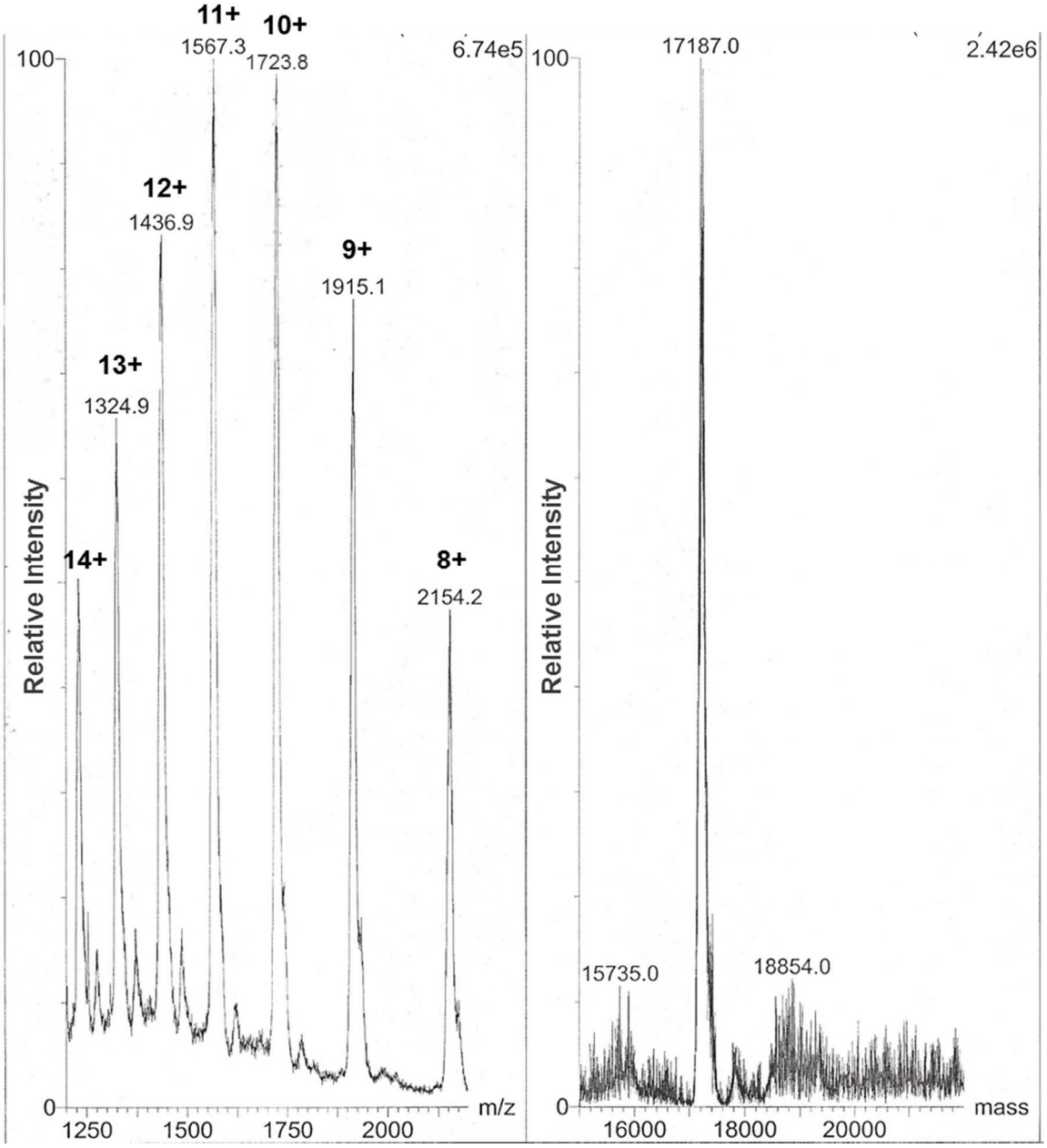

Figure 28. Electrospray ionization mass spectra of native gCYT*b*5-I
(A) Positive-ion ESI mass spectra of a 52 μM solution of his-tagged gCYT*b*5-I obtained with a Quattro™ LC-MS/MS triple-stage quadrupole mass spectrometer (TSQMS) at a cone voltage of 100 V. The numbers above some of the peaks with plus signs refer to the number of positive charges carried by the ion. (B) The average mass calculated by Masslynx NT software is 17187 Daltons. Sample calculation is shown in **Table 4**.

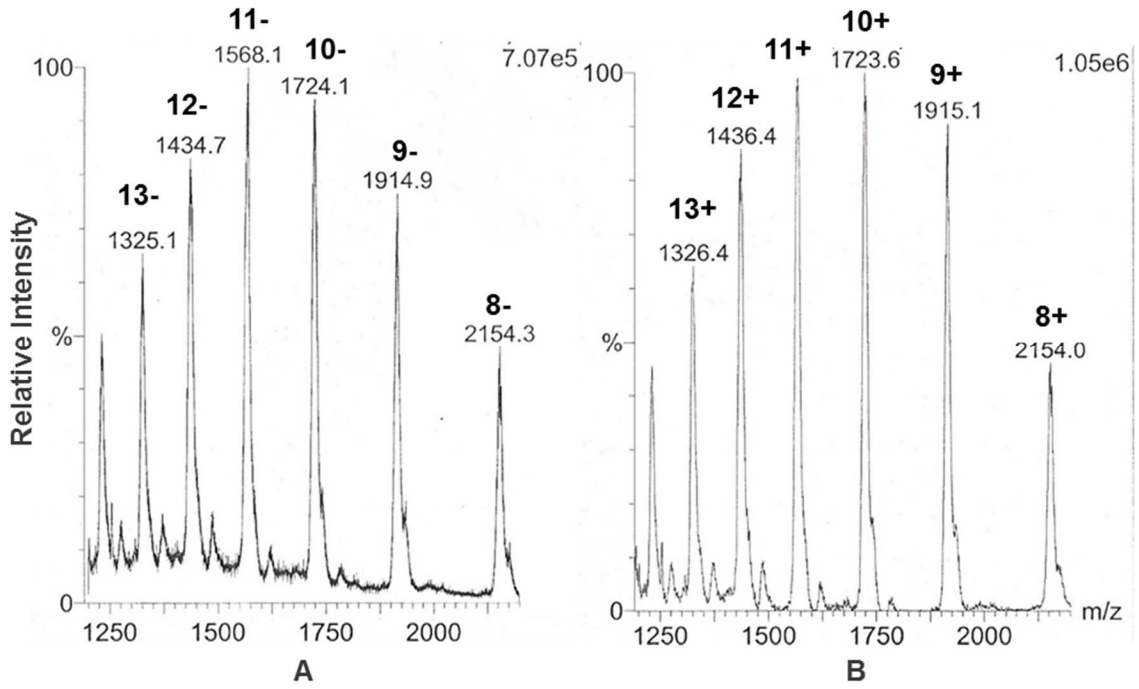

Figure 29. (A) Negative- and (B) positive-ion ESI mass spectra of a 52 μM solution of his-tagged gCYTb_5-I obtained with a Quattro™ LC-MS/MS triple-stage quadrupole mass spectrometer (TSQMS) at a cone voltage of 100 V. The numbers preceding minus or plus signs represent the number of negative or positive charges, respectively, carried by the ion.

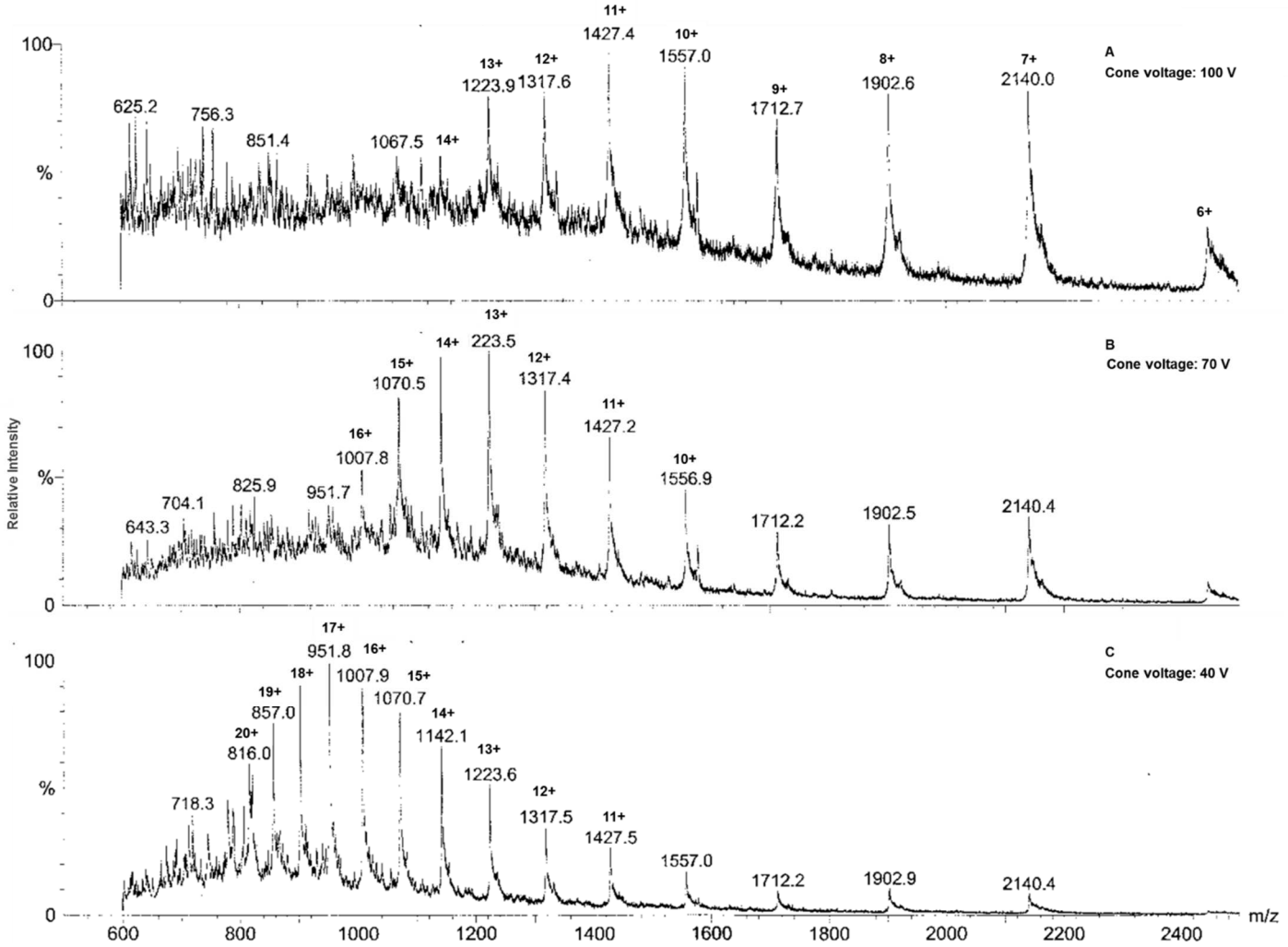

Figure 30 Positive-ion ESI mass spectra of a 52 μM solution of his-tagged Giardia apocytochrome *b*5 (gCYT*b*5-I with heme removed, pH 2.82) obtained with a Quattro™ LC-MS/MS triple-stage quadrupole mass spectrometer (TSQMS) at a cone voltage of (A) 100 V, (B) 70 V and (C) 40 V. The numbers above some of the peaks with plus signs refer to the number of positive charges carried by the ion.

5: *UV-Visible Spectra of Giardia Cytochrome b_5*

The UV-Visible electronic spectra of the oxidized and reduced forms of both full length and the truncated cytochrome b_5 from *Giardia lamblia* are shown in Figure 31. The main features of gCYT*b*5-I are a Soret (γ) peak maximum at 410 nm for the oxidized protein that shifts to 423 nm and increases in magnitude for the reduced protein, and the splitting of α (558 nm) and β (529 nm) peaks in the reduced form of protein. The spectrum of the full-length gCYT*b*5 closely resembles those previously reported from other organisms, including bovine, rat, human (Nóbrega *et al.* 1969). The maximum wavelength of absorbance of gCYT*b*5 in comparison to other organisms is given in Table 5.

The absorption spectrum of the truncated gCYT*b*5 is also identical to the full-length gCYT*b*5. This indicates that the flanking sequences are not required to bind heme. However, the protein expression level of the truncated protein is comparatively low, indicating that the flanking regions have an effect on the stability of the protein.

a

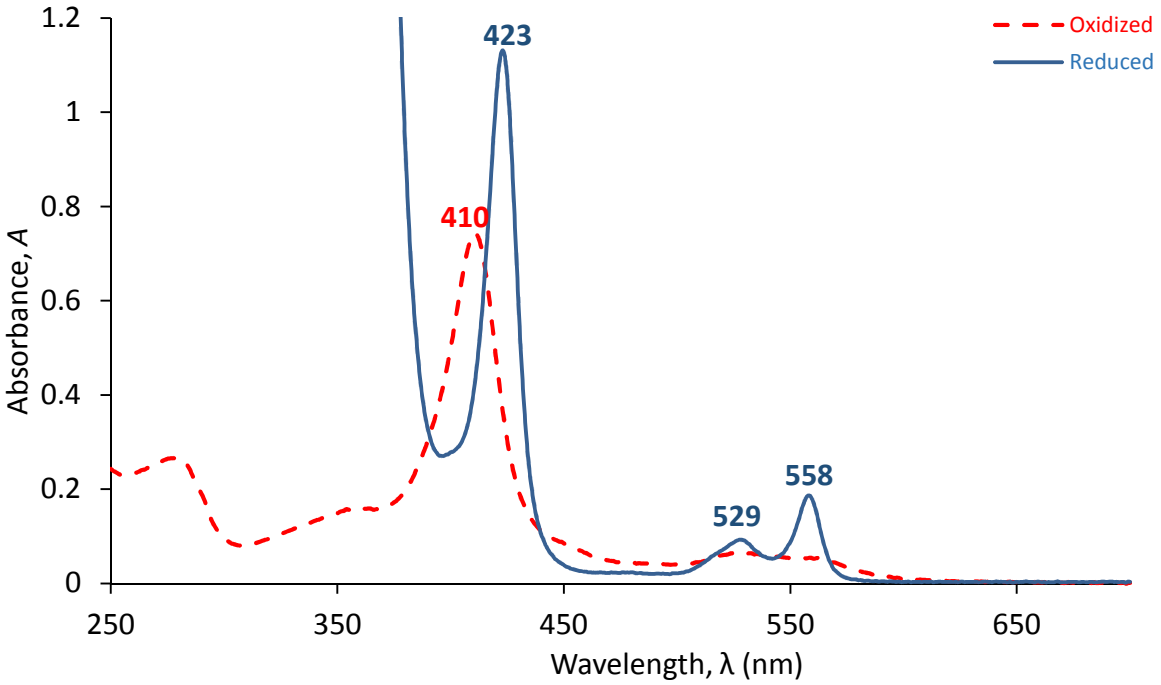

b

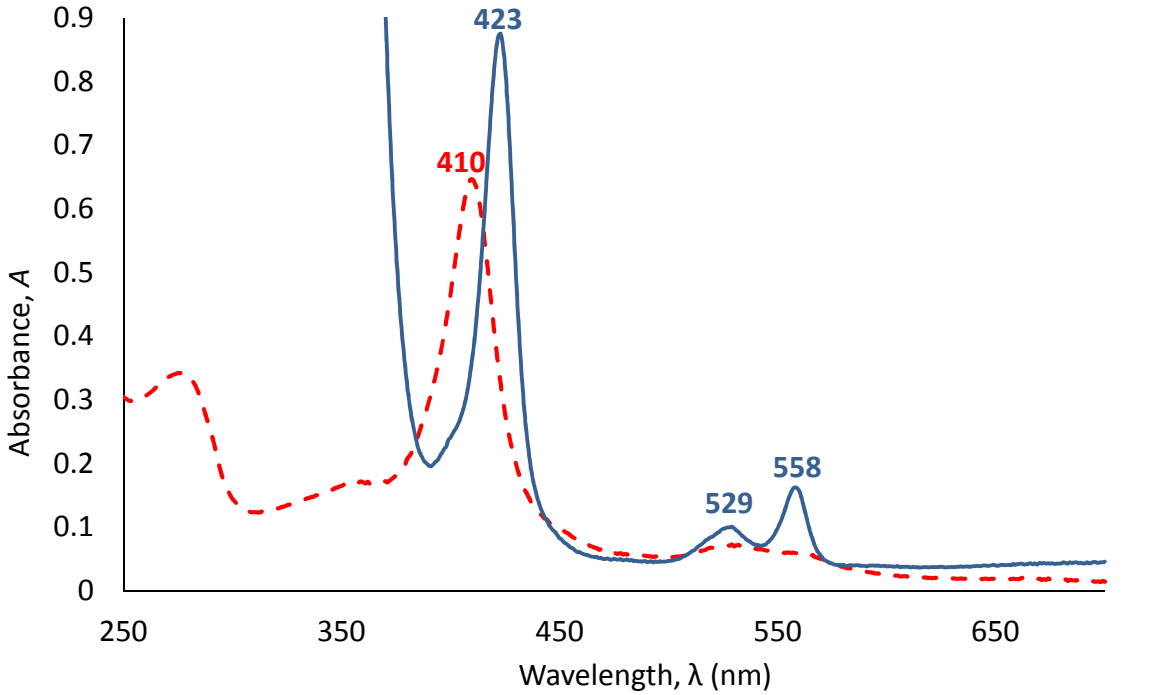

Figure 31: UV-Visible spectra of oxidized (Fe^{3+}) and reduced (Fe^{2+}) states of Giardia cytochrome *b*$_5$. Sodium dithionite ($Na_2S_2O_4$) is used as the reducing agent. (a) Full length protein (b) Truncated protein with only heme binding domain present. The visible bands appear prominently in the reduced spectrum with the α band occurring at 558 nm and the β band occurring at 529 nm. The Soret band shifts from 410 nm in the oxidized state to 423 nm in the reduced state.

Table 5: Comparison of the spectroscopic properties of *Giardia lamblia* cytochrome b_5 to outer mitochondrial membrane cytochrome *b*5 of other organisms

Species	Soret (γ) peak		β peak	α peak
	Oxidized	Reduced	Reduced	Reduced
Giardia lamblia (Alam *et al*. 2012)	410	423	529	558
Bovine heart (Mc*b*5) (Yu *et al*. 1975)	415	429	532	563
***Rattus norvegicus* liver (OM*b*5)** (Ito 1980)	414	423	526	555
***Nicotiana tabacum* leaf *b*5** (Smith *et al*. 1994)	413	423.5	527	558
Saccharomyces cerevisiae (Lin & Beattie 1978)		430	532	562
***Ectothiorhodospira shaposhnikovii b*558** (Kusche & Trüper 1984)	414	425	527	558

6: *Resonance Raman Spectroscopy*

The high-frequency region of gCYT*b*5-I resonance Raman spectra indicates that the protein is six coordinate and low-spin (Figure 32a). The ν_4 vibration mode, which is sensitive to the electron density on the heme and the oxidation state of the heme iron, was found at 1374 cm^{-1} suggesting that the heme iron was in oxidized state. The ν_3 mode, which is sensitive to the coordination and spin state of heme iron, was at 1507 cm^{-1}, indicating a hexa-coordinated low-spin oxidized heme. The ν_2 band at 1582 cm^{-1} further supports a six-coordinate heme in the low spin state. In the ferrous state of gCYTb_5-I (Figure 32a), the frequency of ν_4 (1362 cm^{-1}), ν_3 (1494 cm^{-1}) and ν_2 (1586 cm^{-1}) are also suggestive of six-coordinate low-spin heme similar to those of microsomal cytochrome b_5. Overall, the spectroscopic features of both the ferric and ferrous states are consistent with hexacoordination of the heme, with His^{65} and His^{88} as the likely axial ligands provided by the protein.

In addition to the porphyrin vibrational modes, a vinyl νC=C stretching mode is observed around 1631 cm^{-1} that can provide some information about the interaction between heme and its protein environment. However, its overlap with the ν_{10} vibration mode along with the presence of a spurious band at 1641 cm^{-1} complicates the identification of the vinyl stretch. The band at 1624 cm^{-1} is assigned to the stretching mode of a heme vinyl, while the shoulder near 1630 cm^{-1} could correspond to a second vinyl-stretching mode. These two stretching modes originate from different rotamers in which the double bond C=C has different orientations with respect to the porphyrin ring.

The low frequency region of a resonance Raman spectra is insensitive to the iron oxidation, spin or coordination state and instead the frequencies and relative intensities of these bands characterize the heme pocket and its axial ligands. In the low-frequency region of the resonance Raman spectrum of ferric gCYT*b*5-I (Figure 32b), the heme skeletal modes are assigned as ν_7 (678 cm-1), ν_8 (344 cm-1) and ν_{15} (745 cm-1). In addition to these modes, we note that the line at 377 cm^{-1} is in the frequency region of modes frequently referred to as the propionates bending modes, $\delta(C_\beta C_c C_d)$, although this region also contains contributions from pyrrole ring deformations (Rwere *et al.* 2008). The 377 cm^{-1} frequency is similar to that of other heme proteins in which the propionates form hydrogen bonding interactions with structured surrounding groups, such as amino acids side chains of the polypeptide chain (Chen *et al*. 2003, Chen *et al*. 2004).

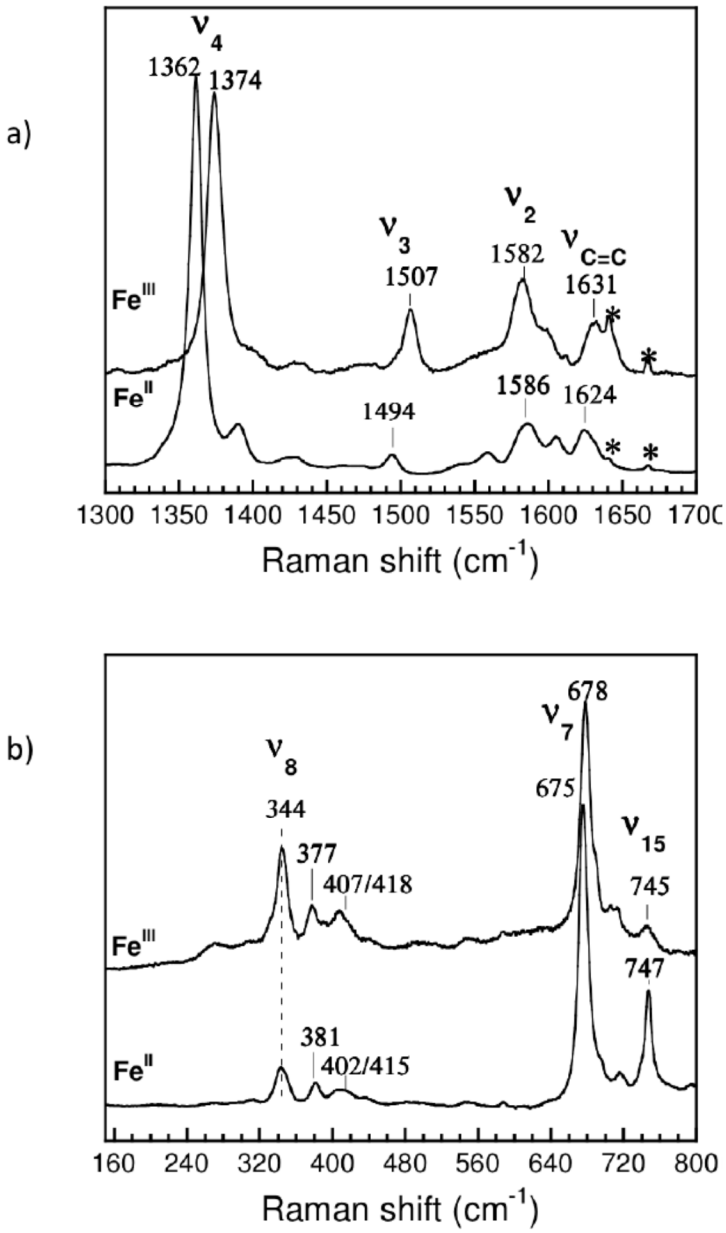

Figure 32: Resonance-Raman spectra of gCYT*b*5-I in the oxidized and reduced states as a function of laser power with 413 nm excitation. (a) High-frequency region. (b) Low-frequency region. The asterisks mark sharp lines arising from light scattering by the experimental set-up, not from the samples. The ν_3 and ν_4 bands of the resonance Raman spectra are sensitive to the iron oxidation states, spin states, and coordination number.

7: *Thermal denaturation*

Cytochrome b_5 was stable at higher temperature as the thermal ramp experiment showed that the protein precipitated at temperatures greater than 40°C.

8: *pH Dependence*

The pH dependence studies revealed that gCYT*b*5-I is unstable below pH 6 and above pH 8 (Figure 33). Cyclic voltammetric experiments at UBC revealed that the protein precipitates at pH 6.0. This was not evident in our pH-dependent studies as precipitation was not observed until pH 5.5. Within this pH range observed there is no significant change in the spectrum of the protein, suggesting that the coordination environment remains intact.

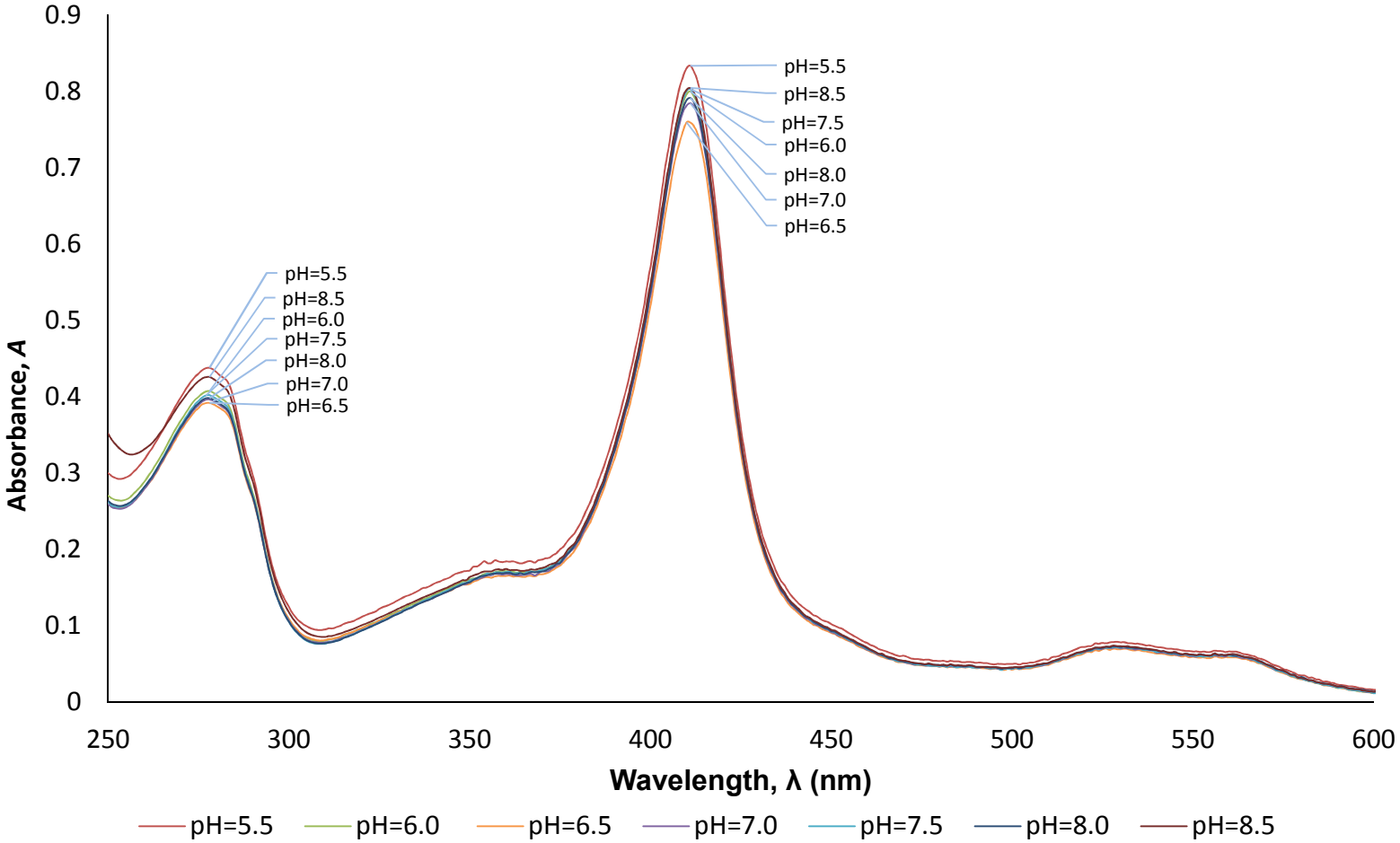

Figure 33: UV-Visible spectra of oxidized (Fe^{3+}) Giardia cytochrome *b*5 in buffer with pH 5.5 to 8.5. The Soret band shifts from 410 nm in the oxidized state to 423 nm in the reduced state.

9: *Oxidation reduction potential of Giardia cytochrome b_5*

9.1: Cyclic voltammetry

The cyclic voltammogram in Figure 34 shows that the half-wave potential of gCYT*b*5-I occurs at approximately -407 mV vs. SCE, which corresponds to -165 mV *vs*. SHE, which is much more negative than the values for cytochrome b_5 from other organisms measured under similar experimental conditions (Table 6).

Table 6: A comparison of the oxidation reduction potential of cytochromes b_5 from different species determined using cyclic voltammetry

Source organism	Potential (mV vs SHE)	Electrode	Electrode modification	References
Giardia lamblia	**-167**	Indium tin oxide		Alam *et al.* 2012
bovine microsomal	**0±2**[a]	gold	β-mercaptopropionic acid	Rivera *et al.* 1994
rat OM	**-78**[a] **-43**[b] **-8**[c] **8**[d]	gold	β-mercaptopropionic acid	Rivera *et al.* 1994
rat OM	**-72**[e] **-63**[f]	gold disk	β-mercaptopropionic acid	Rivera *et al.* 1998
rat OM	**-27**	glassy carbon	thin film of the cationic surfactant DDAB	
rat OM	**-43**[b] **-26**[c,d]	indium tin oxide	poly-L-lysine	Wirtz *et al.* 2000
human erythrocyte	**-9±2**	gold	KCTCCA peptide	Lloyd *et al.* 1994
human cytochrome b_5	**-19.5**	gold	β-mercaptopropionic acid	Aono *et al.* 2010
house fly	**-26**	gold	β-mercaptopropionic acid	Guzov *et al.* 1996

[a]0.2 mM $Cr(NH_3)_6^{3+}$
Poly-L-lysine to b_5 ratio= [b]0.5, [c]1.0, [d]2.0
Poly-L-lysine MW = [e]3970, [f]9000

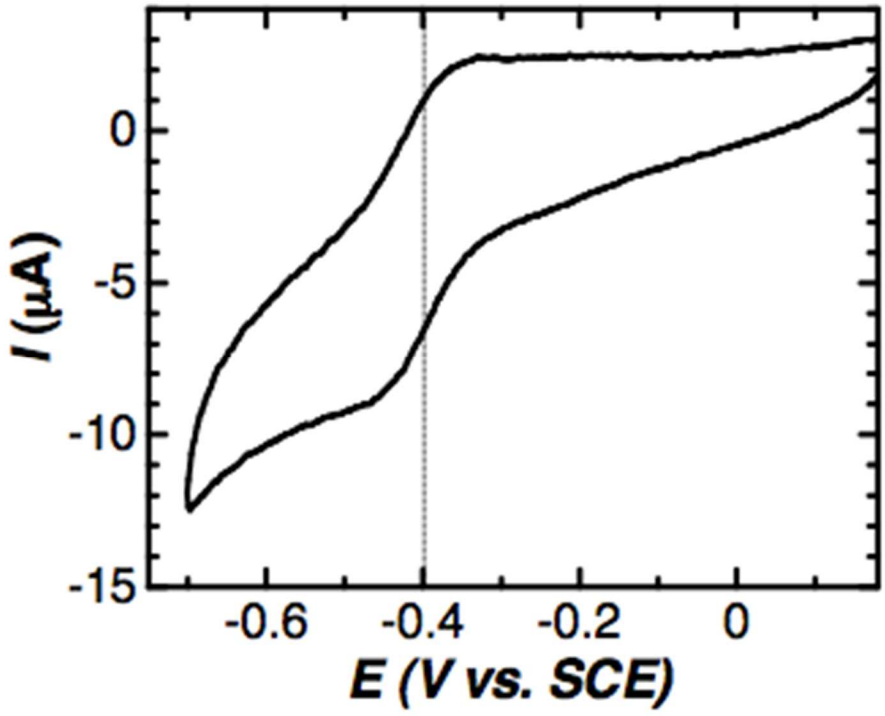

Figure 34: Cyclic voltammogram of gCYT*b*5 in 50 mM sodium phosphate, 150 mM NaCl, pH 7.4. The voltammogram was obtained using an indium tin oxide working electrode, saturated calomel (SCE) reference electrode (E° = +242 mV vs. SHE) and platinum wire counter electrode at a scan rate of 100 mV/second.

9.2: Spectroelectrochemistry

The reduction potential obtained from spectroelectrochemistry differed from that obtained from cyclic voltammetry. For spectroelectrochemistry experiments, changes in oxidation state of heme were monitored using UV/Vis spectrometry at both heme α band (558 nm) and the reduced protein Soret band (422 nm). A sample of these spectra are shown in Figure 35a and Figure 36a. The gCYT*b*5-I took approximately 20 minutes to reach equilibrium at a given potential with two mediators. Isosbestic points were observed at 352, 418, 440, 520, 536, 546 and 568 nm. These absorbance data were analyzed according to the Nernst equation (8) and the corresponding Nernst plots are shown in Figure 35b and Figure 36b. Only two set of experiments yielded a slope (~60) corresponding to one-electron Nernst plot. The potential obtained from these two experiments yield a midpoint potential of -246 and -211 mV vs. SHE at 558 nm, and -269 and -221 mV vs. SHE at 423 nm. The other experiments that were completed, but did not yield theoretical slope are also included in Table 7.

The effect of mediator on the reduction potential was evaluated. Initial titrations of cytochrome b_5 were done without mediators and were unsuccessful because the electrochemical equilibration was so slow that the protein would start to precipitate. Thus, purified gCYT*b*5-I sample had to be mixed with different concentrations of redox mediators to increase equilibration rate. The mediator concentration in the first experiment were 300 μM for hexaammineruthenium(III) chloride (E°= 50 mV *vs*. SHE) and 600 μM for 2-hydroxy-1,4-naphthoquinone (E°= -137 *vs*. SHE). These concentrations were considerably higher than literature values and thus the mediator concentration for rest of the experiments was adjusted to 6 μM of hexaammineruthenium(III) chloride and 3 μM

naphthoquinone. In one experiment both mediators were present at the concentration of 3 μM, however when the potential was changed for reduction, the spectrum starts to shift up rather than change into a reduced state. This may have been due to protein precipitation although no precipitate could be seen.

The results for gCYT*b*5 spectroelectrochemistry experiments were compared with published values of cytochromes b_5 from different mammals (Table 8). The reduction potential obtained through spectroelectrochemistry is much lower than that from cyclic voltammetry and those reported in literature. It has been previously reported that the reduction potential of cytochrome b_5 may slightly differ depending upon the technique used, with CV yielding more positive potentials (Aono *et al*. 2010). Factors that could be responsible for this discrepancy are several experimental design differences. One factor could be a lack of temperature control apparatus in our experiment whereas the setup in published studies carefully monitored the temperature of the system. It has been shown previously that as the temperature increases the potential becomes more negative and thus lack of a stable temperature could cause the variance in data observed (Reid *et al.* 1982). Secondly, a lack of a completely anaerobic environment may cause an increase in time required for the protein to go from oxidized state to reduced state. Although the introduction of nitrogen gas helped in preventing auto-oxidation of the cytochrome, an anaerobic chamber would be useful. Thirdly, the long incubation times required means that not as many steps can be applied as is desirable, as each experiment took a minimum 8 to 10 hours to complete around 30 to 40 steps. Another issue observed was that reactants did not reach equilibrium at each potential, which is why there are many points in the data where change in potential does not result in a change in concentration ratios. Each

equilibrium needed almost 10-15 minutes, which meant experiments took a very long time, and sometimes to strike a balance between protein being denatured and equilibration time, the time between each potential step was shortened. Lastly, our experiment was performed using a very high concentration of protein in a small volume of buffer. Potential measured through spectroelectrochemistry are extremely sensitive to experimental conditions and thus these differences probably led to the more negative redox potential of gCYTb_5 in comparison to others. One way to account for these differences would have been to obtain samples of cytochrome b_5 from other species with well-known potentials and measure their potential using our setup to see if the differences are due to properties of gCYTb_5 or due to experimental conditions.

These experiments were most useful as a method development tool for future spectroelectrochemistry work in this lab, rather than to get accurate reduction potentials. Using these experiments, future students were able to optimize their experiments. For example, owing to the difficulties with baseline drift in the Ocean optics spectrometer, a Cary 400 Bio UV-visible spectrophotometer was used for future studies. The Cary 400 was more sensitive and stable with respect to its baseline as well as at maintaining a constant 22°C temperature in the optic chamber. Another modification that was made was to use argon instead of nitrogen gas for blanketing the sample; argon is 1.4 times denser than nitrogen and thus the gas will blanket the surface of reactants more effectively. In order to prevent evaporation over the course of the experiment by the argon stream, silicone oil was layered on top of the sample. This was important because evaporation of water over the long duration of the experiments could change the concentration of protein in the cuvette affecting the absorbance readings and hence the measured reduction potentials. Lastly, the

equilibration time for each step was increased from 20 minutes to an hour. Following these modifications the reduction potential for gCYTb_5-I through electrochemistry was much closer to the potential obtained through cyclic voltammetry.

(a)

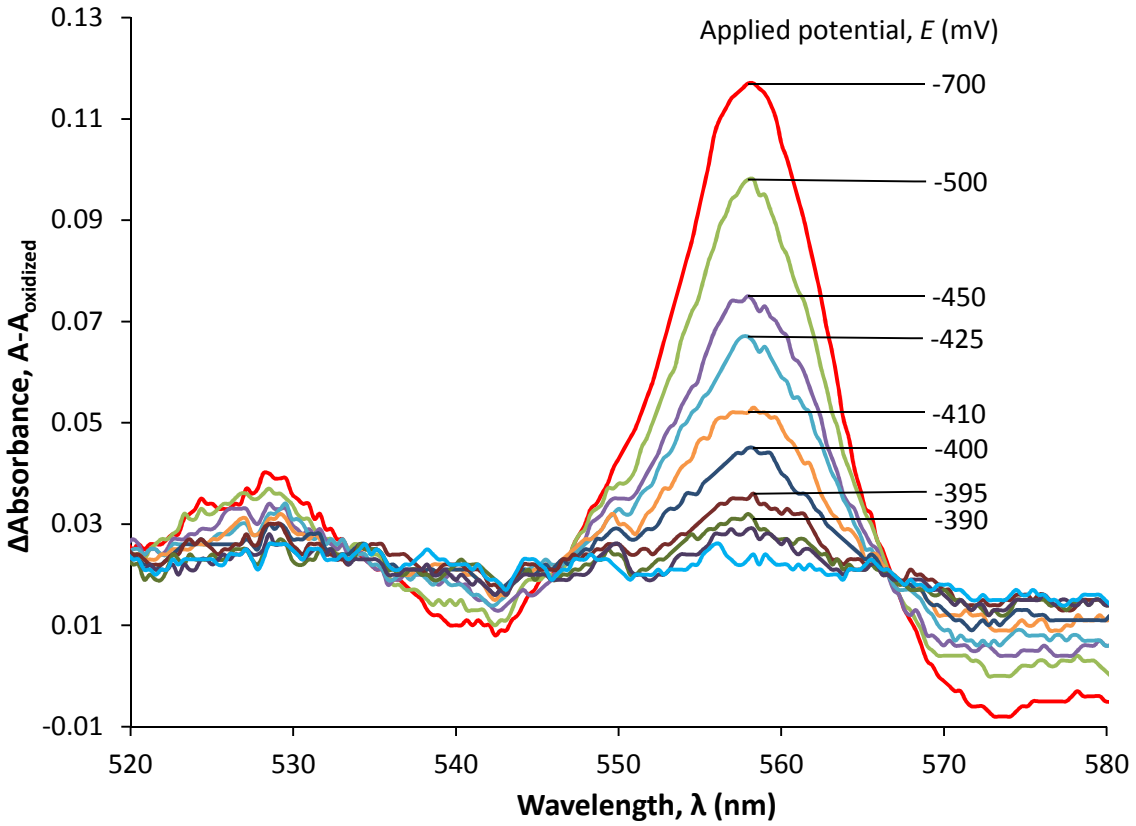

(b)

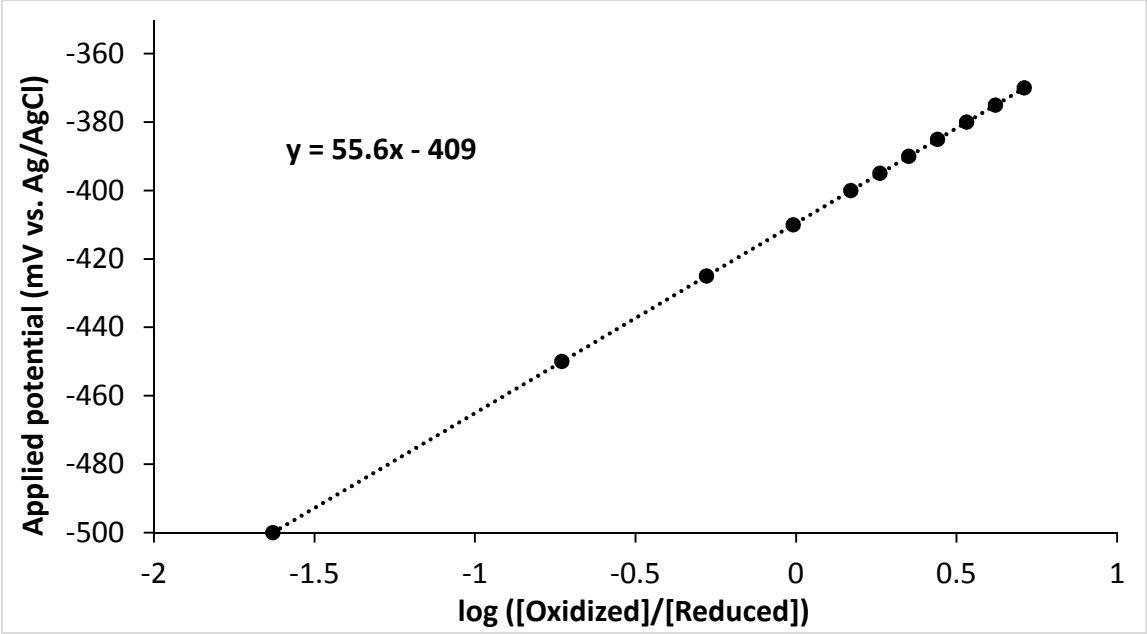

Figure 35: Sample spectroelectrochemical data. **(a)** Difference spectra of Giardia cytochrome b_5 (30 µM) as the applied potential (mV vs. Ag/AgCl) is stepped from reducing to oxidizing values in the presence of hexaammineruthenium(III) chloride and naphthoquinone (3 µM) as mediators in 20mM NaPi buffer (pH=7.4) at 25°C. **(b)** Nernst weighted linear square fit derived from the change in absorbance at α band (558 nm). The calculated midpoint potential is -409 mV vs. Ag/AgCl and Nernst slope is 55.6.

(a)

(b)

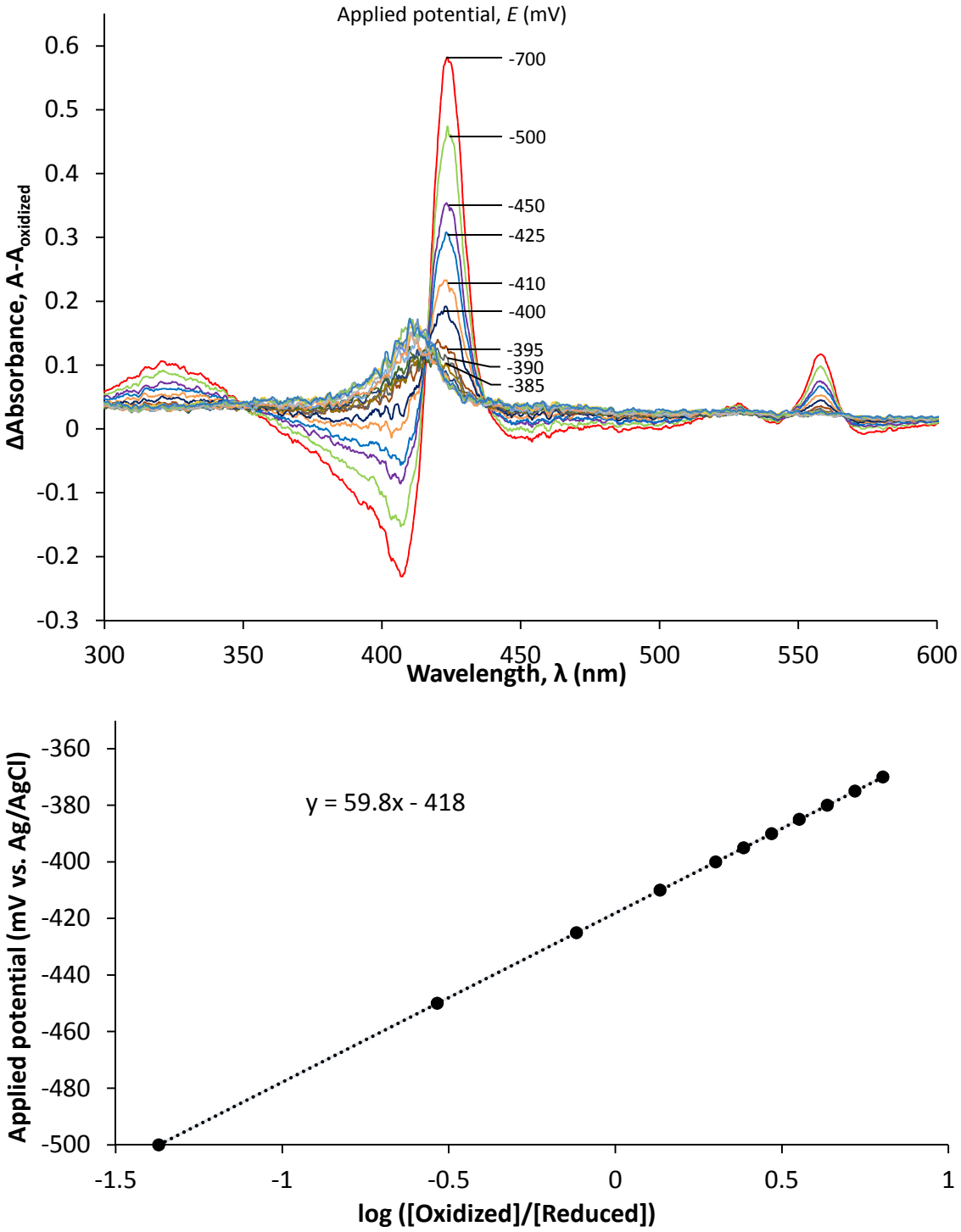

Figure 36: Sample spectroelectrochemical data. **(a)** Difference spectra of Giardia cytochrome b_5 (30 μM) as the applied potential (mV vs. Ag/AgCl) is stepped from reducing to oxidizing values in the presence of hexaammineruthenium(III) chloride and naphthoquinone (3 μM) as mediators and 20 mM NaPi buffer (pH=7.4) at 25°C. **(b)** Nernst weighted linear square fit derived from the change in absorbance at reduced soret peak (422 nm). The midpoint potential is -418 mV vs. Ag/AgCl and Nernst slope is 59.8

Table 7: The nernstian slope and $E_{midpoint}$ vs. Ag/AgCl (y-intercept) values at 558 and 423 nm for gCYTb_5-I from independent experiments.

Exp	λ (nm)	Nernst slope	$E_{1/2}$ vs. Ag/AgCl y-intercept	$E_{1/2}$ vs. SHE	Applied *E* range (mV vs Ag/AgCl)
1	558	165	-259	-62	-450 to -100
	423	137	-288	-91	
2	558	139	-278	-81	-500 to -100
	423	149	-271	-74	
3	558	55	-443	-246	-600 to -360
	423	57	-466	-269	
4	558	56	-408	-211	-500 to -375
	423	59	-418	-221	-500 to -370
5	558	114	-450	-253	-800 to -200
	423	118	-462	-265	
6	558	201	-485	-288	-800 to -200
	423	183	-466	-269	-800 to 0
7	558	116	-428	-231	-700 to -200
	423	141	-444	-247	
8	558	140	-359	-162	-500 to -250
	423	117	-380	-183	

† hexaammineruthenium(III) chloride and naphthoquinone

Table 8: A comparison of the oxidation reduction potential of cytochrome b_5 from different species determined using spectroelectrochemistry. Mc and OM are microsomal and mitochondrial outer membrane cytochrome b_5, respectively.

Source organism	Potential (mV vs SHE)	Electrode	Mediators	References
Giardia	**-237**	gold	$Ru(NH_3)_6^{2+/3+}$ (12 µM) naphthoquinone (3 µM)	this study
bovine Mc	5.1±0.1	gold	$Ru(NH_3)_6^{2+/3+}$ (12 µM)	Reid *et al.* 1982
bovine Mc	-1.9±1.6	gold minigrid	$Ru(NH_3)_6^{2+/3+}$ (0.2 mM) $K_3Fe(CN)_6$ (0.2 mM) methyl viologen (1 mM)	Walker *et al.* 1988
bovine Mc	3±0.1	electrofor med gold	$Ru(NH_3)_6^{2+/3+}$ (12 µM)	Funk *et al.* 1990
bovine Mc	2	gold minigrid	$Ru(NH_3)_6^{2+/3+}$ (10 µM)	Yao *et al.* 1997
rat OM	-102±2	gold minigrid	$Ru(NH_3)_6^{2+/3+}$ (0.4 mM) methyl viologen (1 mM)	Rivera *et al.* 1994
rat OM	-102 -70[a] -40[b]	gold minigrid	$Ru(NH_3)_6^{2+/3+}$ (0.30 mM) methyl viologen (1.41 mM)	Rivera *et al*. 1998
rat OM	-102	platinum-foil dithionite	$Ru(NH_3)_6^{2+/3+}$ (200 µM) 2,5-dihydroxy-*p*-benzoquinone (25 µM) anthraquinone-2,6-disulfonate (25 µM)	Wirtz *et al*. 2000
human testis OM	-40	gold	100 µM of $[Ru(NH_3)_6]Cl_3$ and methyl viologen	Altuve *et al* 2004
human erythrocyte	-2	platinum and AgCl	methylene blue, indigodisulphonate,and indigotetrasulphonate	Abe & Sugita 1979
Rabbit	20			
A. suum	78	Redox titration		Yu *et al*. 1996
b_{558}	-210	Redox titration		Kusche and Trüper 1984
b_5 domain of flavocytochrome *b*2	-31±2		Phenazine ethosulfate, Phenazine methosulfate, 3,6-Diaminodurene and Lawsone dimer	Brunt *et al*. 1992

[a]0.2 mM $Cr(NH_3)_6^{3+}$
Poly-L-lysine to b_5 ratio= [b]0.5, [c]1.0, [d]2.0
Poly-L-lysine MW = [e]3970, [f]9000

Even after considering experimental variance, from table 6 and Table 8 it is apparent that the gCYT*b*5-I reduction potential is significantly more negative compared to other family members. There are four factors that may account for such a negative potential: (1) the orientation of the heme within the protein, (2) steric constraints resulting in distortion of the heme, (3) surface charges, and (4) the hydrophobicity of the heme environment (Paoli *et al.* 2002). Out of these factors, we cannot evaluate heme-ligand orientation or the distortion of the heme because homology models are not detailed enough for such analysis, and high quality crystal structures will be required

Charged residues on the surface of the protein that line the exposed heme edge of cytcochrome b_5 have electrostatic effects on the heme and modulate its reduction potential (Rivera *et al*. 1998). In microsomal cytochromes b_5, negatively charged acidic residues (glutamate and aspartate) stabilize the oxidized (Fe^{3+}) state relative to the reduced state (Fe^{2+}) and cause the redox potential to be more negative (Rodgers and Sligar 1991). When these charges are neutralized by the addition of polylysine, the reduction potential increases (Rivera *et al*. 1998). Consistent with this explanation is the observation that the soluble cytochrome b_5 of *Ascaris suum*, which has few acidic residues near the heme edge, has a higher reduction potential (Yu *et al*. 1996). Interestingly, in gCYT*b*5-I, neutral residues occupy several positions where conserved acidic residues are normally found in the microsomal proteins, including Trp^{64}, Asn^{85}, and Val^{91}, and at position Lys^{69} the charge is actually switched from negative to positive (Figure 37a). Based on mutational studies done on microsomal cytochrome b_5 such differences would be expected to lead to a more positive redox potential in gCYT*b*5-I (Rodgers and Silgar 1991; Xue *et al*. 1999). However, this is not the case, as gCYT*b*5-I has a more negative redox potential as

compared to any other species. However influential surface charges are on the reduction potential of microsomal cytochromes b_5 they have little effect in determining the properties of gCYT*b*5-I.

The hydrophobicity or polarity of the heme environment regulates the stability of the oxidation state of the heme iron. In a nonpolar environment the neutral Fe^{2+} state is more stable than the charged (+1) Fe^{3+} state and thus the reduction potential tends to be more positive for a heme surrounded by nonpolar residues (Funk *et al*. 1990; Kassner 1972). Conversely, in a hydrophilic/polar environment the reduction potential of heme tends to be more negative (Yao *et al*. 1997). Several positions at which conserved hydrophobic amino acids are found within the heme pocket of microsomal and mitochondrial cytochrome b_5 are occupied by polar ones in gCYT*b*5-I (Figure 37b). For example, gCYTb_5-I has a tyrosine at position-61, which in microsomal cytochromes b_5 is a phenylalanine residue (position-35). Previous spectroelectrochemical studies involving bovine cytochrome b_5 has shown that mutation of this residue to tyrosine (position-35) lowers the reduction potential from +2 mV to -64 mV vs SHE due to the stabilization of oxidized state relative to the reduced state (Yao *et al.* 1997). Recently, in our lab the redox potential of a mutant, gCYT*b*5-I Y61F, was measured through electrochemistry and the potential of gCYTb_5 is raised by 100 mV vs SHE. This shows that the tyrosine 61 residue is indeed responsible for the low potentials observed in gCYT*b*5-I.

Conversely, there are also sites where gCYT*b*5-I possesses hydrophobic residues in the heme environment whereas hydrophilic ones occur in the mammalian proteins; these include Phe^{75}, Ile^{80}, and Ile^{93}, which are occupied by Gln^{49}, Ala^{54}, and Ala^{67} respectively in bovine microsomal cytochrome b_5. While these differences should result in a more

positive potential in gCYTb_5-I, their contribution is not as significant as those differences that favor a lower potential. Tyr^{61} has a greater impact on the reduction potential because it is buried deeper in the protein and the presence of a polar tyrosine residue so close to the ligand would disturb the hydrophobicity of the heme pocket more than residues further away from the histidine ligand.

Ectothiorhodospira shaposhnikovii b_{558} is another species, which has replaced the phenylalanine residue with tyrosine. *E. shaposhnikovii* b_{558} has redox potential of −210 mV determined through redox titration (Kusche and Trüper 1984 and Kostanjevecki *et al.* 1999), which is much more negative than other cytochrome b_5.

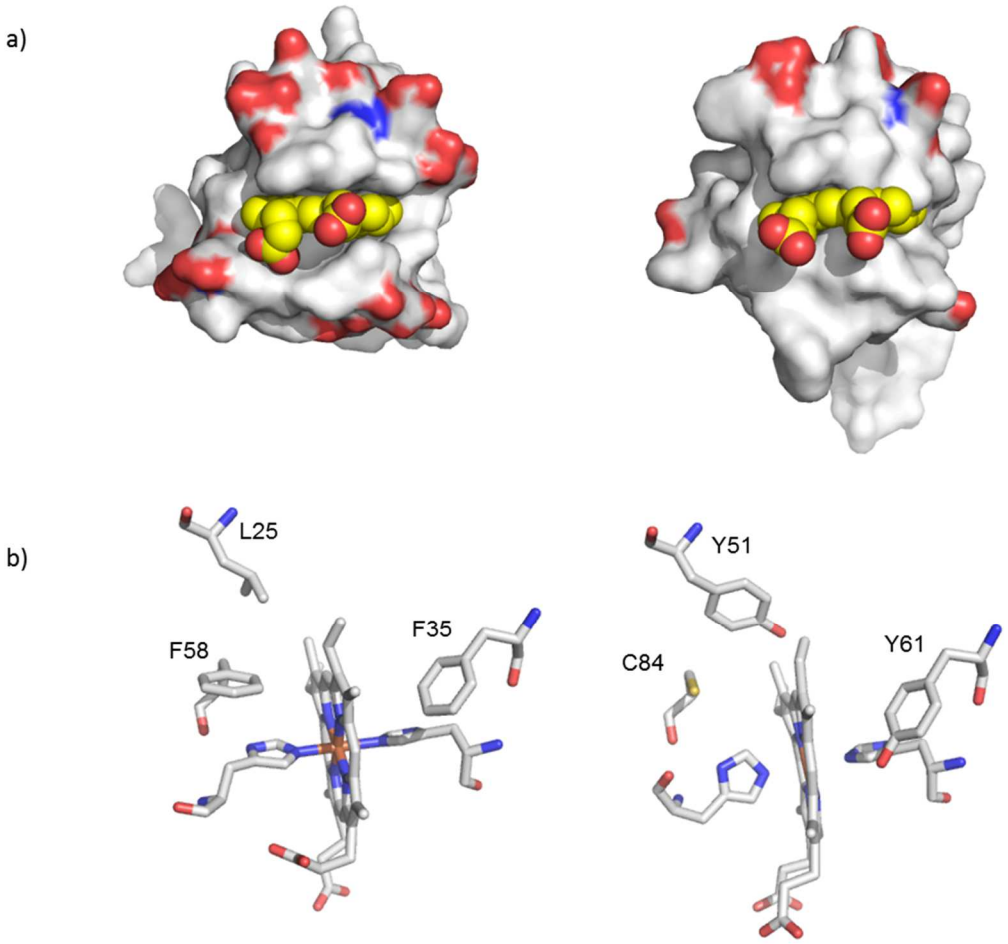

Figure 37: Structural differences between gCYTb_5-I and microsomal cytochrome b_5 (1cyo.pdb). a) Surface charge distribution of acidic residues on microsomal cytochrome b_5 (left) and the model of gCYTb_5-I (right). b) Sites at which hydrophobic residues of microsomal cytochrome b_5 (left) are replaced by hydrophilic residues in gCYTb_5-I (right) in the heme-binding pocket that may contribute to the low oxidation-reduction potential of the Giardia protein.

10: *NMR Spectroscopy*

The homology modeling technique was limiting because it was not able to model the amino and carboxy ends of gCYT*b*$_5$-I and the model also lacked details on the protein structure, such as heme-ligand orientation. Nuclear magnetic spectroscopy (NMR) can provide detailed 3-D structural information, such as orientation of heme-ligands within the protein, interaction of heme with side chains as well as additional information about the electronic structure of protein and process and strength of heme binding. This study was the starting point for further NMR studies on gCYT*b*5-I.

The low spin iron in the heme of cytochrome b_5 has unpaired electrons, which causes the resonance of substituents in porphyrin ring to shift to the low field, high frequency region (10-35 ppm) of the ^{1}H NMR spectrum away from the overlapped diamagnetic region of 0-10 ppm (Walker *et al.* 1988) where most protons on the protein will have peaks. The 1D ^{1}H NMR spectrum of gCYTb_5-I was obtained and analyzed by Shin-ichi J. Takayama at UBC (Figure 38). The spectrum shows very broad paramagnetic signals in comparison to the rat outer mitochondrial cytochrome b_5 (Rivera *et al.* 1992) and bovine cytochrome b_5 (Lee *et al.* 1990). Despite the broad peaks of the spectrum, it can be used to make a few predictions about gCYT*b*5-I. Firstly, there are no broad signals observed above 50 ppm, which indicates that the protein is in the low spin state. Secondly, there are no low spin signals above 25 ppm, which means unpaired electron density is less localized and more uniformly spread upon heme. Thirdly, the quantity of the paramagnetic signals observed are more than what would be expected for a protein with heme incorporated in one orientation. This indicates that gCYT*b*5-I binds heme in two orientations and thus has a rotational isomer (Walker *et al.* 1988). Finally, examination of

the spectrum using Ann Walker's analysis the ligand plane angle is in the range of 140 to 180 degrees, similar to other cytochromes b_5 (Shorkhirev and Walker 1998).

The 2-D Heteronuclear Single Quantum Coherence (HSQC) ^{1}H-^{15}N spectrum (Figure 39) contains around 110 peaks, 102 of them attributed to secondary amide groups and 8 corresponding to the side chain amide groups of glutamine and asparagine. Two of the three tryptophan side-chain Nε-Hε groups are also visible. Considering that gCYTb_5-I has 131 residues, of which 8 are proline, we expect to see 123 backbone amine peaks. However, not all the N-H bonds are observed in HSQC spectrum. It is possible that the unstructured amino and carboxy terminal region of the protein was preventing us from getting the full structure of the protein. Further experiments where these ends are removed and only the core protein with the heme binding domain is present can help us obtain a structure. Removing the heme and getting the structure of the holo and the apoproteins could help determine the process of heme binding.

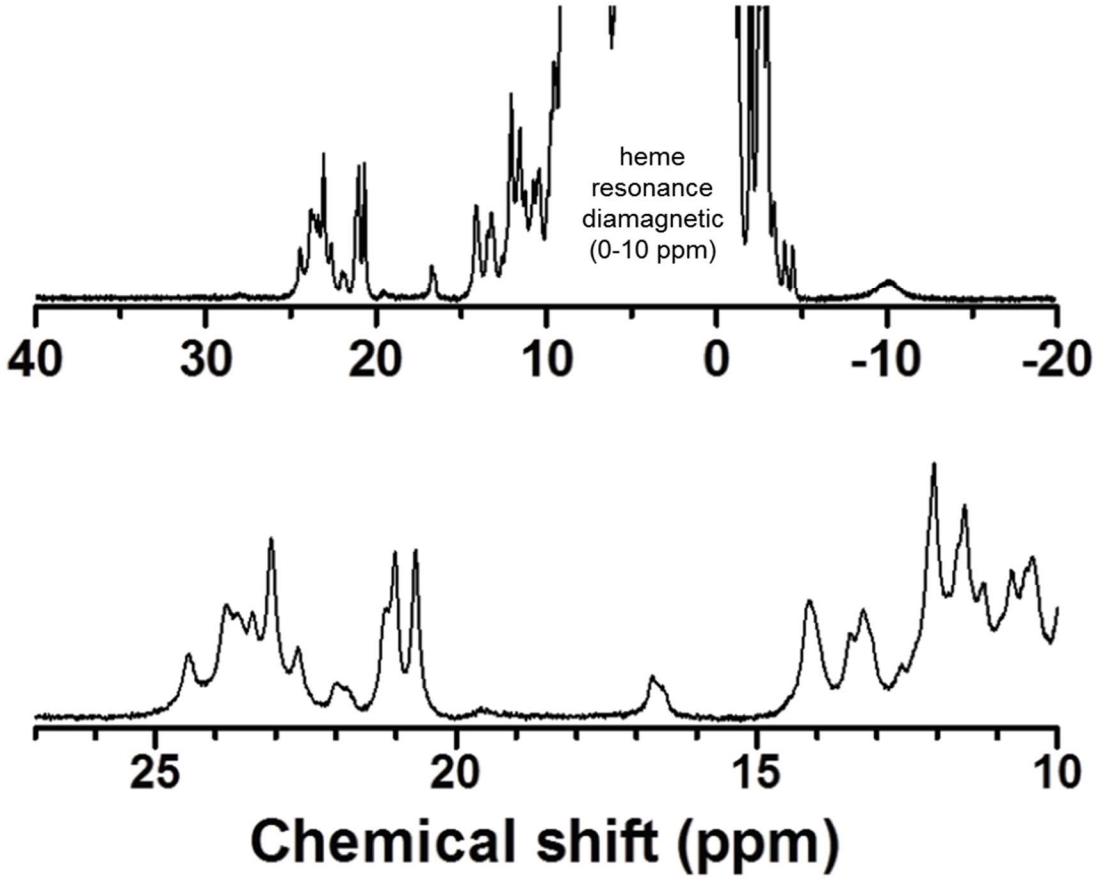

Figure 38: ^{1}H NMR spectrum of oxidized 2 mM Giardia cytochrome b_5-I recorded in D_2O

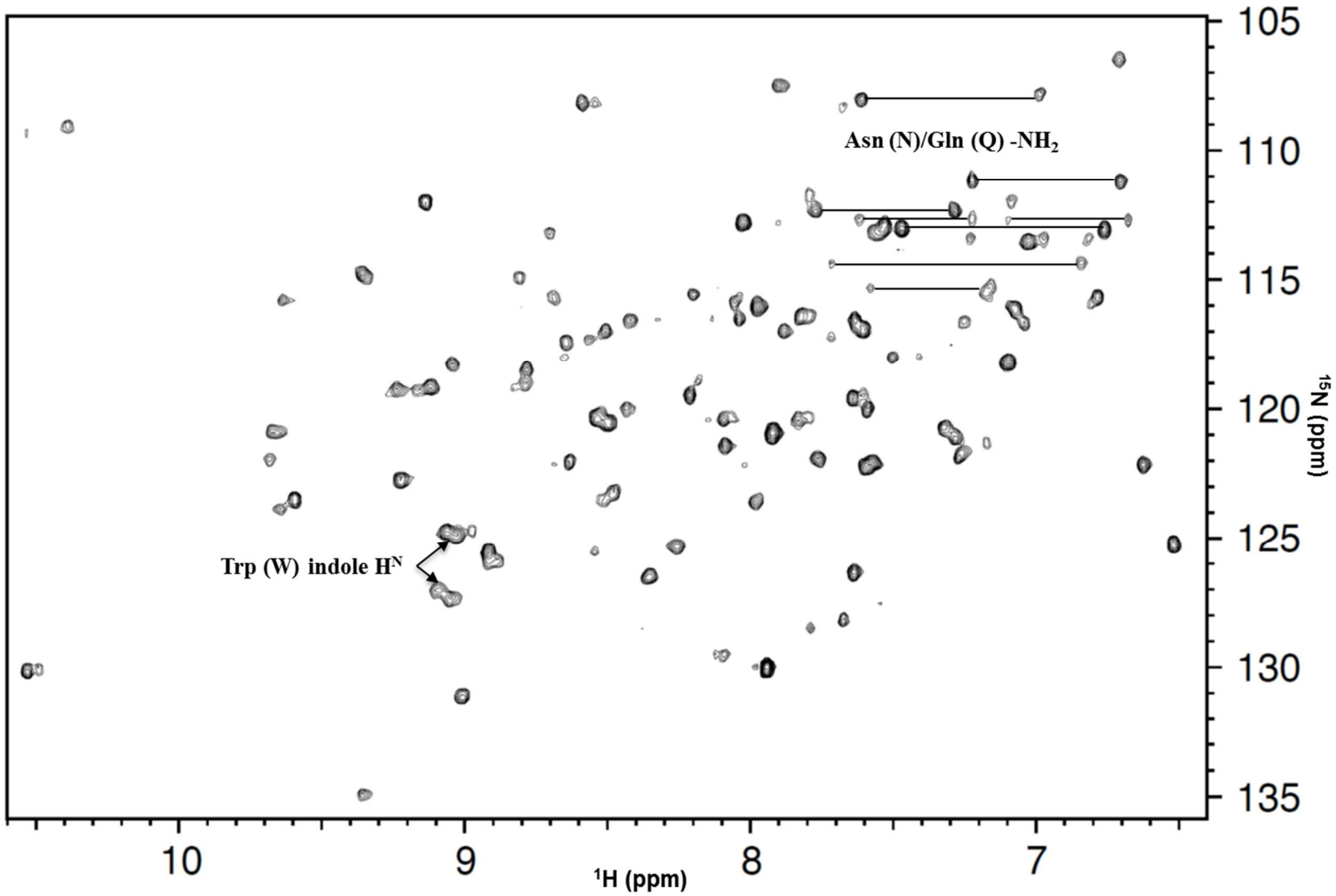

Figure 39: HSQC spectrum of ^{15}N enriched gCYTb_5-I (94 µM) in PBS at 30°C 256 scans/FID

11: *The three isotypes of gCYTb$_5$*

Giardia has three cytochromes b_5 that are similar in their core sequences, sharing 36-41% amino acid identity, as well as unusual variation at position-84 in which small residues replace larger ones typically found in other cytochromes b_5 (Figure 40). Collectively these three sequences have about the same identity in their cores to proteins from the other eukaryotes, including protists, fungi, plants and metazoans, suggesting that Giardia possessed these genes since its divergence from the rest of the eukaryotic lineage.

The amino- and carboxy-terminal flanking sequences of the three gCYTb_5s are not conserved among these isotypes, and BLAST searches of these sequences identify no counterparts in other cytochromes b_5. However, the N-terminal flanking regions of the three Giardia proteins do share similar properties (Figure 40). All of these regions are of similar length, have basic isoelectric points and have the same predicted secondary structure pattern of a central α-helix (11-18 residues) followed by a short β-strand. The latter is likely an extension of the N-terminal sheet common to most cytochromes b_5, as observed in the example of the bovine microsomal cytochrome b_5 (1cyo.pdb). The C-terminal extensions of the Giardia cytochrome sequences are shorter and more hydrophilic than their better-known mammalian counterparts, several of which function as hydrophobic membrane anchors. We note that the C-termini of the Giardia sequences differ in their calculated isoelectric points with those from isotypes I and III being basic (pI ~10) while the one from isotype II is acidic (pI = 4). The variation in charge properties of the flanking sequences could provide a means to target the three cytochromes to different sites within the cell, or to different redox partners.

Figure 40: **Comparison of the Giardia cytochromes b_5 sequences**

(a) The shaded green sequences represent the conserved haem-binding domain, with the predicted axial ligands in bold. The side chains of the boxed residues (C84, A86 and T85 of isotypes I, II, III respectively) are predicted to lie near the coordinating histidine side chain; this position is occupied by a highly-conserved phenylalanine in most other cytochromes b_5. Non-conserved flanking sequences are coloured according to their isoelectric points (red, acidic; blue, basic; cyan, weakly basic). The underlined sequences are the predicted α-helical regions in the N-terminal flanks.

(b) Schematic representation of the variation in isoelectric points of the flanking regions in the three gCYTb_5 proteins. Isoelectric points for the extensions were estimated by the program ProteinParam. The Giardia genome DB accession numbers for these sequences are: GL50803_9089 (gCYTb_5-I), GL50803_27747 (gCYTb_5-II), GL50803_33870 (gCYTb_5-III).

12: *Speculations on gCYTb$_5$ cellular localization and function*

We have shown that *Giardia* encodes at least one functional cytochrome b_5, and subsequent experiments in our lab expressed and characterized isotypes II and III, which are also functional and have the conserved axial histidines residues. The charge variation in the flanking sequences suggests that these might target the cytochromes to specific partners, but the identities of these partners are currently unknown; while the *Giardia* genome has been sequenced, no enzymes known to partner with cytochrome b_5 have been identified. This situation probably reflects the limitations of bioinformatics in identifying homologs of proteins for which sequence divergence is large rather than an absence of such proteins. A pertinent example in *Giardia* is that of fatty acid desaturase activity. *Giardia* lacks genes for recognizable fatty acyl-CoA desaturases, yet axenic cultures of *Giardia* accumulate linoleic (18:9,12) and linolenic acid (18:9,12,15) when grown in the presence of oleic (18:9) acid (Ellis *et al.* 1996)

The likely electron sources for these cytochromes are flavoenzymes that receive their electrons from NAD(P)H, of which several have been characterized. Many more are known by sequence similarity, as it is easier to identify the presence of a folding domain by sequence (such as a Rossmann fold) than it is to assign the precise function of an enzyme that possesses such a domain. Interestingly, *Giardia* possesses a gene for a cytochrome P450 reductase (*Giardia* DB accession number GL50803_91252) although it lacks apparent cytochrome P450-type enzymes. Cytochrome P450 reductases are able to reduce cytochrome b_5, and this may be another member of the electron transfer pathway involving these cytochromes. To identify the electron transfer proteins that are partners of the *Giardia* cytochromes will require direct evidence of interactions rather than bioinformatics alone.

CONCLUSION

Giardia lamblia, a microaerophilic protist long known to lack a mitochondria and have a streamlined metabolism, encodes heme-proteins one of which has ~38% sequence identity to the cytochrome b_5 family.The gCYTb_5-I is able to bind heme and is similar to cytochrome b_5 proteins from other organism, as demonstrated through its UV-visible and resonance-Raman spectroscopy. The gCYTb_5-I differs, however, from other cytochrome b_5 in that it has flanking sequences at the amino and carboxy terminal and lower reduction potential than other cytochrome b_5s. Cloning and characterization of truncated mutant with the flanking regions deleted resulted in a protein with similar heme-binding properties as the full-length gCYTb_5-I. This indicated that the flanks are not necessary for heme binding and perhaps has another role. The reduction potential of gCYTb_5-I was very low using both cyclic voltammetry and spectroelectrochemistry. Using the homology model as a guide, we expect that the substitution of hydrophobic to hydrophilic amino acid in the heme-binding pocket have the greatest impact on the reduction potential.

The presence of one actual and two probable functional cytochromes b_5 in Giardia is evidence of uncharacterized cytochrome-mediated metabolic processes in this protist. While such cytochromes serve as electron shuttles with well-established roles in electron transfer pathways, the function of gCYT*b*5 and the means by which Giardia acquires heme remain unknown. As very little is known about function of heme proteins in Giardia, their characterization will lead to better understanding of parasite and may identify unique aspects of Giardia leading to more effective treatments against giardiasis.

REFERENCES

Abe K and Sugita Y. 1979. Properties of cytochrome *b*5, and methemoglobin reduction in human erythrocytes. *Eur J Biochem*. 101(2): 423-428.

Adam, RD. 2001. Biology of *Giardia lamblia*. *Clin Microbiol Rev*. 14(3): 447-475.

Adman ET. 1979. A comparison of the structures of electron transfer proteins. *Biochimica et Biophysica Acta*. 549(1979): 107-144.

Aebersold R and Mann M. 2003. Mass spectrometry-based proteomics. *Nature.* 422(6928): 198-207.

Altschul SF, Madden TL, Schaffer AA, Zhang J, Zhang Z, Miller W and Lipman DJ. 1997. Gapped BLAST and PSI-BLAST: a new generation of protein database search programs. *Nucleic Acids Res.* 25(17): 3389-3402.

Altuve A, Silchenko S, Lee KH, Kuczera K, Terzyan S, Zhang X, Benson DR, Rivera M. 2001. Probing the differences between rat liver outer mitochondrial membrane cytochrome *b*5 and microsomal cytochromes *b*5. *Biochemistry* 40(32): 9469-83.

Altuve A, Wang L, Benson DR, and Rivera M. 2004. Mammalian mitochondrial and microsomal cytochromes *b*5 exhibit divergent structural and biophysical characteristics. *Biochemical and Biophysical Research Communications*. 314(2): 602-609.

Ankarklev, J., Jerlström-Hultqvist, J., Ringqvist, E., Troell K. & Svärd, S.G. 2010. Behind the smile: cell biology and disease mechanisms of Giardia species. *Nature Reviews Microbiology* 8: 413-422

Aono T, Sakamoto Y, Miura M, Takeuchi F, Hori H and Tsubaki M. 2010. Direct electrochemical analyses of human cytochromes *b*5 with a mutated heme pocket showed a good correlation between their midpoint and half wave potentials. *J. Biomed. Sci.* 17(90): 1-15.

Arnold K, Bordoli L, Kopp J and Schwede T. 2006. The SWISS-MODEL Workspace: A web based environment for protein structure homology modelling. *Bioinformatics*. 22(2): 195-201.

Banerjee S. and Mazumdar S. 2012. Electrospray ionization mass spectrometry: a technique to access the information beyond the molecular weight of the analyte. International journal of analytical chemistry. 2012(282574): 1-40

Bard A and Faulkner LR. 2001. Spectroelectrochemistry and other coupled characterization methods: In: *Electrochemical methods: Fundamentals and applications*. 2nd ed. New York: Wiley and Sons: 680-684

Barker PD, Ferrer JC, Mylrajan M, Loehr TM, Feng R, Konishi Y, Funk WD, MacGillivray RT and Mauk AG. 1993. Transmutation of a heme protein. *Proc. Natl. Acad. Sci. U. S. A*. 90: 6542-6546.

Bhattacharya S, Falzone CJ, and Lecomte JT. 1999. Backbone dynamics of apocytochrome *b*5 in its native, partially folded state. *Biochemistry.* 38: 2577-2589.

Bott AW. 1999. Redox properties of electron transfer metalloproteins. *Current Separations.* 18(2): 47-54

Brunt CE, Cox MC, Thurgood AG, Moore GR, Reid GA and Chapman SK. 1992. Isolation and characterization of the cytochrome domain of flavocytochrome b2 expressed independently in Escherichia coli. *Biochem J*. 283 (1): 87-90

Chen Z, Wang LH and Schelvis JPM. 2003. Resonance Raman Investigation of the Interaction of Thromboxane Synthase with Substrate Analogues. *Biochemistry*. 42: 2542-2551.

Chen Z, Ost TWB and Schelvis JPM. 2004. Phe393 Mutants of Cytochrome P450 BM3 with Modified Heme Redox Potentials Have Altered Heme Vinyl and Propionate Conformations. *Biochemistry*. 43: 1798-1808.

Combet C, Blanchet C, Geourjon C and Deleage G. 2000. NPS@: network protein sequence analysis. *Trends Biochem. Sci*. 25: 147–150.

Davydov, D. R. Microsomal monooxygenase in apoptosis: another target for cytochrome c signaling? *Trends in Biochemical Sciences.* 26(3): 155-160

Dole M, Mack LL, Hines RL, Mobley RC, Ferguson LD and Alice MB. 1968. Molecular Beams of Macroions. *The Journal of Chemical Physics*. 49(5): 2240-2249.

Dunn LA, Burgess AG and Krauer KG. 2010. A new-generation 5-nitroimidazole can induce highly metronidazole-resistant *Giardia lamblia* in vitro. *International Journal of Antimicrobial Agents.* 36(1): 37–42

Dunn TM, Haak D, Monaghan E and Beeler TJ. 1998. Synthesis of monohydroxylated inositolphosphorylceramide (IPC-C) in Saccharomyces cerevisiae requires Scs7p, a protein with both a cytochrome b_5-like domain and a hydroxylase/desaturase domain. *Yeast*. 14: 311-321.

Durley RC and Mathews FS. 1996. Refinement and structural analysis of bovine cytochrome *b*5 at 1.5 a resolution. *Acta Crystallogr D Biol Crystallogr*. 52(Pt. 1): 65-76.

Embley TM and Martin W. 2006. Review Eukaryotic evolution, changes and challenges. *Nature.* 440(7084): 623-30.

Rwere F, Mak PJ and Kincaid JR. 2008. Resonance Raman Interrogation of the Consequences of Heme Rotational Disorder in Myoglobin and Its Ligated Derivatives. *Biochemistry*. 47:12869-12877.

Falzone CJ, Wang Y, Vu BC, Scott NL, Bhattacharya S and Lecomte JT. 2001. Structural and dynamic perturbations induced by heme binding in cytochrome b_5. *Biochemistry.* 40: 4879-4891

Falzone CJ, Mayer MR, Whiteman EL, Moore, CD, and Lecomte, JTJ. 1996. Design challenges for hemoproteins: The solution structure of apocytochrome *b*5. *Biochemistry.* 35: 6519-6526

Fenton DE. 1995. *Biocoordination Chemistry*. 2nd ed. Oxford: Oxford Science Publications: Oxford Chemistry Primers 25.

Funk WD, Lo TP, Mauk MR, Brayer GD, MacGillivray RTA and Mauk AG. 1990. Mutagenic, electrochemical, and crystallographic investigation of the cytochrome *b*5 oxidation-reduction equilibrium: Involvement of asparagine-57, serine-64, and heme propionate-7. *Biochemistry*. 29: 5500–5508.

Gasteiger E, Hoogland C, Gattiker A, Duvaud S, Wilkins MR, Appel RD and Bairoch A. 2005. Protein Identification and Analysis Tools on the ExPASy Server. In: Walker JM (ed): *The Proteomics Protocols Handbook*. Totowa, NJ: Humana Press: pp. 571-607. Available from Springer Science & Business Media E-book.

GiardiaDB Giardia genomics resources. 2008. Retrieved from EuPathDB: http://giardiadb.org/giardiadb/

Gray HB and Ellis WR. 1994. Electron Transfer. In: Bertini I, Gary HB, Lippard SJ and Valentine JS (eds). *Bioinorganic chemistry*. Mill Valley, CA: University Science Books: pp. 315-363.

Gruenke LD, Sun J, Loehr TM and Waskell L. 1997. Resonance Raman spectral properties and stability of manganese protoporphyrin IX cytochrome *b*5. *Biochemistry*. 36(23): 7114-25.

Guiard B and Lederer F. 1977. The "b_5-like" domain from chicken-liver sulfite oxidase: a new case of common ancestral origin with liver cytochrome *b*5 and bakers' yeast cytochrome *b*2 core. *Eur J Biochem*. 74: 181-190.

Guzov VM, Houston HL, Murataliev MB, Walker FA and Feyereisen R. 1996. Molecular cloning, overexpression in *Escherichia coli*, structural and functional characterization of house fly cytochrome *b*5. *Journal of Biological Chemistry*. 271(43):26637-45.

Hamza I. 2006. Intracellular trafficking of porphyrins. *ACS Chem Biol.* 1(10): 627-9.

Han J. and Collins LJ. 2012. Reconstruction of Sugar Metabolic Pathways of *Giardia lamblia*. *Int J Proteomics*. 2012: 980829: 1-9

Hegesh E, Hegesh J and Kaftory A. 1986. Congenital methemoglobinemia with a deficiency of cytochrome *b*5. *N. Engl. J. Med.* 414: 757–761.

Hoffmann E and Stroobant V. 2007. Mass Spectrometry: Principles and Applications. 3rd Ed. Chichester, West Sussex, UK: John Wiley & Sons: pp. 502.

Holler DA, Skoog FJ and Crouch SR. 2006. Introduction to Ultraviolet-Visible Molecular Absorption Spectrometry. In: *Principles of Instrumental Analysis*. 6th Ed. Boston: Brooks Cole: 335-336

Huntley TE and Strittmatter P. The effect of heme binding on the tryptophan residue and the protein conformation of cytochrome *b*5. *Journal of Biological Chemistry*. 247(14): 4641 1972.

Ihara M, Takahashi S, Ishimori K and Morishima I. 2000. Functions of Fluctuation in the Heme-Binding Loops of Cytochrome *b*5 Revealed in the Process of Heme Incorporation. *Biochemistry*. 39(20): 5961–5970

Im SC and Waskell L. 2011. The interaction of microsomal cytochrome P450 2B4 with its redox partners, cytochrome P450 reductase and cytochrome *b*5. *Archives of Biochemistry and Biophysics*. 507(1): 144-153

Iribarne JV and Thomson BA. 1976. On the evaporation of small ions from charged droplets. *J. Chem. Phys*. 64(6): 2287-2289.

Ito A, Hayashi S and Yoshida T. 1981. Participation of a cytochrome *b*5-like hemoprotein of outer mitochondrial membrane (OM cytochrome b) in NADH semidehydroascorbic acid reductase activity of rat liver. *Biochem. Biophys. Res. Commun*. 101: 591-8.

Ito A. 1980. Cytochrome *b*5-like Hemoprotein of Outer Mitochondrial Membrane; OM Cytochrome *b*5. Purification of OM Cytochrome b from Rat Liver Mitochondria and Comparison of Its Molecular Properties with Those of Cytochrome b_5. *J. Biochem.* 87: 63-71.

Iyanagi T. 1977. Redox properties of microsomal reduced nicotinamide adenine dinucleotide-cytochrome b_5 reductase and cytochrome b_5. *Biochemistry.* 16: 2725-2730.

Jagow G. 1980. *b*-Type Cytochromes. *Annual Review of Biochemistry*. 49: 281–314.

Källberg M, Wang H, Wang S, Peng J, Wang Z, Lu H and Xu J. 2012. Template-based protein structure modeling using the RaptorX web server. *Nature Protocols*. 7: 1511-1522.

Katoh S. 2013. MAFFT multiple sequence alignment software version 7: improvements in performance and usability. *Molecular Biology and Evolution*. 30: 772-780

Kawano T, Kozutsumi Y, Kawasaki T and Suzuki A. 1994. Biosynthesis of N-glycolylneuraminic acidcontaining glycoconjugates. Purification and characterization of the key enzyme of the cytidine monophospho-N acetylneuraminic acid hydroxylation system. *J Biol Chem.* 269: 9024-9029

Kennepohl P and Solomon E I. 2003. A New Look at Biological Electron Transfer: Electronic Relaxation in Rubredoxins. *Science Highlight*. June 2003.

Konermann L, Ahadi E, Rodriguez AD and Vahidi S. 2013. Unraveling the Mechanism of Electrospray Ionization. *Analytical Chemistry*. 85: 2-9.

Konermann L, Rodriguez AD and Liu J. 2012. On the formation of highly charged gaseous ions from unfolded proteins by electrospray ionization. Analytical chemistry. *American Chemical Society*. 84(15): 6798–804.

Kostanjevecki V, Leys D, Van-Driessche G, Meyer TE, Cusanovich MA, Fischer U, Guisez, Y and Van-Beeumen J. 1999. Structure and characterization of *Ectothiorhodospira vacuolata* cytochrome *b*(558), a prokaryotic homologue of cytochrome *b*(5). *J. Biol. Chem*. 274: 35614-35620

Kotrbová V, Aimová D, Ingr M, Borek-Dohalská L, Martínek V, and Stiborová M. 2009. Preparation of a biologically active apo-cytochrome *b*5 via heterologous expression in *Escherichia coli*. *Protein Expression and Purification*. 66: 203-209

Kuroda R, Ikenoue T, Honsho M, Tsujimoto S, Mitoma JY and Ito A. 1998. Charged amino acids at the carboxyl-terminal portions determine the intracellular locations of two isoforms of cytochrome *b*5. *J Biol Chem*. 273(47): 31097-102.

Kusche WH and Trüper HG 1984. Cytochromes of the Purple Sulfur Bacterium *Ectothiorhodospira shaposhnikovii*. *Z. Naturforsch. Sect. C Biosci*. 39(C): 894-901

Lacan P, Becchi M, Zanella-Cleon I, Aubry M, Quinsat D and Couprie N. 2005. Identification by mass spectrometry of a hemoglobin variant with an elongated beta-globin chain. *Clinical chemistry*. 51(1): 213-5.

Landfried DA, Vuletich DA, Pond MP and Lecomte JTJ. 2007. Structural and thermodynamic consequences of b heme binding for monomeric apoglobins and other apoproteins. *Gene*. 398(1-2): 12-28.

Lederer F. 1994. The cytochrome *b*5 fold: An adaptable module. *Biochimie*. 76(7): 674–692.

Lee KB, Jun E, LaMar GN, Rezzano IN, Pandey RK, Smith KM, Walker FA and Buttlaire DH. 1991. Influence of heme vinyl- and carboxylate-protein contacts on the structure and redox properties of bovine cytochrome *b*5. *J. Am. Chem. Soc*. 113: 3576.

Lee KB, LaMar GN, Kehres LA, Fujinari EM and Smith KM. 1990. ^{1}H NMR Study of the Influence of Hydrophobic Contacts on Protein-Prosthetic Group Recognition in Bovine and Rat Ferricytochrome b_5. *Biochemistry*. 29: 9623-9631

Lin LH and Beattie DS. 1978. Purification and properties of a major cytochrome *b* peptide from baker's yeast. *J Biol Chem.* 253(7): 2412-8.

Lin YW, Ying TL and Lioa LF. 2009. Molecular modeling and dynamics simulation of histidine-tagged cytochrome *b*5. *J. Mol Model*. 17(5): 971-8

Lippard SJ and Berg JM. 1994. *Principles of bioinorganic chemistry*. Mill Valley, CA: University Science Books.

Lloyd D and Harris JC. 2002. Giardia: highly evolved parasite or early branching eukaryote? *Trends in Microbiology*. 10(3): 122-127

Lloyd E, Ferrer JC, Funk WD, Mauk MR and Mauk AG. 1994. Recombinant human erythrocyte cytochrome *b*5. *Biochemistry.* 33: 11432-11437.

Silvestris MD, D'Arrigo A and Borgese N. The targeting information of the mitochondrial outer membrane isoform of cytochrome *b*5 is contained within the carboxyl-terminal region. *FEBS letters*. 370(1-2): 69-74.

Chudaev MV, Gilep AA and Usanov SA. 2001. Site-Directed Mutagenesis of Cytochrome *b*5 for Studies of Its Interaction with Cytochrome P450. *Biochemistry (Moscow).* 66(6): 667-681. *Translated from Biokhimiya,* 66(6): 822-838.

Marcus RA and Sutin N. 1985. Electron transfers in chemistry and biology. *Biochimica et Biophysica Acta*. 811: 265–322.

Martinis SA, Sotiriou C, Chang CK and Sligar SG. 1989. Characterization of cytochrome *b*5 reconstituted with a ferric chlorin and a ferric oxochlorin. *Biochemistry*. 28: 879-884.

Mastronicola D, Testa F, Forte E, Bordi E, Pucillo LP, Sarti P and Giuffrè A. 2010. Flavohemoglobin and nitric oxide detoxification in the human protozoan parasite Giardia intestinalis. *Biochem Biophys Res Commun*. 399(4): 654-658

Mathews FS, Levine M and Argos P. 1971. Structure of calf liver cytochrome *b*5 at 2.8 A resolution. *Nature-New Biology*. 233(35): 15

Mathews FS, Czerwinsky EW and Argos P. 1979. The X-ray crystallographic structure of calf liver cytochrome *b*5. In: Dolphin D. (ed.) *The Porphyrins*. 7th Ed. New York: Academic Press: pp. 107-147.

Mauk G and Moore GR. 1997. Control of metalloprotein redox potentials: what does site-directed mutagenesis of hemoproteins tell us? *Journal of Biological Inorganic Chemistry.* 2(1): 119-125.

Mayer TE, Rivera M, Walker FA, Mauk MR, Mauk AG, Cusanovich M and Tollin G. 1993. Laser Flash Photolysis Studies of Electron Transfer to the Cytochrome *b*5-Cytochrome c Complex. *Biochemistry.* 32: 622-27

Mitoma J. and Ito A. 1992. The carboxy-terminal 10 amino acid residues of cytochrome b_5 are necessary for its targeting to the endoplasmic reticulum. *The EMBO Journal.* 11: 4197–4203

Moore CD, and Lecomte JTJ. 1990. Structural properties of apocytochrome *b*5: Presence of a stable native core. *Biochemistry.* 29: 1984-1989

Morrison HG. 2007. Genomic minimalism in the early diverging intestinal parasite *Giardia lamblia*. *Science.* 317: 1921-1926.

Mukhopadhyay K. and Lecomte JTJ. 2004. A relationship between heme binding and protein stability in cytochrome b_5. *Biochemistry*. 43(38): 12227–36.

Murphy D, Parker J, Zhou M, Fadlelmola FM, Steidl C, Karsan A, Gascoyne RD, Chen H and Banerjee D. 2010. Constitutively overexpressed 21 kDa protein in Hodgkin lymphoma and aggressive non-Hodgkin lymphomas identified as cytochrome B5b (CYB5B). *Mol Cancer*. 9(14).

Nishino H and Ito A. 1986. Subcellular distribution of OM cytochrome *b*-mediated NADH-semidehydroascorbate reductase activity in rat liver. *J. Biochem.* 100: 1523-31.

Nóbrega FG, Araujo PS, Pasetto M and Raw I. 1969. Some properties of cytochrome *b*5 from liver microsomes of man, monkey, pig and chicken. *The Biochemical journal*. 115(4): 849–56.

Ogishima T, Kinoshita J, Mitani F, Suematsu M and Ito A. 2003. Identification of Outer Mitochondrial Membrane Cytochrome b_5 as a Modulator for Androgen Synthesis in Leydig Cells. *The Journal of Biological Chemistry* 278: 21204-21211.

Olea C, Kuriyan J and Marletta M. 2010. Modulating heme redox potential through protein-induced porphyrin distortion. *Journal of the American Chemical Society*. 132(37): 12794–5.

Paoli M, Marles-Wright J and Smith A. 2002. Structure-function relationships in hemeproteins. *DNA and Cell biology*. 21(4): 271–80.

Paul K, Theorell H and Akenson A. 1953. The molar light absorption of pyridine ferroprotoporphyrin (pyridine hemochromagen). *Acta Chem. Scand*. 7: 1284-1287

Philippe H, Lopez P, Brinkmann H, Budin K, Germot A, Laurent J, Moreira D, Muller M. and LeGuyader H. 2000. Early-branching or fast-evolving eukaryotes? An answer based on slowly evolving positions. *Proc. R. Soc. Lond. B: Biol. Sci.* 267: 1213-1221.

Qian W, Wang YH, Wang WH, Yao P, Zhuang JH, Xie Y and Huang ZH. Redox properties of cytochrome *b*5: a mutagenesis and DPV study of the pH and ionic strength dependence of redox potentials and interactions with myoglobin by DPV. *Journal of Electroanalytical Chemistry*. 535 (2002): 85-96.

Rafferty S, Luu B, March RE and Yee J. 2010. *Giardia lamblia* encodes a functional flavohemoglobin. *Biochem Biophys Res Commun*. 399(3): 347-51.

Rafferty SP. 1992. *Functional properties of active site variants of yeast cytochrome c.* Ph.D. thesis, The University of British Columbia (Canada).

Reedy CJ and Gibney BR. 2004. Heme protein assemblies. *Chemical reviews*. 104(2): 617–49.

Reid LS, Taniguchi VT, Gray HB and Mauk AG. 1982. Oxidation reduction equilibrium of cytochrome *b*5. *J. Am. Chem. Soc*. 104: 7516-9.

Reid EL, Weynberg KD, Love J, Isupov MN, Littlechild JA, Wilson WH, Kelly SL, Lamb DC and Allen MJ. 2013. Functional and structural characterisation of a viral cytochrome *b*5. *FEBS Letters*. 587: 3633–3639

Rivera M, Seetharaman R, Ghirdhar D, Wirtz M, Zhang X, Wang X and White S. 1998. The reduction potential of cytochrome *b*5 is modulated by its exposed heme edge. *Biochemistry*. 37: 1485-94.

Rivera M and Walker FA. 1995. Biosynthetic preparation of isotopically labeled heme. *Anal. Biochem.* 230: 295-302.

Rivera M, Wells MA and Walker FA. 1994. Cation-promoted cyclic voltammetry of recombinant rat outer mitochondrial membrane cytochrome b_5 at a gold electrode modified with 8-mercaptopropionic acid. *Biochemistry* 33: 2161-70.

Rivera M, Barillas-Mury C, Christensen KA, Little JW, Wells MA and Walker FA. 1992. Gene synthesis, bacterial expression, and ^{1}H NMR spectroscopic studies of the rat outer mitochondrial membrane cytochrome *b*5. *Biochemistry*. 31(48): 12233-40.

Kassner RJ. 1972. Effects of nonpolar environments on the redox potentials of heme complexes. *Proceedings of the National Academy of Sciences*. 69(8): 2263–2267.

Roat-Malone R M. 2007. *Bioinorganic Chemistry: A Short Course*. 2nd Ed. New York: John Wiley & Sons Inc.

Rodgers KK and Sligar SG. 1991. Surface electrostatic, reduction potentials, and the internal dielectric constant of proteins. *J. Am. Chem. Soc*. 113: 9419-21.

Rodriguez-Maranon MJ, Qiu F, Stark RE, White SP, Zhang X, Foundling SI, Rodriguez V, Schilling CL, Bunce RA and Rivera M. 1996. ^{13}C NMR spectroscopic and X-ray crystallographic study of the role played by mitochondrial cytochrome *b*5 heme propionates in the electrostatic binding to cytochrome c. *Biochemistry*. 35(50): 16378-90.

Savioli L, Smith H and Thompson A. 2006. Giardia and Cryptosporidium join the 'Neglected Diseases Initiative.' *Trends Parasitol*. 22 (5): 203-208

Schenkman JB and Jansson I. 2003. The many roles of cytochrome b_5. *Pharmacology and Therapeutics*. 97(2): 139–152.

Scott AS, Mauk AG and Gray HB. 1985. Experimental Approaches to Studying Biological Electron Transfer. *Journal of Chemical Education*. 62(11):932-938.

Sergeev GV, Gilep AA, Estabrook RW and Usanov SA. 2006. Expression of Outer Mitochondrial Membrane Cytochrome *b*5 in *Escherichia coli*. Purification of the Recombinant Protein and Studies of Its Interaction with Electron Transfer Partners. *Biochemistry*. 71(7): 790-799.

Severance S and Hamza I. 2009. Trafficking of Heme and Porphyrins in Metazoa. *Chem Rev*. 109(10): 4596–4616.

Shan L, Lu JX, Gan JH, Wang YH, Huang ZX and Xia ZX. 2005. Structure of the F58W mutant of cytochrome *b*5: the mutation leads to multiple conformations and weakens stacking interactions. *Acta Crystallographica*. 61(2D): 180-189.

Shokhirev NV and Walker FA. 1998. The effect of axial ligand plane orientation on the contact and pseudocontact shifts of low-spin ferriheme proteins. *JBIC*. 3: 581–594

Silchenko S, Sippel ML, Kuchment O, Benson DR, Mauk AG, Altuve A, Rivera M. 2000. Hemin is kinetically trapped in cytochrome *b*(5) from rat outer mitochondrial membrane. *Biochem. Biophys. Res. Commun*. 271: 467-72.

Smith LJ, Kahraman A and Thornton JM. Heme proteins-diversity in structural characteristics, function, and folding. *Proteins*. 78(10): 2349-68.

Smith MA, Napier JA, Stymne S, Arthur T, Tatham S, Peter T, Shewryt R and Stobart AK. 1994. Expression of a biologically active plant cytochrome *b*5 in *Escherichia coli*. *Biochem*. *J*. 30373-79.

Soucy P and Luu-The V. 2002. Assessment of the ability of type 2 cytochrome *b*5 to modulate 17,20-lyase activity of human P450c17. *J. Steroid Biochem*. *Mol. Biol*. 80: 71–75

Parthasarathy S, Altuve A, Terzyan S, Zhang X, Kuczera K, Rivera M and Benson DR. Comparison of Human and Rat Type B (Mitochondrial) Cytochrome b_5. *Biochemistry* 2011.

Svärd, S. G., Hagblom, P. and Palm, J. E. (2003) *Giardia lamblia*- a model organism for eukaryotic cell differentiation. *FEMS Microbiol Lett.* 218: 3–7

Yokota T, Nakajima Y, Fumiyuki Yamakura, Shigetoshi Sugio, Muneaki Hashimoto, and Shinzaburo Takamiya. 2006. Unique structure of *Ascaris suum b*5-type cytochrome: an additional alpha-helix and positively charged residues on the surface domain interact with redox partners. *The Biochemical Journal*. 394(2): 437-47.

Takematsu H, Kawano T, Koyama S, Kozutsumi Y, Suzuki A and Kawasaki T. 1994. Reaction mechanism underlying CMP-N-acetylneuraminic acid hydroxylation in mouse liver: formation of a ternary complex of cytochrome *b*5, CMP-N-acetylneuraminic acid, and a hydroxylation enzyme. *J Biochem*. 115(3): 381-6.

Teale FWJ. 1959. Cleavage of the haem-protein link by acid methyl ethyl ketone. *Biochim. Biophys. Acta*. 35: 543

Tovar J, Leon-Avila G, Sanchez LB, Sutak R, Tachezy J, Giezen MV, Hernandez M, Muller M and Lucocq JM. 2003. Mitochondrial remnant organelles of Giardia function in iron-sulphur protein maturation. *Nature.* 426: 172–176.

Vergéres G, Chen DY, Wu FF and Waskell L. 1993. The Function of Tyrosine 74 of Cytochrome *b*5. *Archives of Biochemistry and Biophysics*. 305(2): 231–241

Vergéres G and Waskell L. 1995. Cytochrome *b*5, its functions, structure and membrane topology. *Biochimie:* 77(7-8): 604–20.

Walker FA, Emrick D, Rivera JE, Hanquet BJ and Buttlaire DH. 1988. Effect of Heme Orientation on the Reduction Potential of Cytochrome *b*5. *Journal of the American Chemical Society*. 110(15): 6234–6240

Wang J. 2000. Study of electrode reactions: Cyclic voltammetry and Spectroelectrochemistry in *Analytical Electrochemistry*. Second Edition. John Wiley & Sons, Inc., New York, USA: 28-30 and 40-44

Wass MN, Kelley LA and Sternberg MJ. 2010. 3DLigandSite: predicting ligand-binding sites using similar structures. *Nucleic Acids Res*. 2010 Jul 38(Web Server issue):W469-73.

Waterhouse AM, Procter JB, Martin DMA, Clamp M and Barton GJ. 2009. Jalview Version 2: a multiple sequence alignment editor and analysis workbench *Bioinformatics*. 25 (9):1189-1191

Weissman Z and Kornitzer D. 2004. A family of Candida cell surface haem-binding proteins involved in haemin and haemoglobin-iron utilization. *Mol Microbiol*. 53: 1209-1220.

Wirtz M, Oganesyan V, Zhang X, Studer J and Rivera M. 2000. Modulation of redox potential in electron transfer proteins: Effects of complex formation on the active site microenvironment of cytochrome b_5. *Faraday Discuss*. 221-268

Wu CM, Chiou HG, Lin SL, Lin JM. 2012. Effects of Electrostatic Polarity and the Types of Electrical Charging on Electrospinning Behavior. *J Appl Polym Sci*. 126: E89.

Wu Y and Hu S. 2007. Biosensors based on direct electron transfer in redox proteins. *Microchimica Acta*. 159(1-2): 1-17.

Xue LL, Wang YH, Xie Y, Yao P, Wang WH, Qian W, Huang ZX, Wu J and Xia ZX. 1999. Effect of mutation at valine 61 on the three-dimensional structure, stability, and redox potential of cytochrome *b*5. *Biochemistry*. 38(37): 11961–72.

Yu Y, Yamasaki H, Kita K and Takamiya S. 1996. Purification and Molecular Characterization of a Novel *b*5-Type Cytochrome of the Parasitic Nematode, *Ascaris suum*. *Archives of Biochemistry and Biophysics*. 328(1): 165–172

Yao P, Xie Y, Wang YH, Sun YL, Huang ZX, Xiao GT and Wang SD. 1997. Importance of a conserved phenylalanine-35 of cytochrome *b*5 to the protein's stability and redox potential. *Protein Engineering Design and Selection*. 10(5): 575–581.

Younas M, Shah S and Talaat A. 2008. Frequency of *Giardia lamblia* infection in children with recurrent abdominal pain. *Journal of Pakistan Medical Association.* 58(4): 171-174

Yu C, Yu L and King TE. 1975. Studies on cytochrome *b*. I. Isolation, purification, and some properties of cytochrome *b* from beef heart muscle. *Biochem. Biophys. Res. Commun*. 66: 1194-1200

Zhang Y. 2008. I-TASSER server for protein 3D structure prediction. *BMC Bioinformatics*: 9: 40.

APPENDIX

Appendix I- Primer design for cloning cytob_5 into pET14b vector: N-term cleavable His6tag

Cytob_5 GL50803_9089 coding sequence

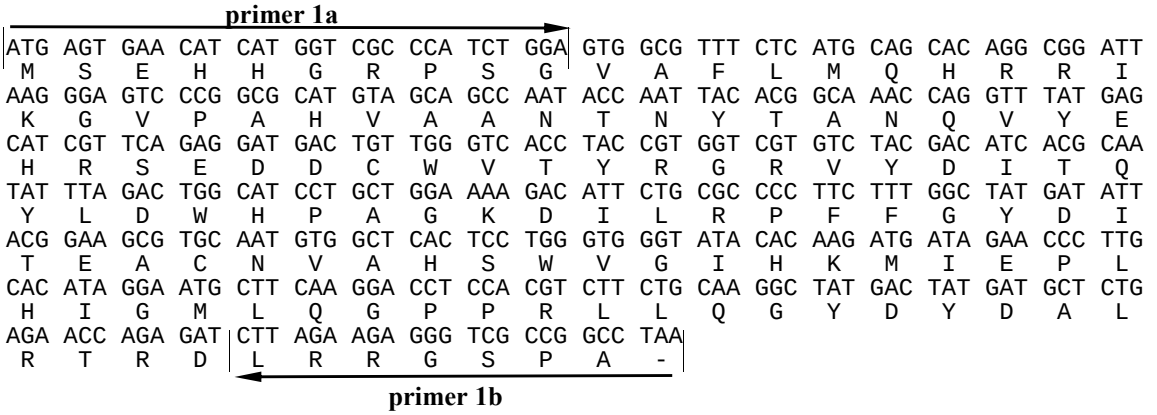

Cytob_5/*Nde*I-1a:

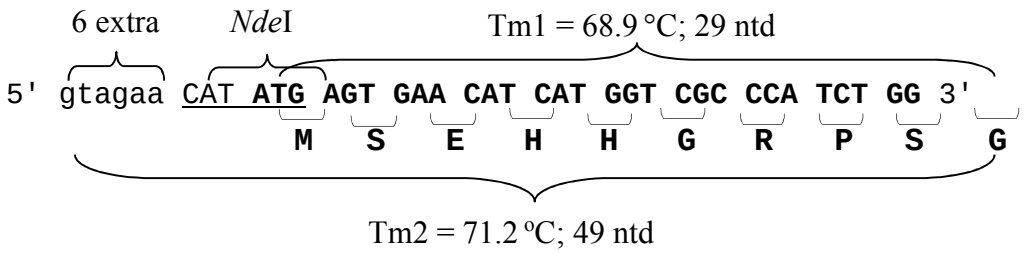

Cytob_5/*Bam*HI-1b:

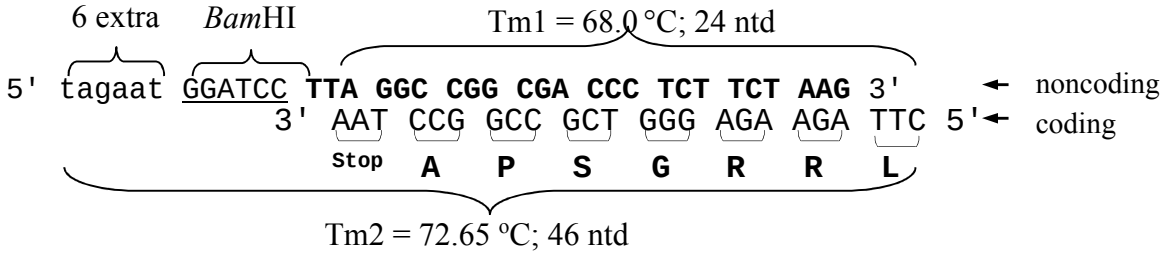

Appendix II- Vector map of pET-14b expression vector

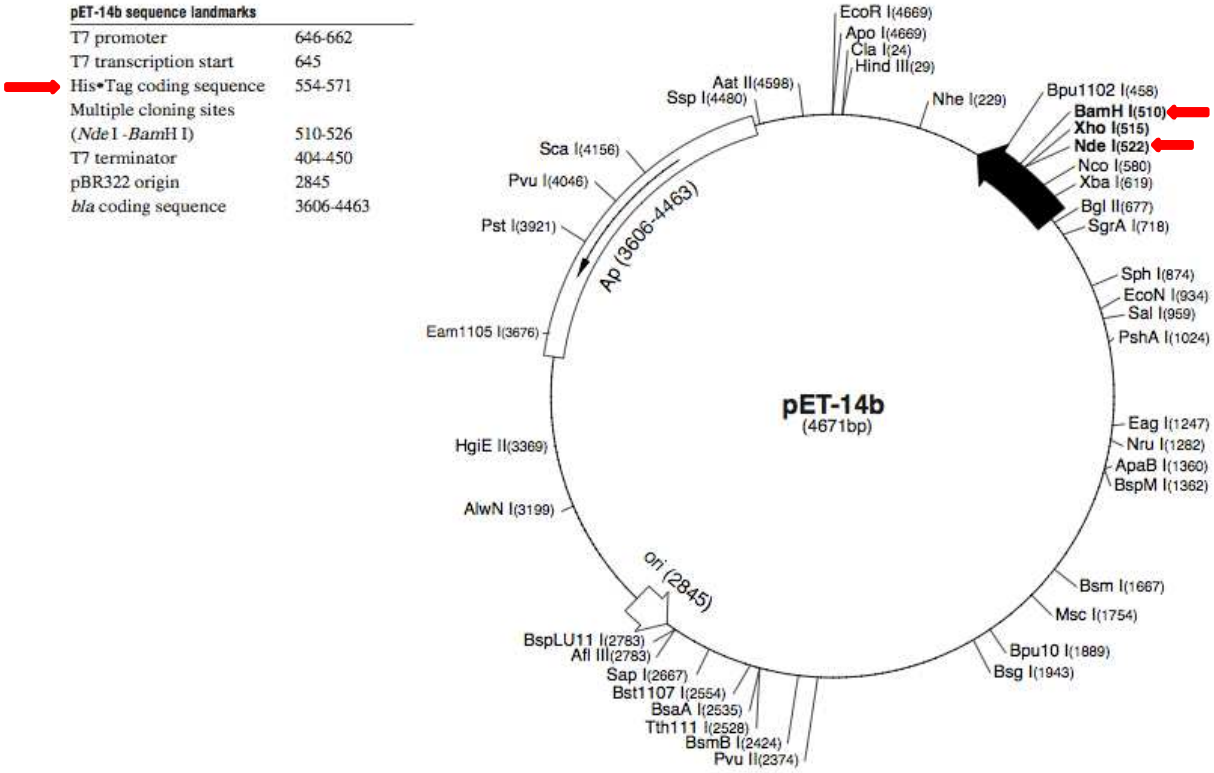

pET-14b Cloning/Expression Region

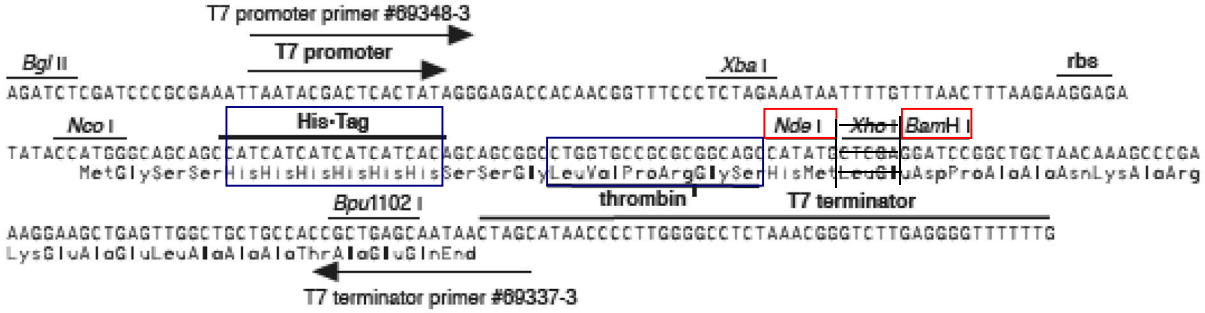

Appendix III- PCR of Cytob_5 from Giardia genomic DNA

(Designed by Dr. J. Yee)

Master mix set-up for PCR with Phire hot start polymerase

PCR component	[Stock]	1x
dH_2O	—	31.5 µl
5x Phire buffer	5x	10
dNTPs	5 mM	2
Forward primer	25 µM	1
Reverse primer	25 µM	1
Giardia genomic DNA€	20 ng/µl	2.5
DMSO	100 %	1.5
$MgCl_2$ ¥	—	—
Phire DNA polymerase*	2 units/ml	0.5
Total reaction volume		**50 µl**

€ 50 ng of DNA was used per 50 µl reaction.

¥ Phire 5x buffer contains 7.5 mM $MgCl_2$ and gives a final [$MgCl_2$] = 1.5 mM

Use Mastercycler EP "Genomic PCR no gradient" program in Samiah's folder

Segment	Step	Temperature (°C)	Time	# Cycles
1	1	98	3 min	1
2	1 2 3	98 60 72	15 sec 30 sec 15 sec	6
3	1 2 3	98 64 72	15 sec 30 sec 15 sec***	30
4	1	72	1 min	1
5	1	4	HOLD	—

*** Based on Phire activity ~1 kb/20 sec, and expected ~ size of amplicon (396 bp + primers 24 bp = 420 bp)

Appendix IV- PCR screening of transformed *E. coli* DH5α and JM109 cells for presence of cytochrome b_5 insert

PCR Setup

PCR Component	[Stock]	[Final]	µL for 1x Rx
dH_2O	—	—	38
Taq Buffer	10x	1x	5
$MgCl_2$ [¥]	25 mM	2 mM	4
Cytob_5/*Nde*I-1a primer	25 µM	0.25 µM	0.5
Cytob_5/*Bam*HI-1b primer	25 µM	0.25 µM	0.5
dNTPs	5 mM	100 µM	1
Taq pol (Bioshop)	5 units/µL	1 unit total	0.20
			*49.2 µL

[¥] The 10x buffer associated have no $MgCl_2$—so need to add it to 2 mM.
* 1 µL of bacterial solution was added to make a total reaction volume of 50.2 µL.

PCR Parameters for colony screening for Cytochrome b_5 inserts in pJET1.2

Step	Segment	Temperature (°C)	Duration	# of Cycles
1	1	94.0	8 min	1
2	1 2 3	94.0 68.0 72.0	15 sec 30 sec 40 sec	25
3	1	4.0	HOLD	—

* Use the mid-range T_{m2} from the original PCR amplification of the gene from genomic DNA

Appendix V- Primer design for cloning core heme-binding domain gCYTb$_5$-1$_{(32-107)}$ into pET14b vector

Cyto*b*$_5$ GL50803_9089 coding sequence

```
ATG AGT GAA CAT CAT GGT CGC CCA TCT GGA GTG GCG TTT CTC ATG CAG CAC AGG CGG ATT
M   S   E   H   H   G   R   P   S   G   V   A   F   L   M   Q   H   R   R   I
                                                        primer 2a
AAG GGA GTC CCG GCG CAT GTA GCA GCC AAT ACC AAT TAC ACG GCA AAC CAG GTT TAT GAG
 K   G   V   P   A   H   V   A   A   N   T   N   Y   T   A   N   Q   V   Y   E
CAT CGT TCA GAG GAT GAC TGT TGG GTC ACC TAC CGT GGT CGT GTC TAC GAC ATC ACG CAA
 H   R   S   E   D   D   C   W   V   T   Y   R   G   R   V   Y   D   I   T   Q
GAC ATT CTG CGC CCC TTC TTT GGC TAT GAT ATT TAT TTA GAC TGG CAT CCT GCT GGA AAA
 Y   L   D   W   H   P   A   G   K   D   I   L   R   P   F   F   G   Y   D   I
ACG GAA GCG TGC AAT GTG GCT CAC TCC TGG GTG GGT ATA CAC AAG ATG ATA GAA CCC TTG
 T   E   A   C   N   V   A   H   S   W   V   G   I   H   K   M   I   E   P   L
CAC ATA GGA ATG CTT CAA GGA CCT CCA CGT CTT CTG CAA GGC TAT GAC TAT GAT GCT CTG
 H   I   G   M   L   Q   G   P   P   R   L   Q   G   Y   D   L   Y   D   A   L
                    primer 1b
AGA ACC AGA GAT CTT AGA AGA GGG TCG CCG GCC TAA
 R   T   R   D   L   R   R   G   S   P   A   -
```

Cyto*b*$_5$/NdeI-2a:

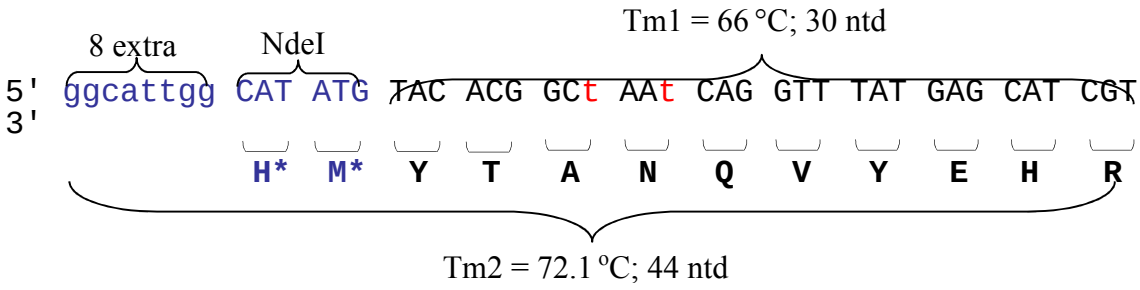

***Amino acids encoded by NdeI site on pET14 b vector**

Cyto*b*$_5$/BamHI-2b:

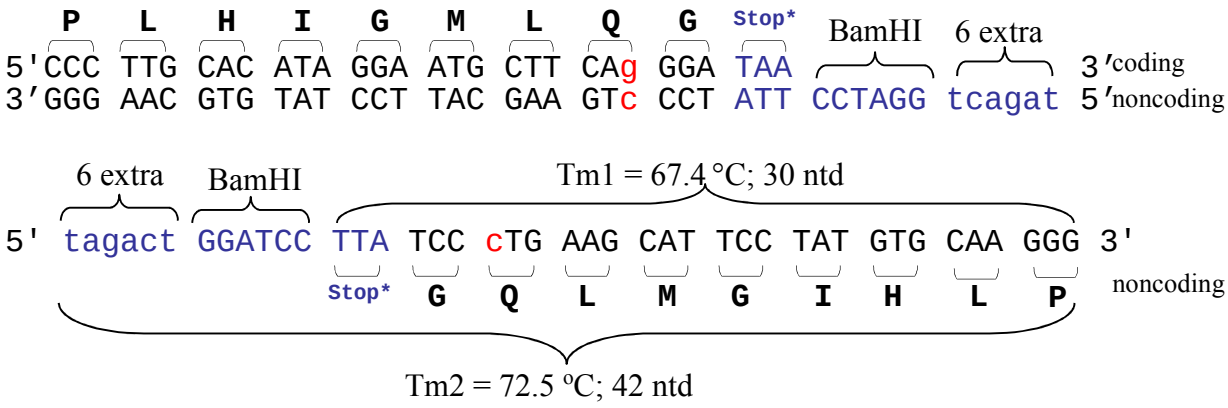

Appendix VI- Primer design for cloning N-terminal truncated gCYTb$_5$-I$_{(32-131)}$ into pET14b vector

Cyto*b*$_5$ GL50803_9089 coding sequence

```
ATG AGT GAA CAT CAT GGT CGC CCA TCT GGA GTG GCG TTT CTC ATG CAG CAC AGG CGG ATT
M   S   E   H   H   G   R   P   S   G   V   A   F   L   M   Q   H   R   R   I
                                                        primer 2a
AAG GGA GTC CCG GCG CAT GTA GCA GCC AAT ACC AAT TAC ACG GCA AAC CAG GTT TAT GAG
 K   G   V   P   A   H   V   A   A   N   T   N   Y   T   A   N   Q   V   Y   E
CAT CGT TCA GAG GAT GAC TGT TGG GTC ACC TAC CGT GGT CGT GTC TAC GAC ATC ACG CAA
 H   R   S   E   D   D   C   W   V   T   Y   R   G   R   V   Y   D   I   T   Q
GAC ATT CTG CGC CCC TTC TTT GGC TAT GAT ATT TAT TTA GAC TGG CAT CCT GCT GGA AAA
 Y   L   D   W   H   P   A   G   K   D   I   L   R   P   F   F   G   Y   D   I
ACG GAA GCG TGC AAT GTG GCT CAC TCC TGG GTG GGT ATA CAC AAG ATG ATA GAA CCC TTG
 T   E   A   C   N   V   A   H   S   W   V   G   I   H   K   M   I   E   P   L
CAC ATA GGA ATG CTT CAA GGA CCT CCA CGT CTT CTG CAA GGC TAT GAC TAT GAT GCT CTG
 H   I   G   M   L   Q   G   P   P   R   L   Q   G   Y   D   L   Y   D   A   L
AGA ACC AGA GAT CTT AGA AGA GGG TCG CCG GCC TAA
 R   T   R   D   L   R   R   G   S   P   A   -
                 primer 1b
```

Cyto*b*$_5$/NdeI-2a:

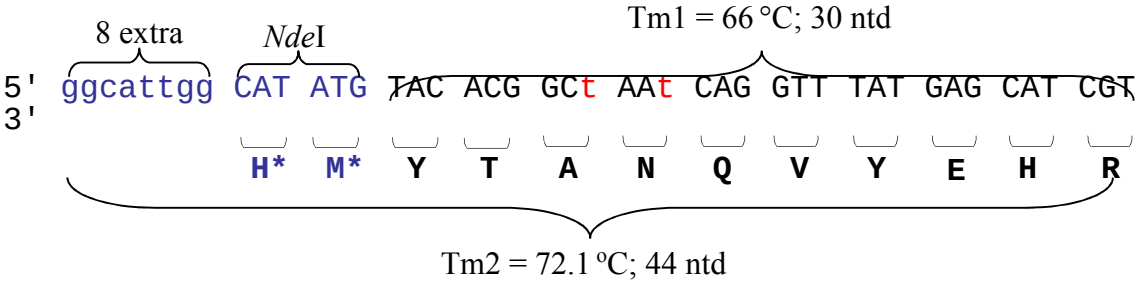

***Amino acids encoded by NdeI site on pET14 b vector**

Cyto*b*$_5$/BamHI-3b:

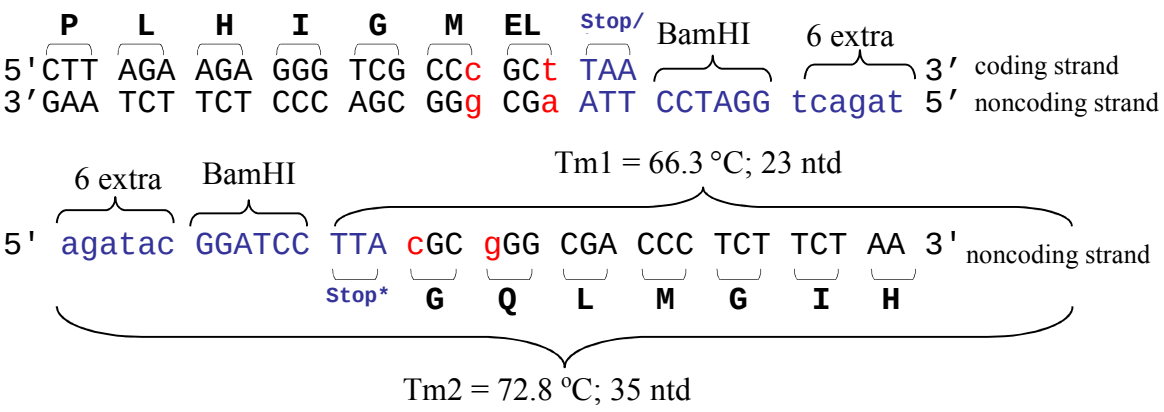

Appendix VII- Primer design for cloning C-terminal truncated Cytob_5-I$_{(1\text{-}107)}$ into pET14b vector

Cytob_5 GL50803_9089 coding sequence

primer 1a

```
ATG AGT GAA CAT CAT GGT CGC CCA TCT GGA GTG GCG TTT CTC ATG CAG CAC AGG CGG ATT
M   S   E   H   H   G   R   P   S   G   V   A   F   L   M   Q   H   R   R   I
AAG GGA GTC CCG GCG CAT GTA GCA GCC AAT ACC AAT TAC ACG GCA AAC CAG GTT TAT GAG
 K   G   V   P   A   H   V   A   A   N   T   N   Y   T   A   N   Q   V   Y   E
CAT CGT TCA GAG GAT GAC TGT TGG GTC ACC TAC CGT GGT CGT GTC TAC GAC ATC ACG CAA
 H   R   S   E   D   D   C   W   V   T   Y   R   G   R   V   Y   D   I   T   Q
GAC ATT CTG CGC CCC TTC TTT GGC TAT GAT ATT TAT TTA GAC TGG CAT CCT GCT GGA AAA
 Y   L   D   W   H   P   A   G   K   D   I   L   R   P   F   F   G   Y   D   I
ACG GAA GCG TGC AAT GTG GCT CAC TCC TGG GTG GGT ATA CAC AAG ATG ATA GAA CCC TTG
 T   E   A   C   N   V   A   H   S   W   V   G   I   H   K   M   I   E   P   L
CAC ATA GGA ATG CTT CAA GGA CCT CCA CGT CTT CTG CAA GGC TAT GAC TAT GAT GCT CTG
 H   I   G   M   L   Q   G   P   P   R   L   Q   G   Y   D   L   Y   D   A   L
                                primer 2b
AGA ACC AGA GAT CTT AGA AGA GGG TCG CCG GCC TAA
R   T   R   D   L   R   R   G   S   P   A   -
```

Cytob_5/NdeI-1a:

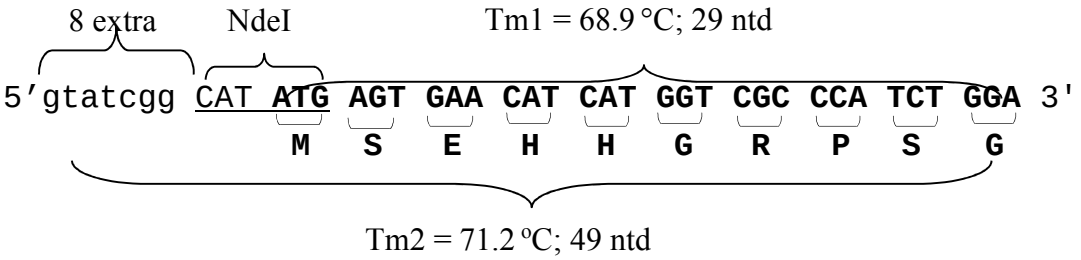

Cytob_5/BamHI-2b:

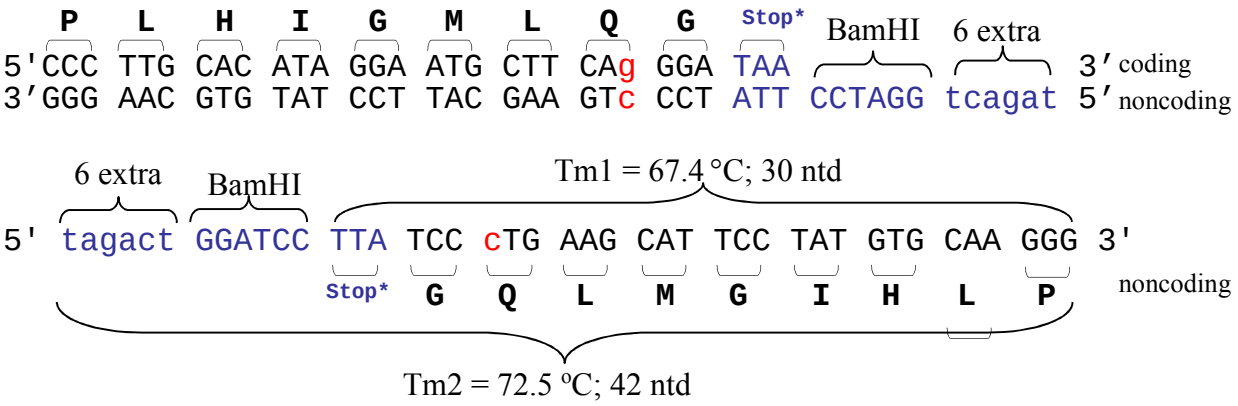

342 bp

Appendix VIII- PCR amplification of truncated Cytob$_5$-I gene from Giardia Cyto*b*$_5$ plasmid DNA

Master mix set-up for PCR with Phire hot start polymerase

PCR component	[Stock]	1x	3.2x
dH_2O	—	28.5 µl	91.2
5x Phire buffer	5x	10	32
dNTPs	5 mM	2	6.4
Forward primer: NdeI-1a	25 µM	1	3.2
Reverse primer: BamH1- 2b	25 µM	1	3.2
Recombinant DNA plasmid Full length Cytob$_5$	5 ng/µl	5	16
DMSO	100 %	1.5	4.8
$MgCl_2$ ¥	—	—	—
Phire DNA polymerase*	2 units/ml	1	3.2
Total reaction volume		**50 µl**	**160**

€ 50 ng of DNA was used per 50 µl reaction.
¥ Phire 5x buffer contains 7.5 mM $MgCl_2$ and gives a final [$MgCl_2$] = 1.5 mM

Use Mastercycler EP "Genomic PCR gradient" program in Samiah's folder

Segment	Step	Temperature (°C)	Time	# Cycles
1	1	98	3 min	1
2	1 2 3	98 57 - 77°C* 72	15 sec 30 sec 15 sec	6
3	1 2 3	98 61 - 81°C** 72	15 sec 30 sec 15 sec***	30
4	1	72	1 min	1
5	1	4	HOLD	—

*T_{m1} was used at 60°C (col 4), 65°C (col 6), and 70°C (col 8) in heat block set at temperature gradient from 58.8 - 73°C on thermocycler
**T_{m2} was used at 64°C (col 4), 69°C (col 6), and 74°C (col 8) in heat block set at temperature gradient from 63.8 - 78°C on thermocycler
*** Based on Phire activity ~1 kb/20 sec, and expected ~ size of amplicon (321 bp + primers 21 bp = 342 bp)

Appendix IX- M9 Minimal Media Stock Solutions

5X Concentrate, M9 Salt Stock Solution
30g/L Na_2HPO_4 (Sodium phosphate, dibasic, anhydrous)
15g/L KH_2PO_4 (Potassium phosphate, monobasic)
5 g/L NH_4Cl (Ammonium chloride)
2.5 g/L NaCl (Sodium Chloride)
Sterilize by autoclave, 15 minutes

$MgSO_4$ Stock Solution, 1 M
12.3 grams of magnesium sulfate heptahydrate, *made up to* 5*0 mL*
Sterilize by autoclave, 15 minutes

Glycerol Stock Solution, 10% (w/v)
50 g glycerol *made up to* 5*00 mL*
Sterilize by autoclave, 15 minutes

Ferric Chloride Stock Solution, 2 mM
55 mg $FeCl_3$ hexahydrate, (molecular weight 270.3 g/mol) *in 100 mL*
"Sterilize" by microcentrifugation of the required portion (~ 1 mL) prior to use.

Aminolevulinic Acid Stock Solution, 100 mM
84 mg 5-aminolevulinic acid hydrochloride (molecular weight 167.59 g/mol) *in* 5 *mL*. Sterilize by filtration through a 0.20 micron filter unit mounted on a syringe. Store at -20° C.

Deionized water, sterilized by autoclave, is also required, as is Ampicillin stock solution and a sterile beaker (600 to 1000 mL)

For 1 liter of complete M9+Glycerol+ALA+Fe ("M9-GAFe") media, add the following, under sterile conditions:

200 mL 5X concentrate M9 Salt Stock Solution
1 mL 1 M $MgSO_4$ Stock Solution
20 mL of 10% Glycerol Stock Solution
1 mL Ferric Chloride Stock Solution
1 mL Aminolevulinic Acid Stock Solution
1 mL Ampicillin Stock Solution
Add sterile deionized water up to 1 L

Begin your 2 mL starter cultures using LB+Ampicillin, and use this to inocululate 1 L of M9-GAFe